INVESTIGATING THE RESPONSE OF BOLTED WOOD CONNECTIONS SUBJECTED TO BLAST LOADS

by

Andrew McGrath

Thesis submitted to the in partial fulfillment of the requirements for the degree of

Master of Applied Science

in Civil Engineering

Under the auspices of the Ottawa-Carleton Institute for Civil Engineering

uOttawa

Department of Civil Engineering

Faculty of Engineering

University of Ottawa

Abstract

With recent improvement in wood manufacturing technologies, taller and larger wooden structures are being constructed, thereby increasing the risk for potential damage due to a blast threat against such structures. Recent studies on the effects of high strain rate in wood have been undertaken, however the vast majority of these studies have focussed on structural elements with idealized boundary conditions. Some studies included realistic connections as the boundary conditions, but little progress has been made to date in order to quantify the behaviour of connections in isolation. The current study aims to investigate the response of steel-wood-steel bolted connections when subjected to blast loads. This includes determining the dynamic increase in resistance and stiffness for stocky and slender bolts in both the parallel and perpendicular to grain directions. The study also explores analytical solutions to predict the joint behaviour and discusses the validity of current blast design provisions.

Bolted wood connections were investigated under both static and simulated blast loading using the University of Ottawa's shock tube. The study found a dynamic increase in resistance and stiffness when the failure mode was dominated by wood crushing in both the parallel and perpendicular to grain directions. No increase in resistance or stiffness was observed when bolt yielding dominated the failure. A loss of ductility was observed under dynamic loading for the parallel to the grain connections designed to fail in wood crushing. It was found that the use of self-tapping screw reinforcement was an effective method of preventing premature splitting failures and enhancing the performance of a connection. The results showed that connections which engaged the fastener in bending exhibited more favourable behaviour than connections which engaged only in wood crushing. A two degree-of-freedom model was capable of modelling the connections even when the support frame system had some flexibility. The validated model was used to investigate cases where the connection could contribute to the energy dissipation. It was found that the performance of the assembly improved when the connections were considered.

Recommended future work includes an investigation of brittle failure modes in bolted connections, exploring connections with more deformation capacities, and expanding the experimental component of the study to include full-scale structural assemblies with wood elements and boundary connections. Limited design recommendations have been proposed in the current study, however testing at the assembly level could shed more light on such an important topic.

Acknowledgements

Throughout my graduate studies I have had the privilege of being surrounded by people who have believed in my potential and helped me grow extensively as an individual over the last two years.

I would especially like to thank my thesis supervisor Dr. Ghasan Doudak for his time, flexibility, patience, and thorough support. Without his timely and supportive feedback, this project would not have been the success that it was.

I would like to extend my deepest appreciation to my fiancée Ms. Alison Rose for making all the personal sacrifices required to allow me to pursue my passion and complete this thesis. Your support was instrumental to me being able to complete this work and has never gone unnoticed.

The finical support I received throughout my studies has allowed me to focus solely on my research and course work; resulting in a more comprehensive and quality thesis. I would like to thank the National Sciences and Engineering Research Council of Canada and the University of Ottawa for this finical support.

I would like to take this opportunity to thank my fellow graduate student Mr. Christian Viau for the assistance and advice he has provide me. I am especially grateful for all his guidance and assistance in the laboratory work. I would also like to thank him for providing me with the analysis tool *BlasTDOF*.

Last but certainly not least, I would like to send countless thanks to my mother and father for their endless support and always believing in me.

Table of Contents

List of Tables

List of Figures

Notations

Symbol	Definition
b	Waveform parameter
c	Damping coefficient
d	Fastener diameter
d_u	Displacement at failure
d_y	Displacement at yield
F(t)	Forcing function
F(x,t)	Distributed load per unit length relative to time
F_o	Initial peak load
F_u	Ultimate strength
F_y	Yield load
f_1	Embedment strength of side member
f_2	Embedment strength of main member
f_y	Yield strength of fastener in bending
I^-	Negative impulse
I^+	Positive impulse
I_R	Reflected impulse
K	Stiffness
K_L	Load transformation factor
K_{LM}	Load-mass factor
K_M	Mass transformation factor
K_R	Resistance transformation factor
m	Mass
$\bar{m}(x)$	Mass per unit length
P(t)	External pressure function
P_D	Driver pressure
P_R	Peak reflected pressure
R	Standoff distance
R(y)	Member resistance function

Symbol	Definition
t	Time
t_a	Arrival time of shock wave
t_d	Idealized positive phase duration
t_o	Positive phase duration
t_o^-	Negative phase duration
t_1	Thickness of side member
t_2	Thickness of main member
W	Charge weight
y	Displacement
$\dot{y}$	Velocity
$\ddot{y}$	Acceleration
Z	Scaled distance
μ	Ductility
ω	Natural angular frequency
$\varphi(x)$	Shape function
$\dot{\varepsilon}$	Strain rate

Acronym	Definition
ASTM	American Society for Testing and Materials
CLT	Cross laminated timber
CSA	Canadian Standards Association
DIF	Dynamic increase factor
LSL	Laminated strand lumber
LVDT	Linear variable differential transformer
MOE	Modulus of elasticity
MOR	Modulus of rupture
OSB	Oriented strand board
PSL	Parallel strand lumber
SDOF	Single degree-of-freedom
SHPB	Split Hopkinson pressure bar
SIF	Strength increase factor
SPF	Spruce-pine-fir
TDOF	Two degree-of-freedom
UTM	Universal testing machine

CHAPTER 1 – Introduction

1.1 Introduction and research needs

In recent decades, the mitigation of risk to structures and critical infrastructure associated with terrorist attack and accidental explosions has become a topic of interest among researchers and engineers. This rise of interest largely stems from high profile incidents, including intentional attacks (e.g. World Trade Center, 2001; Oklahoma City Bombing, 1995) and accidental explosions (e.g. Texas City refinery explosion, 2005; Ronan Point, 1968; Lac-Mégantic rail disaster, 2013). Understanding a structure's response to blast loading and proper design of the structure is an important step in reducing risk and ensuring the safety of building occupants. To provide designers with information on how to design against blast loading and its effects, several documents and standards have been published around the world (CSA, 2012; DHS, 2011; USACE, 2008; USADD, 2008, 2009).

The majority of research on the topic of blast resistance of structures has focused on reinforced concrete (e.g. Burrell, 2012; Mays et al., 1999; Silva & Lu, 2009; Williams & Williamson, 2011; Yu et al., 2014) and steel structures (e.g. Krishnappa et al., 2014; Nassr et al., 2014; Soroushian & Choi, 1987; Warn & Bruneau, 2009). There has been comparatively little research into the response of wood to blast loading, although some recent research in the area has aimed to change this (e.g. Viau & Doudak, 2016; Poulin et al., 2018; Lacroix & Doudak, 2018).

With recent improvement in wood manufacturing technologies producing more advanced engineered wood products, taller and larger wooden structures are being constructed. In addition, as a renewable building material, wood will likely be utilized more frequently in the future as sustainability and considerations for environmental impact become more important in building design. These factors will result in an increasing number of wood structures, thereby increasing the risk of a wooden structure being subjected to blast loading.

In Canada, the governing blast design standard is that published by the Canadian Standards Association (CSA, 2012). The standard includes design considerations for concrete, masonry, steel, fiber reinforced polymer, and wood materials. The standard specifies strength increase factors (SIF) and dynamic increase factors (DIF) that are to be applied to the static strength of the material. The SIF is a scaling factor applied to material strength which reflects the difference

between the specified strength and the average strength found in installations. The DIF reflects the apparent increase in material strength or stiffness to account for strain rate effects (CSA, 2012). For the design of heavy wood connections, the standard requires the SIF and DIF to be taken as unity. In addition, the connection must fail in a ductile manner and be designed for forces 1.2 times greater than the capacity of the connected members. This approach aims to allow the structural members to reach their full capacity prior to failure in the connections. Assigning no increase factors to the connection capacity can be primarily attributed to the lack of current knowledge on the response of wood connections subjected to blast loading.

Published research on wood subjected to blast loading has primarily focused on overall member behaviour with idealized simply supported boundary conditions (Jacques et al., 2014; Lacroix & Doudak, 2015; Poulin et al., 2018). The inclusion of realistic boundary conditions has been the focus of some studies (e.g. Cote, 2017; Viau, 2016), with the aim of understanding how realistic connections impact the response of the overall assembly being tested. These studies have shown that under blast loading, connections between subsystems have the potential to fail before the members if not detailed properly. While these studies have been instrumental in understanding the behaviour of wood structural assemblies subjected to blast loads and have identified the importance of proper connection design and detailing, there has been no direct contribution to the behaviour of wood connections in isolation under the effects of blast loading. The current study aims to establish a fundamental understanding of the response of bolted wood connections to blast loads. Bolted connections are the most widely used type of connections in heavy timber applications. The focus of the current study is on investigating bolted steel-wood-steel connections with failure in wood crushing (embedment) or in combination of bolt yielding and wood crushing. The study covers cases in both the parallel and perpendicular to the grain directions.

1.2 Bolted wood connection behaviour

The load carrying capacity of dowel-type connectors is typically determined using the European Yield Model. This model was first developed by Johansen (1949) and is based on the assumption that both the embedment strength of the wood and the bending resistance of the fastener exhibit rigid-plastic behaviour. Equations were developed for three distinct failure modes:

- Mode I: wood crushing (embedment) failure with no bending in the fastener,

- Mode II: bending in the fastener with plastic hinges in one member only, accompanied by wood crushing,
- Mode III: bending in the fastener with plastic hinges in each member, accompanied by wood crushing at the member interfaces.

The slenderness of the fastener (ratio of length to diameter) is one of the most important factors to determine which failure mode occurs in the connection. Mode I is obtained when the fastener slenderness is low and the fastener is sufficiently stiff, preventing it from bending. Mode II occurs at intermediate slenderness ratios, while Mode III occurs at high slenderness ratios. An example relationship between slenderness, resistance, and failure mode can be seen in Figure 1.1.

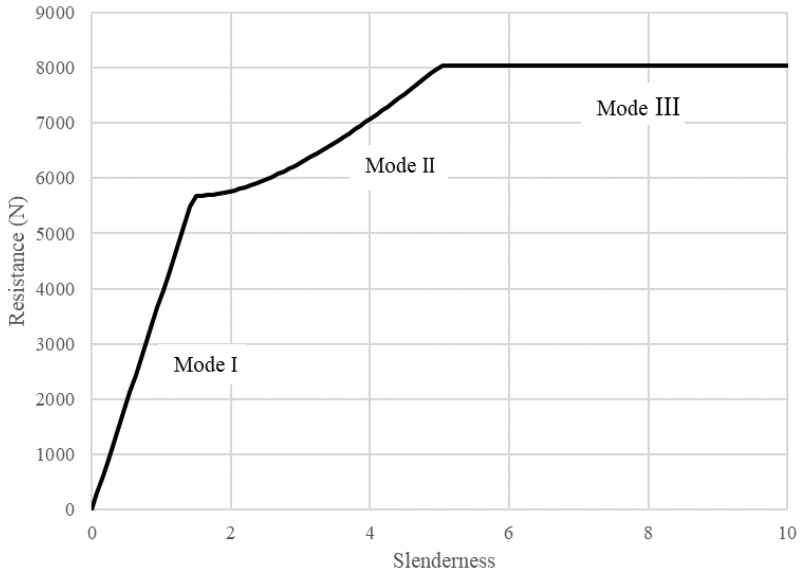

Figure 1.1: Example of a resistance vs. slenderness curve showing different failure modes

The original equations developed by Johansen (1949) were formulated based on the elastic section modulus of the fastener and were limited to symmetric connections between wood members of equal embedment strength. Both two-member and three-member connections were considered. Möller (1950) extended the yield theory to include non-symmetrical two-member connections and connection members of different embedment strengths. Larsen (1979) presented the yielding equations in their general form, based on the full derivation given in (Larsen, 1973). CSA O86 (2014) adopted modified forms of the equations proposed by Larsen (1979) as developed by Whale et al. (1987). The possible failure modes are shown in Figure 1.2. The equations given in CSA

O86 (2014) are presented in Equations 1.1 to 1.10. For a particular connection, the load carrying capacity is taken as the minimum of the applicable equations.

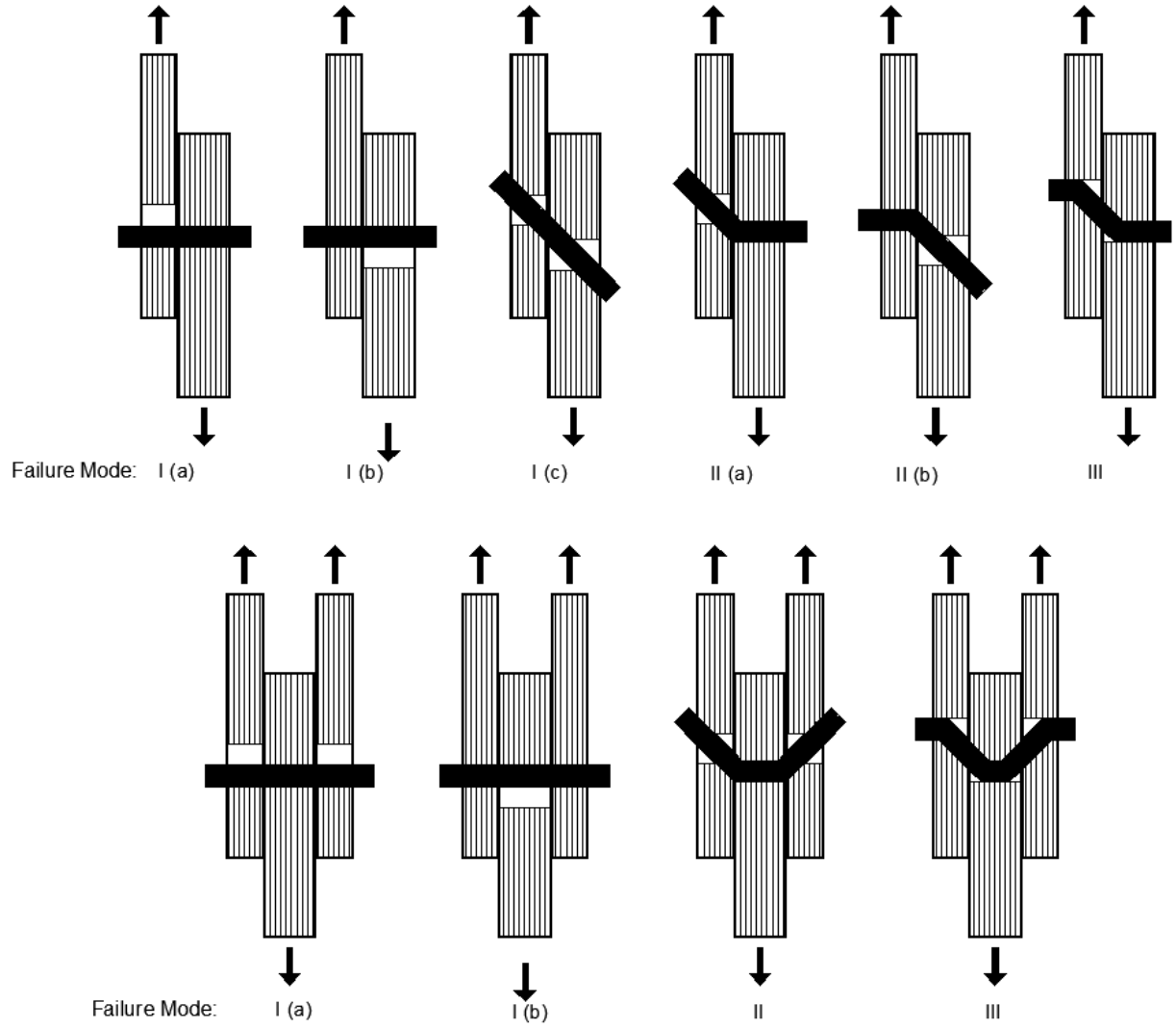

Figure 1.2: Yielding failure modes (CSA, 2014)

For two-member joints:

$$F_y = f_1 d t_1 \qquad \text{Ia} \qquad (1.1)$$

$$F_y = f_2 d t_2 \qquad \text{Ib} \qquad (1.2)$$

$$F_y = f_1 d^2 \frac{1}{5}\left(\frac{t_1}{d} + \frac{f_2}{f_1}\frac{t_2}{d}\right) \qquad \text{Ic} \qquad (1.3)$$

$$F_y = f_1 d^2 \left(\sqrt{\frac{1}{6} \frac{f_2}{(f_1 + f_2)} \frac{f_y}{f_1}} + \frac{1}{5} \frac{t_1}{d} \right) \quad \text{IIa} \quad (1.4)$$

$$F_y = f_1 d^2 \left(\sqrt{\frac{1}{6} \frac{f_2}{(f_1 + f_2)} \frac{f_y}{f_1}} + \frac{1}{5} \frac{t_2}{d} \right) \quad \text{IIb} \quad (1.5)$$

$$F_y = f_1 d^2 \sqrt{\frac{2}{3} \frac{f_2}{(f_1 + f_2)} \frac{f_y}{f_1}} \quad \text{III} \quad (1.6)$$

For three-member joints:

$$F_y = f_1 d t_1 \quad \text{Ia} \quad (1.7)$$

$$F_y = \frac{1}{2} f_2 d t_2 \quad \text{Ib} \quad (1.8)$$

$$F_y = f_1 d^2 \left(\sqrt{\frac{1}{6} \frac{f_2}{(f_1 + f_2)} \frac{f_y}{f_1}} + \frac{1}{5} \frac{t_1}{d} \right) \quad \text{II} \quad (1.9)$$

$$F_y = f_1 d^2 \sqrt{\frac{2}{3} \frac{f_2}{(f_1 + f_2)} \frac{f_y}{f_1}} \quad \text{III} \quad (1.10)$$

Where F_y is the connection strength per shear plane, f_1 and f_2 are the embedment strength of the side and main member respectively, d is the fastener diameter, t_1 and t_2 are the thickness of the side and main member respectively, and f_y is the yield strength of the fastener in bending.

When considering these equations for bolted connections, they neglect the partial rotational restraint imposed by the bolt head and nut, as well as the "rope-effect" in the bolt. The rotational restraint from the bolt head and nut suppresses Mode II failures and makes Mode III failures more dominant. The "rope-effect" occurs after yielding when the bolt bends to the extent where tension in the bolt contributes to the connection capacity. The tension force also creates friction between the connection members and thereby further adds to the capacity of the joint. This effect is typically not considered in design because excessive deformations are required in order to generate the required tension in the bolt. Pre-tension can also be applied to the bolt, but such tension force

cannot be relied upon since it is expected to dissipate in service due to anticipated shrinkage in the wood members.

A brittle failure in the wood around the connection may occur before it reaches its yield load. For parallel to the grain loading this can take the form of row shear, group tear out, or net tension, while for perpendicular to the grain loading splitting is the possible brittle failure mode. Row shear is the failure of a wood plug along a row of bolts. Group tear out is the failure of a wood block around the perimeter of a connection. Net tension is the failure of the member in tension at the net section through the bolt holes. Splitting is the fracture of the wood across connection due to tension perpendicular to the grain stresses. Figure 1.3 depicts these four failure modes. For bolted connections, the Canadian wood design standard (CSA, 2014) accounts for these failure modes through mechanics-based equations. Since brittle failure modes are not permitted in a blast resistant design in accordance with the CSA S850 standard (2012), the connection configurations investigated in the current study were designed and detailed such that brittle failure was not expected to govern. As such, brittle failures modes are deemed outside the scope of the current research project.

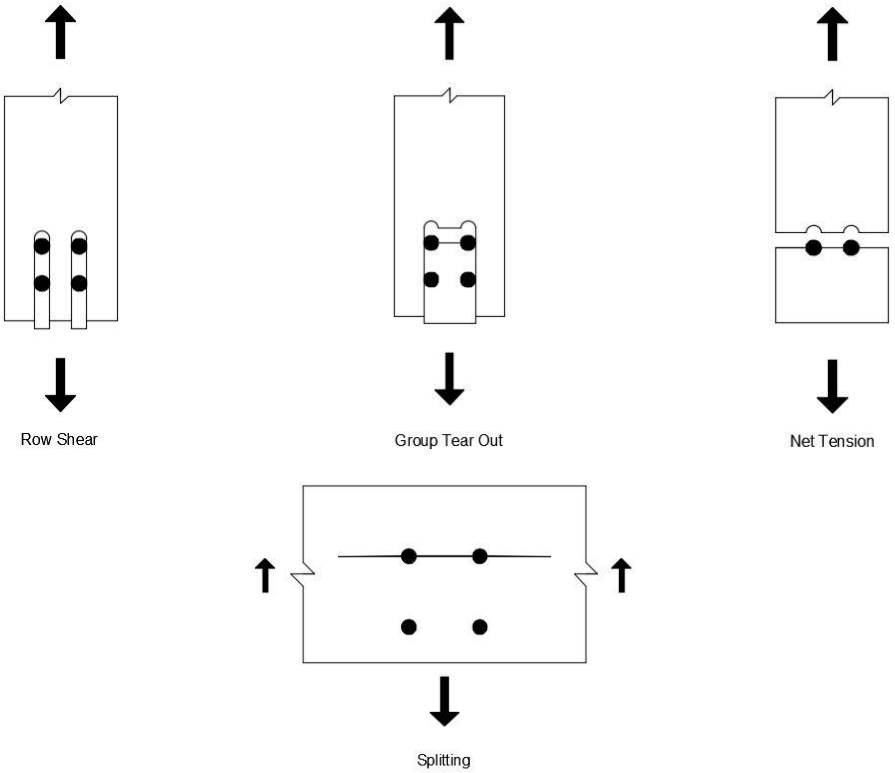

Figure 1.3: Brittle failure modes

1.3 Blast loading

The detonation of high explosives is a burning process occurring at rates exceeding the speed of sound (Krauthammer, 2008). The chemical reaction produces gaseous reaction products that rapidly expand and displace the air surrounding the explosive charge. This displaced air becomes highly compressed, resulting in high pressures and the formation of a shock wave. The shock wave then travels outward from the source of the explosion due to the difference in pressure between the undisturbed air and the high-pressure shock wave. As the shock wave travels away from the explosion source, it will expand in a spherical pattern if unobstructed. This expansion is accompanied by a drop in the pressure of the shock wave because the total energy of the system is constant once the detonation is completed (Cormie et al., 2009).

As the shock wave passes a fixed point there is a near instantaneous rise in pressure followed by a decline back towards ambient pressure; this is known as the positive phase. The positive phase is followed by a further drop in pressure below that of ambient pressure, also known as the negative phase. This drop below ambient pressure is caused by the overexpansion of the air at the shock front, leading to a partial vacuum behind the shock front. Typically, the peak negative pressure is significantly less than the peak positive pressure but lasts for a longer duration. For this reason, the positive phase generally has a much greater impact on structural performance than the negative phase, which is often ignored in design of primary structural elements (Dusenberry, 2010). Ignoring the negative phase may be acceptable if the structural element is designed for multidirectional loading but could be unconservative if the direction of loading is important to the structural response. Figure 1.4 shows a typical pressure-time history diagram.

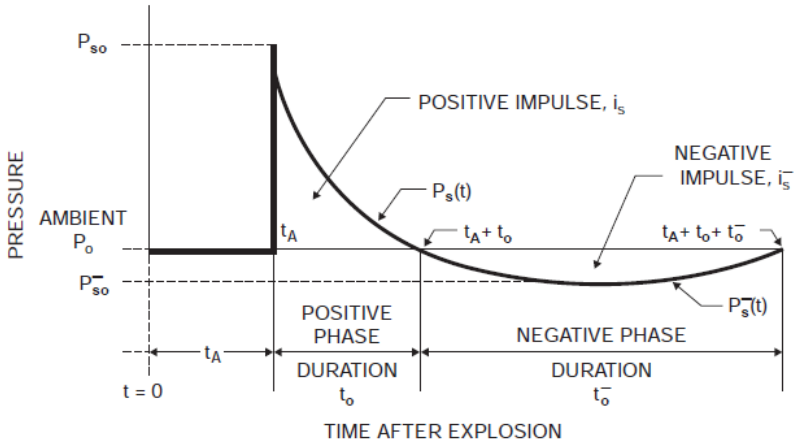

Figure 1.4: Typical pressure-time history of a blast wave (Dusenberry, 2010)

The pressure-time history of a shock wave can be represented by an exponential function such as the Friedlander expression shown in Equation 1.11 (Cormie et al., 2009). For design purposes, approximating the pressure-time history as an instantaneous rise to peak pressure followed by a linear decrease to ambient pressure is often sufficient. The amount of energy in the shock wave is given as the area under the pressure-time history curve; also known as the impulse. There are both positive and negative impulses associated with a shock wave and these are represented by Equations 1.12 & 1.13, respectively.

$$P(t) = P_r\left(1 - \frac{t}{t_d}\right)e^{\frac{-bt}{t_d}} \tag{1.11}$$

$$I^+ = \int_{t_a}^{t_a+t_o} P(t)dt \tag{1.12}$$

$$I^- = \int_{t_a+t_o}^{t_a+t_o+t_o^-} P(t)dt \tag{1.13}$$

Where P_r is the peak reflected pressure, t is the time, t_d is the positive phase duration, and b is the waveform parameter.

A shock wave's interaction with structures can be quite complicated. The shock wave will reflect off surfaces and diffract around objects and through openings. The reflection of the shock wave results in an increase in pressure above the free-air pressure of the shock wave (incident pressure). The amount of increase depends on the angle at which the shock front approaches the structure (Cormie et al., 2009).

The comparison of different charge weights at different distances is an important issue in blast engineering. One concept that allows this comparison is the cube root scaling. A scaled distance, Z, is determined using the standoff distance, R, and charge weight, W, as shown in Equation 1.14. This scaling law requires similar atmospheric conditions, charge geometry, and materials between charges. Two different charge weights at different standoff distances can produce a similar shock wave if they have the same scaled distance (Krauthammer, 2008).

$$Z = \frac{R}{W^{1/3}} \tag{1.14}$$

1.4 Dynamic analysis

Blast events involve the near instantaneous application of a load on a structural element for a short duration. This implies that inertial forces and kinetic energy are both important factors in the analysis of the structure. For this reason, the equivalent static approach that is often used for other dynamic loads (e.g. wind and earthquake) is generally unacceptable for blast loading, and a dynamic analysis approach must be used. Generally, a simplified approach, such as single degree-of-freedom SDOF) modelling, is sufficient to describe the important parameters needed (e.g. displacement). Two degree-of-freedom (TDOF) models may be required if deformations in the supporting structure or connections is expected. This type of modeling is utilised by the USADD's (2008) design guide, because the extra accuracy and effort of more robust modeling techniques, such as finite element, may not be required due to the high degree of uncertainty inherit in determining the blast loading. Single degree-of-freedom analysis

A typical SDOF system used for structural analysis consists of a single point mass connected to a linear spring and viscous damper, subjected to an external force as depicted in Figure 1.5. The equation of motion of the system is described by Equation 1.15.

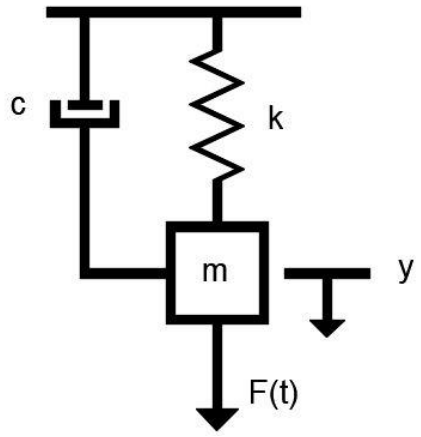

Figure 1.5: Typical damped SDOF system

$$m\ddot{y}(t) + c\dot{y}(t) + ky(t) = F(t) \tag{1.15}$$

Where m is the mass of the system, c is the damping coefficient, k is the stiffness, and F(t) is the forcing function. y, $\dot{y}$, and $\ddot{y}$ represent the unknown values of displacement, velocity, and acceleration, respectively.

In blast engineering, it is common practice to ignore damping, since only the maximum response is desired (Biggs, 1964). If the forcing function can be integrated, a closed-form solution can be developed to the above differential equation. For blast loading, a triangular pulse load is often used as an estimation of the forcing function (Equation 1.16). Using this forcing function, the solution to Equation 1.15 can be expressed as shown in Equation 1.17.

$$F(t) = F_0\left(1 - \frac{t}{t_d}\right) \tag{1.16}$$

$$y = \frac{F_0}{k}(1 - \cos\omega t) + \frac{F_0}{kt_d}\left(\frac{\sin\omega t}{\omega} - t\right) \tag{1.17}$$

$$\omega = \sqrt{\frac{k}{m}} \tag{1.18}$$

Where F_0 is the initial peak load, t_d is the duration of load, and ω is the natural angular frequency of the system in rad/sec, as defined by Equation 1.18.

Closed-form solutions for other forcing functions, both with and without damping, are available throughout the literature (e.g. Biggs, 1964; Paultre, 2011). In general, closed-form solutions are reserved for forcing functions that are mathematically simple. More complex forcing functions may make a closed-form solution unattainable. In these cases, numerical methods can be used to solve the governing differential equation.

A simple linear elastic resistance function was assumed in Equation 1.15, but any resistance-deformation function could be utilised in the model. Selecting a resistance function that accurately represents the behaviour of the material being modeled is crucial to the model's performance.

1.4.1 Equivalent SDOF analysis

A SDOF system assumes the mass, loads, and resistance of the system are all concentrated at a single point. This prevents SDOF models from being directly used to represent structural elements because they have distributed mass and loading, and the displacement varies along the length of the element. In order to use SDOF analysis on real structural elements the mass, loading and resistance must be transformed into an equivalent SDOF system. To perform this transformation, a point of interest is selected (e.g. mid-span of a beam) where the mass and resistance of the structural element and the applied forces are considered to act. Transformation factors are then

applied on the mass, resistance and forces of the real system. These factors depend on the deformed shape of the element, which is typically taken as the static deformed shape (Biggs, 1964). The equivalent system preserves the time scale of the real system, such that any deformation in the equivalent SDOF system is always the same as the deformation at the selected point of interest of the structural element throughout the displacement-time history. The equation of motion for the equivalent SDOF is shown in Equation 1.19, where K_M is the mass transformation factor, K_R is the resistance transformation factor, K_L is the load transformation factor, and R(y) is the member resistance function.

$$K_M m\ddot{y}(t) + K_R R(y) = K_L F(t) \tag{1.19}$$

The mass transformation factor, K_M, is determined by equating the kinetic energy of the real system to that of the equivalent SDOF (Biggs, 1964). This results in Equation 1.20 or 1.21 for a system with continuous or concentrated mass, respectively.

$$K_M = \frac{\int_0^L \bar{m}(x)\varphi^2(x)dx}{\int_0^L \bar{m}(x)dx} \tag{1.20}$$

$$K_M = \frac{\sum_{r=1}^{i} m_r \varphi_r^2}{\sum_{r=1}^{i} m_r} \tag{1.21}$$

Where $\bar{m}(x)$ is the mass per unit length, $\varphi(x)$ is the assumed shape function of the element, m_r is the r^{th} mass and i is the number of concentrated masses.

In general, the load factor, K_L, is equal to the resistance factor, K_R, because the resistance is the internal forces and typically have a similar distribution as the applied load (USADD, 2008). K_L is determined by equating the work done by the external forces on the real system to that of the equivalent SDOF. This results in Equation 1.22 or 1.23 for a system with continuous or concentrated mass, respectively.

$$K_L = \frac{\int_0^L F(x,t)\varphi(x)dx}{\int_0^L F(x,t)dx} \tag{1.22}$$

$$K_L = \frac{\sum_{r=1}^{i} F_r \varphi_r}{\sum_{r=1}^{i} F_r} \tag{1.23}$$

Where F(x,t) is the distributed load per unit length as a function of time, F_r is the r^{th} concentrated load, and i is the number of concentrated loads.

A single factor, termed the load-mass factor (K_{LM}), can be defined as the ratio between the load factor and the mass factor (Equation 1.24). The use of this single factor simplifies the equation of motion for the equivalent SDOF system to Equation 1.25. Transformation factors are available in the literature for a variety of different structures subjected to different loading and boundary conditions (Biggs, 1964).

$$K_{LM} = \frac{K_M}{K_L} \tag{1.24}$$

$$K_{LM} m \ddot{y}(t) + R(y) = F(t) \tag{1.25}$$

1.4.2 Two degree-of-freedom analysis

Equivalent single degree-of-freedom models may not be adequate to describe systems where, for example, different failure modes are expected. For example, a flexural member where the effect of the connections is to be included may require a two degree-of-freedom model with a degree-of-freedom for the flexural member and another for the connection. A typical TDOF system is depicted in Figure 1.6 and consists of two point masses, two springs and an externally applied load. The equation of motion for the first and second degree-of-freedom are presented in Equations 1.26 and 1.27, respectively. Where m is the mass, R is the resistance, and F(t) is the forcing function. y and $\ddot{y}$ represent the unknown values of displacement, and acceleration of the mass respectively. Subscripts 1 and 2 identify if the variable is referring to the first or second degree-of-freedom, respectively. These equations need to be solved simultaneously to reach a solution.

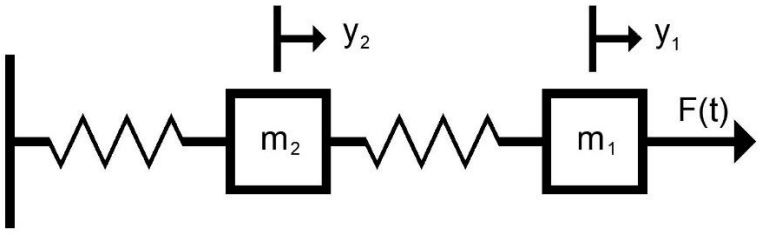

Figure 1.6: Typical TDOF system

$$m_1 \ddot{y_1}(t) + R_1(y_1(t) - y_2(t)) = F(t) \tag{1.26}$$

$$m_2 \ddot{y_2}(t) + R_2\big(y_2(t)\big) - R_1(y_1(t) - y_2(t)) = 0 \tag{1.27}$$

1.5 Research objectives

The main objective of this research project is to investigate the response of steel-wood-steel bolted connections when subjected to blast loads. More precisely, the goals of this project are to investigate:

1. the ability of a shock tube used in conjunction with a load transfer device and support frame to produce high deformation rate response in wood connections;
2. static and dynamic connection response to determine the dynamic increase in resistance and stiffness for two main cases, namely: stocky bolts leading to wood crushing failure and slender bolts with bolt yielding failure. The behaviour is investigated in both the parallel and perpendicular to grain directions;
3. the ability of self-tapping screws to reinforce wood connections subjected to dynamic load;
4. the ability of simplified analytical solutions to predict the behaviour of structural members with connections;

1.6 Scope

The above stated objectives are achieved through the following courses of action:

- Carry out a detailed literature review on the behaviour of wood, and specifically wood connections, subjected to high strain rates;
- Conduct static and dynamic tests on 35 single bolt steel-wood-steel connections loaded in the parallel or perpendicular to grain direction, using stocky or slender bolts;
- Conduct static bending tests on bolt fasteners to characterize material behaviour;
- Analyze the experimental results to determine the dynamic increase in resistance and stiffness for the connection configurations studied;
- Model the connection and support frame system to establish the joint behaviour;
- Model beam-connections assemblies to extend knowledge obtained at joint level, and;
- Discuss the results and code implications regarding design of wood connections subjected to blast loading.

1.7 Structure of thesis

Chapter 1 introduces the topics of blast loading, wood connections, dynamic analysis, and presents the research needs and objectives.

Chapter 2 provides a detailed literature review of studies related to the behaviour of wood and wood connections subjected to blast and impact loads.

Chapter 3 presents a detailed description of the experimental setup and methodology employed in this research project.

Chapter 4 presents the experimental program results, including the bolt bending tests, static and dynamic connection tests for the four connection configurations.

Chapter 5 presents the analytical modelling techniques utilized including single degree-of-freedom modelling of the support frame, and two degree-of-freedom modelling of the connection-support frame system.

Chapter 6 discusses the experimental and analytical results. This includes the dynamic increase in resistance and stiffness, the post yielding behaviour of the connections, the effects of reinforcing on connection behaviour, and the effects of different grain directions and failure modes. Analytical modelling of beam-connections assemblies is also presented, and the implications of the results on the blast standard are discussed.

Chapter 7 summarizes key findings and proposes potential future work

Appendix A and B present details about the test results and analysis for all specimens tested under static and dynamic loading, respectively.

CHAPTER 2 – Literature Review

2.1 Wood subjected to high strain rates

2.1.1 Wood subjected to impact loading

Markwardt & Liska (1956) investigated the effect of loading rate on the compression and flexure strength of small clear wood samples. All compression tests were undertaken using a mechanical-type testing machine, while the flexure tests were conducted on a hydraulic controlled testing machine. Multiple loading rates were investigated. The time to failure in the fastest tests for both compression and flexure was approximately 1 s, while in the control tests the time to failure varied from 300 s to 700 s. The authors compared the ultimate strengths from the rapid tests to that of the control tests and found approximately an 8% increase in the ultimate strength for a tenfold increase in rate of loading for both the compression and the flexure tests.

Nadeau et al. (1982) investigated the rate-of-loading effect on the strength of clear Douglas Fir wood using a servo-hydraulic machine. Of particular interest was the effects of the test sample relative strength (i.e. comparing the top percentile and the bottom percentile results). To investigate this, half of the specimens were intentionally notched on the tension side to promote flexural failure and represent members with defects. The notched specimens were tested at strain rates between $3.2 \times 10^{-7} – 8.4 \times 10^{-3}$ s^{-1} while the unnotched specimens were tested between $3.2 \times 10^{-7} – 6.5 \times 10^{-2}$ s^{-1}. For the unnotched specimens an increase in ultimate strength of 30% was observed when comparing the lowest to the highest strain rate. For the notched specimens no correlation between ultimate strength and rate-of-loading was observed. This is in agreement with Spencer (1978) who found that at the 95^{th} percentile of strength the rate-of-loading effect was present, but this effect was absent for specimens at the 5^{th} percentile. The authors attributed this difference in rate-of-loading effect to the fact that weaker specimens, having larger cracks, are less influenced by a small amount of subcritical crack growth, while stronger specimens, having small initial cracks, will be influenced more by the growth of subcritical cracks. The subcritical cracks require time to grow and therefore at high strain rates they do not have sufficient time to grow and deteriorate the ultimate strength of the stronger specimens.

The stress rate sensitivity of the bending strength of parallel strand lumber (PSL) beams was investigated by Sukontasukkul et al. (2000). Eighteen 100 mm x 100 mm x 650 mm PSL beams were tested; six under static load, and twelve under impact load using a drop hammer apparatus.

Two different drop heights were used; 500 and 1000 mm. The tests had a relatively short clear span of 550 mm, which resulted in a mixed shear and flexural failure mode. For the impact tests, the true bending load was taken as the measured load between the drop hammer and the beam minus the generalised inertial load, which was determined based on the measured acceleration of the beam. It was found that the bending strength increased by approximately 30% from the static to the impact tests.

The strain rate dependant behaviour of two different grades of laminated strand lumber (LSL) was studied by (Syron, 2008). Testing was completed at strain rates of 1×10^{-5}, 1×10^{-3}, and 0.1 s^{-1}. The strength and modulus of elasticity were evaluated in both the longitudinal and transverse direction for compression and in the longitudinal direction for tension. The longitudinal compressive strength of the LSL increased by 37% and 31%, while the transverse compressive strength increased by 41% and 16% for the 1.35E and 1.75E grade, respectively. No statistically significant increase in the longitudinal modulus of elasticity was observed for the 1.35E grade, while an increase of 16% was noted for the 1.75E grade. The transverse modulus of elasticity increased by 28% and 18% for the 1.35E and 1.75E grade, respectively. There were no significant strain rate effects observed for the LSL in tension.

Widehammar (2004) studied effects of strain rate and moisture content on the crushing behaviour of spruce wood. Three different strain rates were investigated 8×10^{-3}, 17, and 1000 s^{-1}. The two slower tests were conducted using a displacement-controlled servo-hydraulic testing machine. The faster tests were performed using split Hopkinson pressure bar (SHPB). In addition, three different moisture contents were studied; oven dry, fiber saturated, and fully saturated. The specimens measured 12 mm x 12 mm by 6 mm in length and were all cut from the same tree. The crushing behaviour was studied in the three principal directions, i.e. radially, tangentially and axially. For all sets of tests, it was found that there was an increase in crushing strength with an increase in strain rate. The relative increase over static tests was not directly quantified by the author, but it was shown to vary over the three moisture contents and the three loading directions tested.

High strain rate compression tests were conducted on small pine and maple specimens using a SHPB apparatus. The specimens tested were cylindrical with a diameter of 63.5 mm and a height of 38 mm. Tests were conducted across a variety of strain rates between 69 and 337 s^{-1}. A significant difference in material properties was observed over this range of strain rates. At

increased strain rates, the time to ultimate stress decreased, the modulus of elasticity increased, and so did the compressive strength and the maximum strain. The ultimate compressive stress was compared to the static strength of the material (7.5 min duration) and a DIF between 1.9 and 2.4 was obtained (Gilbertson & Bulleit, 2013).

2.1.2 Wood structural elements subjected to blast loading

Jacques et al. (2014) studied the dynamic bending response of stud grade spruce-pine-fir (SPF) lumber using simulated blast loading generated by a shock tube. The goal of the research was to determine the DIF for the modulus of rupture (MOR), the modulus of elasticity (MOE) and the strain at failure. For the strain rate range of 0.1 to 0.4 s^{-1}, a statistically significant average DIF on the MOR of 1.41 was observed. There was an increase in the MOE and strain at rupture, but due to the high variability and relatively small sample size it could not be considered statistically significant.

The dynamic flexural response of full-scale light frame stud walls was investigated using the University of Ottawa's shock tube and compared to static test results (Lacroix & Doudak, 2015). The objective of the study was to determine a DIF for both the flexural resistance and stiffness of the walls. Ten walls were tested under static loading and ten walls were subjected to simulated blast loading. Simply supported boundary conditions were used to ensure that flexural failure was achieved. Under static loading the studs failed in a splintering tension manner, while under dynamic loading the failure mode switched to a brash tension failure. This was attributed to the high rate of loading not providing enough time for the splintering failure to develop. Strain rates of 0.12 - 0.55 s^{-1} were achieved in the dynamic tests. Average DIFs of 1.40 and 1.18 were found on the resistance and stiffness, respectively. The results from this study were combined with past results to derive an equation relating the dynamic increase factor (DIF) on the resistance to strain rate. The proposed equation is presented in Equation 2.1 where $\dot{\varepsilon}$ is the strain rate. Figure 2.1 presents the data that was utilized in deriving Equation 2.1.

$$DIF = 1.46 + 0.1 \log_{10} \dot{\varepsilon} \tag{2.1}$$

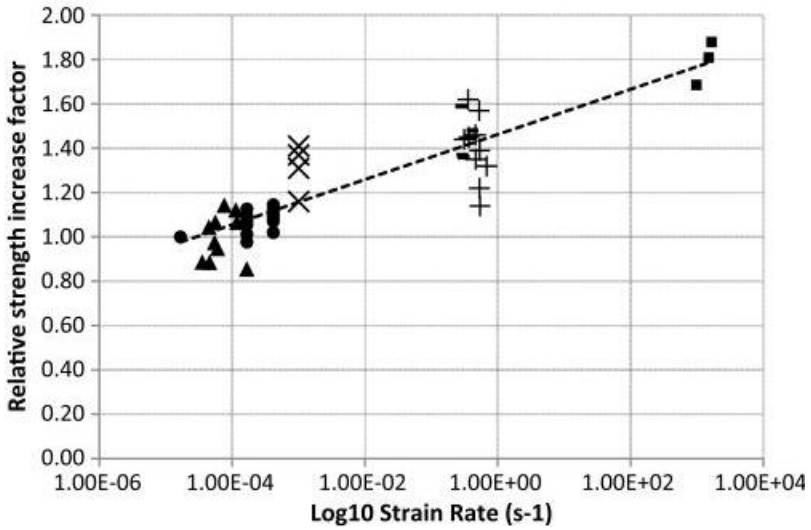

Figure 2.1: Relative increase in strength compared to strain rates (Lacroix & Doudak, 2015)

Viau & Doudak (2016a) investigated the flexural response of full-scale wood stud walls subjected to blast loading that produced severe damage levels. Sixteen wood stud walls were tested with different sheathing configurations including 11 mm thick oriented strand board (OSB), and 18.5 mm plywood. It was found that the 11 mm OSB sheathing was inadequate in transferring enough pressure to fail the wall studs and generated significant flying debris. The 18.5 mm plywood sheathing could transfer enough pressure to the studs to initiate flexural failure in them. Welded wire mesh was installed on some of the walls either as a catcher system or as reinforcement for the sheathing and it was found to be successful in both applications.

Lacroix & Doudak (2018a) performed a series of dynamic and static tests on simply supported glulam beams. The aim of the research program was to determine the DIF for the glulam beams. It was observed that the presence of a finger joint through the entire width of the member in the high moment region of the beam had a detrimental effect on its dynamic performance. For beams without this defect, a statistically significant DIF of 1.14 on the MOR was observed. When this defect was present a dynamic increase in strength was not observed. No statistically significant increase was observed in beam stiffness (MOE). SDOF modeling with a linear elastic resistance curve was shown to adequately capture the dynamic response of the simply supported glulam beams subjected to dynamic loading. As part of the same research program, Lacroix & Doudak (2018b) investigated the effects of axial load on the dynamic response of glulam structural members subjected to combined lateral-blast and axial loading and developed a material predictive model to capture these effects. In addition, Lacroix & Doudak (2018c) investigated the potential

of fiber-reinforced polymers as a strengthening option for glulam beams subjected to simulated blast loads.

The behaviour of cross laminated timber (CLT) panels subjected to simulated blast loading was investigated by Poulin, et al. (2018). A total of twelve panels were tested dynamically and six were tested under static loading. For the resistance, an average DIF of 1.28 was observed for strain rates between 0.119 and 0.213 s^{-1}. There was no observed DIF on the panel's stiffness. The failure mode under static loading was initially flexural failure with rolling shear present at or following the peak response. Under dynamic loading, the failure mode was rolling shear for five specimens and flexural failure for seven specimens. Two models were developed to account for the two failure modes observed. Comparisons between the proposed models and test results showed reasonable accuracy.

2.1.3 Wood connections subjected to high strain rates

The rate-of-loading effect on nailed wood connections was investigated in an experimental program (Girhammar & Andersson, 1988). Six different loading rates were tested, with the slowest being static loading at 2 mm/min and the fastest being 1,250 mm/s. The connections consisted of three-members connected with four nails in single shear (two driven from each side). Plastic shims were placed between the wood members to reduce the friction, and the nails were not fully driven in to the side members to prevent the nail head from influencing the load carrying capacity. Connections were designed to fail in either wood crushing or combined nail yielding and wood crushing. Both parallel and perpendicular to the grain tests were performed for each joint configuration and testing speed. The ultimate load capacity of the yielding connection tests increased as the loading rate increased. The increase in strength obtained for the fastest dynamic test relative to the static tests were 1.33 and 1.38 for the parallel and perpendicular to the grain tests, respectively. At the fastest loading rates both sets of yielding connection tests had reduced ductility when compared to other loading rates. The DIF for the embedment tests were 1.58 and 1.43 for the parallel and perpendicular to the grain tests, respectively. The ductility of these tests was not dependant on the loading rate. In addition to the connection tests, bearing tests and nail bending tests were performed at the six different loading rates. The bearing tests showed a DIF of 1.50 and 1.22 for parallel and perpendicular to the grain respectively; while the nail bending tests had a DIF of 1.19.

Rosowsky & Reinhold (1999) performed lateral testing and withdrawal testing at a variety of different loading rates on nailed and screwed connections. For the withdrawal tests, the nails/screws were installed into dimensioned lumber and the heads were left protruding approximately 13 mm. Load was applied directly to the fasteners using grips. Time for fastener withdrawal varied from about 0.1 – 10 s. Lateral loading test specimens consisted of plywood nailed to dimensioned lumber. Displacement rates ranging from 0.25 to 25,000 mm/min were tested. An air cylinder had to be utilized to produce the highest loading rate. Overall, no rate-of-loading effects were observed for nails or screws loaded laterally or in withdrawal.

Light-frame wood stud walls with realistic boundary conditions were tested under simulated blast loading through the use of a shock tube (Viau & Doudak, 2016b). Several different connection types were investigated including: typical nailed connections based on prescriptive requirements, two different joist hangers, twist straps, and angle brackets. The prescriptive connections proved to be inadequate for the out of plane blast loads and failed before the studs could reach their ultimate flexural capacity. The premature failure of these connections caused the entire wall to become a projectile and fly across the laboratory. This type of connection is intended to resist gravity and in-plane shear loads and is not optimised for out of plane loads. The two joist hanger connections and the angle brackets provided enough resistance for the studs to reach their ultimate resistance and performed significantly better than the prescriptive connections. The twist strap connection performed poorly and failed in strap rupturing or stud splitting at the connection. The authors also investigated the validity of using a SDOF model to predict the behaviour of stud walls with realistic boundary conditions. The model gave accurate predictions for the joist hanger connections because they behaved similar to simple supports and did not add significant rotational restraint or energy dissipation. For the angle bracket connections, there was energy dissipation at the connections that could not be accounted for in the simple SDOF model. This caused the model to over predict displacement. The model was also unable to account for the different failure mode introduced by the twist straps.

Côté & Doudak (2019) investigated the behaviour of CLT panels with realistic boundary conditions subjected to simulated blast loads. End grain connections, typically used to resist gravity loads, were tested to determine if typical connections have any inherent blast resistance. These connections performed poorly and resulted in brittle splitting failures; not allowing the panel

to reach its ultimate strength. Even when the connections were reinforced to prevent tension perpendicular to the grain failure, splitting was still evident. Tests on angled, double threaded screws also showed unfavourable behaviour and did not provide the ductility desired for out of plane blast loads. Bearing type connections proved most favourable for resisting blast loads. This type of connection does not create any tension perpendicular to the grain splitting failures. Three different bearing connections were tested: thin angle brackets, stiff angle brackets, and balloon construction. The thin angle brackets provided large amounts of energy dissipation through the steel yielding and wood crushing. This type of connection is suitable for blast loading, provided it has enough ductility to absorb the energy of the blast wave. SDOF modeling with the assumption of simply supported boundary conditions was shown to be unable to accurately predict the performance of CLT panels with realistic connections.

2.2 Steel subjected to high strain rates

Wood connections with mechanical fasteners often deform in such a way that the fastener is engaged in bending. In order to understand the response of such connections to blast loading, the dynamic material properties of the fasteners are needed. Most commonly, these fasteners are made from steel. In general, both the yield and ultimate tensile strength of steel increases with an increase in strain rate, although, the magnitude of increase is greater for the yield strength. The modulus of elasticity is not sensitive to the strain rate (USADD, 2008). For blast loading, the Canadian blast design standard (CSA, 2012) assigns a DIF of 1.2 for the flexural yield strength of 350W steel subjected to a far field explosion. Bolted wood connections typically utilize ASTM A307 bolts (ASTM, 2014) that have a minimum tensile strength of 413 MPa. With a strength similar to 350W steel, a DIF of 1.2 for ASTM A307 bolt's yield strength is reasonable.

2.3 Summary

This chapter presented an overview of the knowledge base surrounding wood elements and connections subjected to dynamic short-term loading. The majority of research shows the strength of wood increasing with the rate of loading. It has also been shown that there are significant differences between the rate-of-loading effects for clear wood and for wood with defects. This leads to the conclusion that test results from small clear wood specimens are not be representative of the behaviour of in grade wood members. High strain rate tests have been performed in tension,

and compression parallel to the grain, as well as in compression perpendicular to the grain directions, with different dynamic increases in strength being observed in each loading direction.

Some of the testing of wood at high strain-rates has been conducted using the split Hopkins pressure bar technique. This test method produces strain rates that are several orders of magnitude greater than what is observed in impact or blast loading, therefore the observed dynamic properties cannot be directly applied to blast design, but these tests can give insight into the general trends of how wood's mechanical properties are affected by strain-rate.

Dynamic shock tube testing on dimensioned lumber, light frame stud walls, glulam and CLT have all shown a dynamic increase in strength at the strain rates associated with blast loading. Studies of light frame stud walls and CLT walls with realistic boundary conditions revealed that the type of connections and detailing play a significant role in the performance of the wall systems when subjected to blast loading. Typical connection details used to resist gravity and in plane shear loads were shown to cause premature failure of the wall system and were deemed inadequate for out of plane blast loads. While these studies highlighted the need to understand the behaviour of wood connections subjected to blast loading, little progress has been made to quantify the behaviour of the connections themselves under high rates of loading. Research into the rate of loading effects on nailed connections has been undertaken but no effort has been made to establish the performance of bolted connections subjected to blast loading.

The current study is the first of its kind to investigate the behaviour of bolted connections under static and simulated blast loading. Characteristics of various parameters under static and dynamic loading are investigated, and implications on analysis techniques and design approached are presented and discussed.

CHAPTER 3 – Experimental Program

3.1 General

A total of thirty-five single bolt steel-wood-steel connections were tested under static or dynamic loading. Connections were designed to fail either in wood crushing (Failure Mode I) or a combination of bolt bending and wood crushing (Failure Mode III). Each failure mode was investigated both parallel and perpendicular to the wood grain. All connection tests consisted of two steel side plates, a wood member and a steel bolt connecting the side plates to the member. Steel was used as the side plates because this is the most typical configuration. Each test utilised the same two 152 mm x 76 mm x 6.4 mm ASTM A500 Grade B hollow steel sections as the side plates. The nomenclature of the specimens is such that the first letter (E or Y) refers to failure mode (Mode I (crushing) or Mode III (yielding)), the first number (0 or 90) refers to loading direction relative to the wood grain (parallel or perpendicular), the second letter (S or D) refers to the type of loading (static or dynamic), and the last number in square brackets indicates the specimen number. For example, E90S[3] is the static test involving the third specimen that failed in Mode I in the perpendicular to the grain direction.

Connections designed to fail in failure Mode I consisted of a 25.4 mm ASTM A307 Grade A hex bolt and an 86 x 178 mm 24f-ES Spruce-Pine glulam wood member. This provided a length to diameter aspect ratio for the bolt of 3.4. All wood specimens were 356 mm in length (14 times the diameter of the bolt). For the parallel to the grain tests, both edge distances were 89 mm, and the loaded and unloaded end distances were 178 mm. For the perpendicular to the grain tests, the loaded edge distance was 127 mm, the unloaded edge distance was 51 mm, and both end distances were 178 mm. Figures 3.1 and 3.2 show the dimensions of the parallel and perpendicular to the grain specimens, respectively. The 25.4 mm bolt used for these connections can be seen in Figure 3.3.

Connections designed to fail in failure Mode III consisted of a 12.7 mm ASTM A307 Grade A hex bolt and a 137 x 178 mm 24f-ES Spruce-Pine glulam wood member. This provided a length to diameter aspect ratio for the bolt of 10.8. All specimens were 178 mm in length (14 times the diameter of the bolt). For the parallel to the grain tests, both edge distances and the loaded and unloaded end distances were 89 mm. For the perpendicular to the grain tests the loaded edge distance was 127 mm, the unloaded edge distance was 51 mm, and both end distances were 89

mm. Figures 3.4 and 3.5 show the dimensions for the parallel and perpendicular to the grain specimens, respectively. The 12.7 mm bolt used for these connections can be seen in Figure 3.6.

The edge and end distances for all four connection configurations were selected to meet the minimum dimensions required by ASTM D5652 Standard Test Methods for Single-Bolt Connections in Wood and Wood-Based Products (ASTM, 2015).

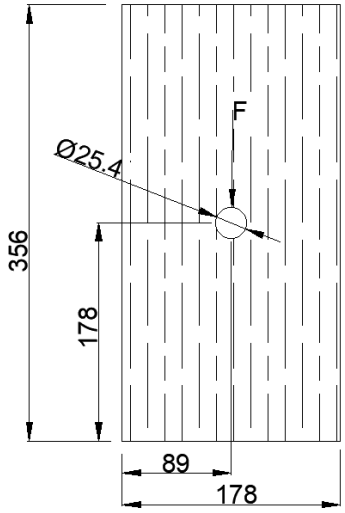

Figure 3.1: Parallel to the grain specimen designed to fail in Mode I (dimensions in mm)

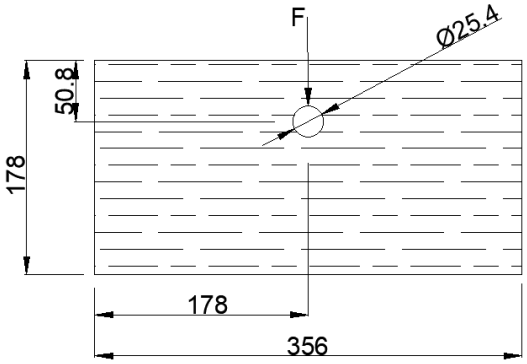

Figure 3.2: Perpendicular to the grain specimen designed to fail in Mode I (dimensions in mm)

Figure 3.3: 25.4 mm ASTM A307 Grade A hex bolt

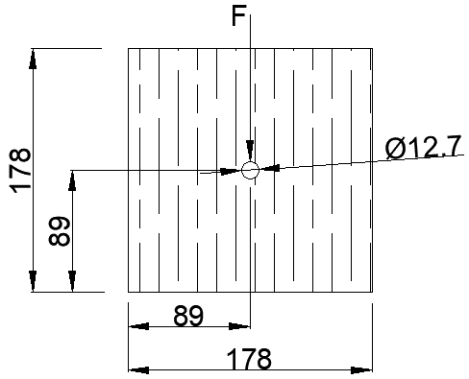

Figure 3.4: Parallel to the grain specimen designed to fail in Mode III (dimensions in mm)

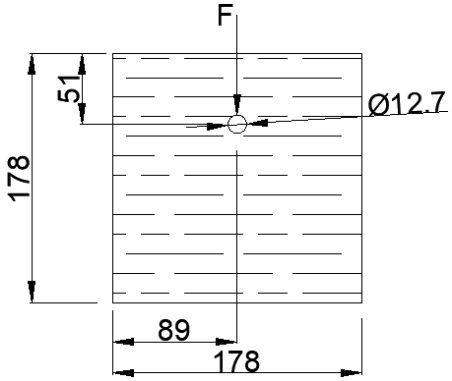

Figure 3.5: Perpendicular to the grain specimen designed to fail in Mode III (dimensions in mm)

Figure 3.6: 12.7 mm ASTM A307 Grade A hex bolt

Fourteen connections were tested under static loading to establish the load-displacement behaviour of the connections including yield point, stiffness, ultimate strength, failure displacement, and ductility. Twenty-one connections were tested under dynamic loading. Table 3.1 shows the test matrix, which summarises the connection failure mode, grain direction, loading type and whether the connection was retrofitted with self-tapping screws.

To investigate the ability of self-tapping screws to reinforce a connection, a total of seven parallel to the grain dynamic specimens were reinforced with 8x120 mm Heco-Topix screws. The screws were not expected to affect the yield strength or stiffness of the connection but were used to improve their post peak performance. Four of those specimens were designed to fail in Mode I and three in Mode III. The screws were driven perpendicular to the load direction to reinforce the splitting perpendicular to the grain failure mode. In the loaded portion of the specimen (in front of the bolt), the maximum number of screws based on the manufacture's recommended spacing and edge distances was used. This was done to provide the maximum resistance to splitting in order to investigate the effectiveness of this form of reinforcement. In the unloaded portion of the specimen (behind the bolt), an additional two screws were used. Figure 3.7 shows the screw used for the reinforcement while Figures 3.8 and 3.9 show the reinforcement pattern of the connections designed to fail in Mode I and Mode III, respectively.

Figure 3.7: 8x120 mm Heco-Topix self-tapping screw

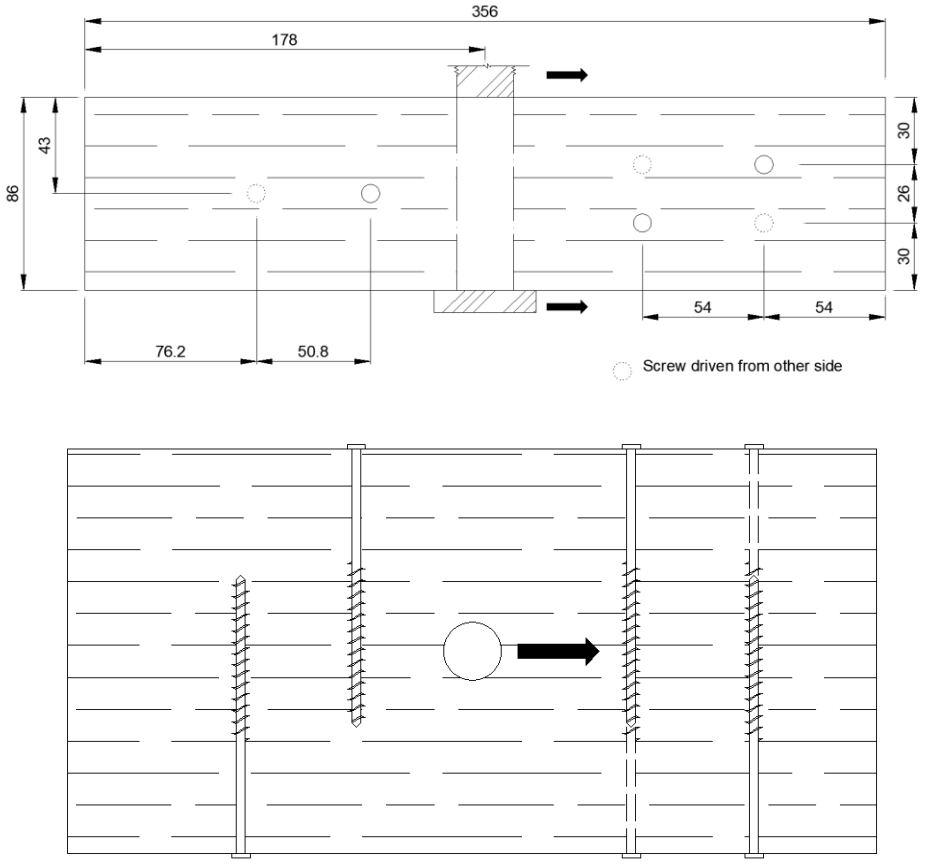

Figure 3.8: Screw reinforcement pattern for connections designed to fail in Mode I

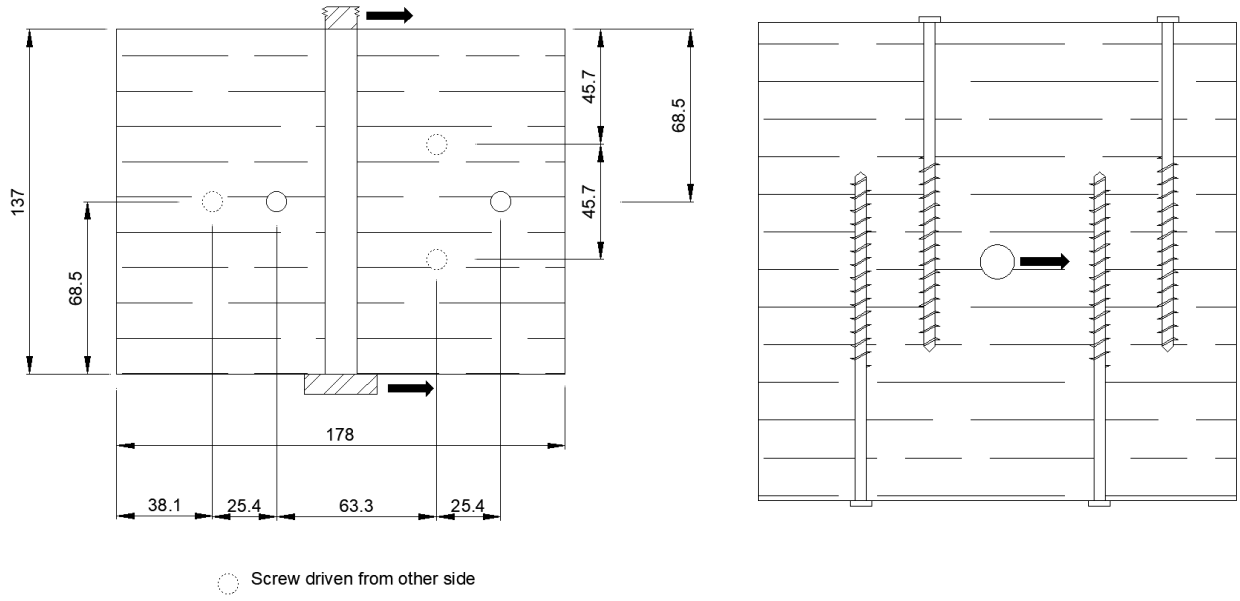

Figure 3.9: Screw reinforcement pattern for connections designed to fail in Mode III

Table 3.1: Test matrix

Connection Failure Mode	Grain Direction	Loading Type	Retrofitted	Specimens
Mode I	Parallel	Static	No	E0S[1] – [5]
Mode I	Perpendicular	Static	No	E90S[1] – [3]
Mode III	Parallel	Static	No	Y0S[1] – [3]
Mode III	Perpendicular	Static	No	Y90S[1] – [3]
Mode I	Parallel	Dynamic	No	E0D[1] – [5]
Mode I	Perpendicular	Dynamic	No	E90D[1] – [3]
Mode III	Parallel	Dynamic	No	Y0D[1] – [3]
Mode III	Perpendicular	Dynamic	No	Y90D[1] – [3]
Mode I	Parallel	Dynamic	Yes	E0D[6] – [9]
Mode III	Parallel	Dynamic	Yes	Y0D[3] – [6]

3.2 Bolt bending tests

Three-point bending tests were performed on the slender 12.7 mm ASTM A307 Grade A hex bolts to characterize their material behaviour. These tests were conducted in accordance with the ASTM F1575 – 17: Standard Test Method for Determining Bending Yield Moment of Nails (ASTM, 2017). The standard specifies that for diameters larger than 4.8 mm a span to diameter ratio of 11.5 shall be used. This allows the standard to be applicable to bolts as well. Tests were performed in a universal testing machine (UTM). The distance between supports was set as 146 mm to meet the required span to diameter ratio of 11.5. A constant loading rate of 2 mm/min was used. A point load was applied at the mid span of the bolt, with roller supports on either end. Figure 3.10 shows the bolt bending test setup. Tests were conducted until the bolts reached a bending angle of 45°.

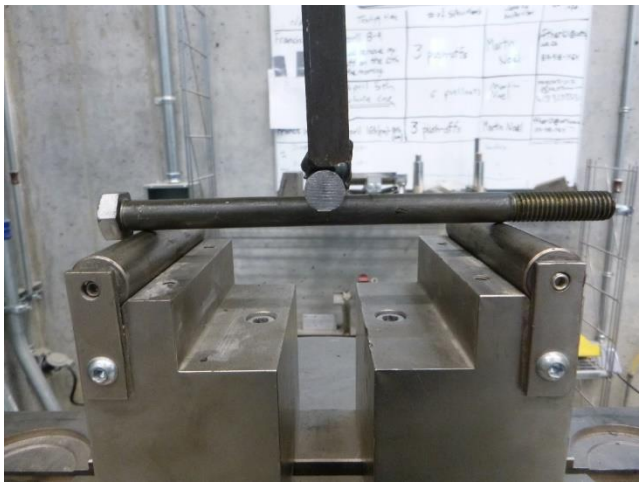

Figure 3.10: Typical bolt bending test setup

3.3 Static connection testing

Testing was performed in a UTM according to ASTM D5652 Standard Test Methods for Single-Bolt Connections in Wood and Wood-Based Products (ASTM, 2015). The specimens were fully supported along their bottom edge to avoid the brittle failure modes such as row shear and net tension (in the parallel to grain direction) and splitting (in the perpendicular to grain direction). The side plates were brought into contact with the wood member by tightening the bolt. The bolt's nut was then slightly loosened and retightened to "finger tightness" as per the procedure in ASTM D5652. A steel rod was used to connect the two side plates to maintain their alignment throughout the test. All tests were deformation controlled at a constant rate of 2 mm/min. An example of each testing configuration can be seen in Figure 3.11.

(a) Mode 1 parallel to the grain

(b) Mode I perpendicular to the grain

(c) Mode III parallel to the grain

(d) Mode III perpendicular to the grain

Figure 3.11: Typical static test setups

3.4 Dynamic connection testing

This section describes the University of Ottawa's shock tube, which was used to simulate blast loading conditions. The test setup and experimental methodology are also described in detail.

3.4.1 Description of the shock tube

The shock tube is used to produce shock waves similar to those created by the far-field detonation of high-explosives through the rapid release of compressed air. The shock tube consists of three main sections: the driver section, diaphragm section, and expansion section, as seen in Figure 3.12.

Sheets of aluminum foil are used to separate the three sections. The number and thickness of the foils are determined based on the desired driver pressure. The length of the driver section can be varied from 305 to 5185 mm. This, in combination with the ability to vary the driver pressure, allows the shock wave parameters of reflected pressure and impulse to be varied and selected for each test. The shock tube is capable of producing reflected pressures up to 100 kPa and impulses up to 2200 kPa-ms.

Compressed air is introduced into the driver and diaphragm sections and the aluminum foils between the driver and diaphragm are selected to be sufficiently strong to withstand the pressure difference between the two sections, and the foils between the diaphragm and the expansion section need to withstand the pressure in the diaphragm. Once the desired pressure is reached in the driver, air is released from the diaphragm section through a control valve. This causes the pressure difference between the driver and diaphragm sections to increase until it is greater than the capacity of the aluminum foils, resulting in the foils rupturing. Subsequently, the set of foils between the diaphragm and expansion section rupture and the compressed air is released and travels along the 6096 mm expansion section.

The opening at the end of the expansion sections is 2032 x 2032 mm. The opening size necessitates the use of a load transfer device to collect the pressure from the shock wave and transfer it to the side plates of the connection. The load transfer device consists of rigid steel panels that are connected to the end frame of the expansion section through slotted hinges. These hinges allow the entire load transfer device to translate freely up to 200 mm without transferring any forces through the hinges or adding to the stiffness of the tested specimen. This LTD has been used successfully to test glulam beams (Lacroix & Doudak, 2018a), cross laminated timber (Poulin et al, 2018), and dimension lumber (Jacques et al., 2014). The LTD, in its undeformed position and attached to the end frame of the shock tube, can be seen in Figure 3.13.

(a) Driver and diaphragm sections (b) Expansion section

Figure 3.12: University of Ottawa's shock tube before installation of aluminum foils

3.4.2 Description of dynamic test setup

The connection specimens were supported by a steel support frame, which consisted of two vertical 152.4 x 76.2 mm HSS members that were tied to the end frame of the shock tube with eight threaded rods. To reduce deflections in the frame, four sets of diagonal bracing were used to brace against the laboratory floor and ceiling. The diagonal braces consisted of back to back 76.2 x 76.2 x 6.4 mm angles. Additionally, top and bottom chords of 76.2 x 76.2 mm HSS were required to tie the diagonal bracing back to the main vertical members. Horizontal 152.6 x 152.6 mm HSS were used at the top and bottom of the frame to connect the two vertical frames and allow for more threaded rod connection points. Attached to the front of the support frame were two horizontal HSS with welded brackets to support the two load cells. The distance between these HSS members could be adjusted, allowing for different size connections to be tested. A stiffened W section was clamped to the front of the load cells to provide a bearing surface for the connection specimens. The connection specimen was lightly clamped to the W section to hold it in position during testing. The dynamic test setup is shown in Figures 3.13 to 3.15.

Two dynamic piezoelectric pressure sensors located at the bottom and side walls near the end frame of the shock tube were used to record the reflected pressure time history. Two linear variable differential transformers (LVDT) connected to a post were used to measure displacements in the connection. One LVDT measured the movement of the steel side plates, while another measured the movement of the wood specimen. The difference between these two measurements provided a value for the displacement in the connection itself. A third LVDT attached to the laboratory floor

was used to measure the displacement of the shock tube itself. Two load cells were placed between the wood specimen and the support frame to measure the force transmitted through the connection. A data acquisition system with a sampling rate of 100,000 samples per second was used to collect the data from these instruments. In addition, two high speed cameras recording at a frame rate of 2,000 frames per second were used to observe the test and act as a back-up method of determining displacements.

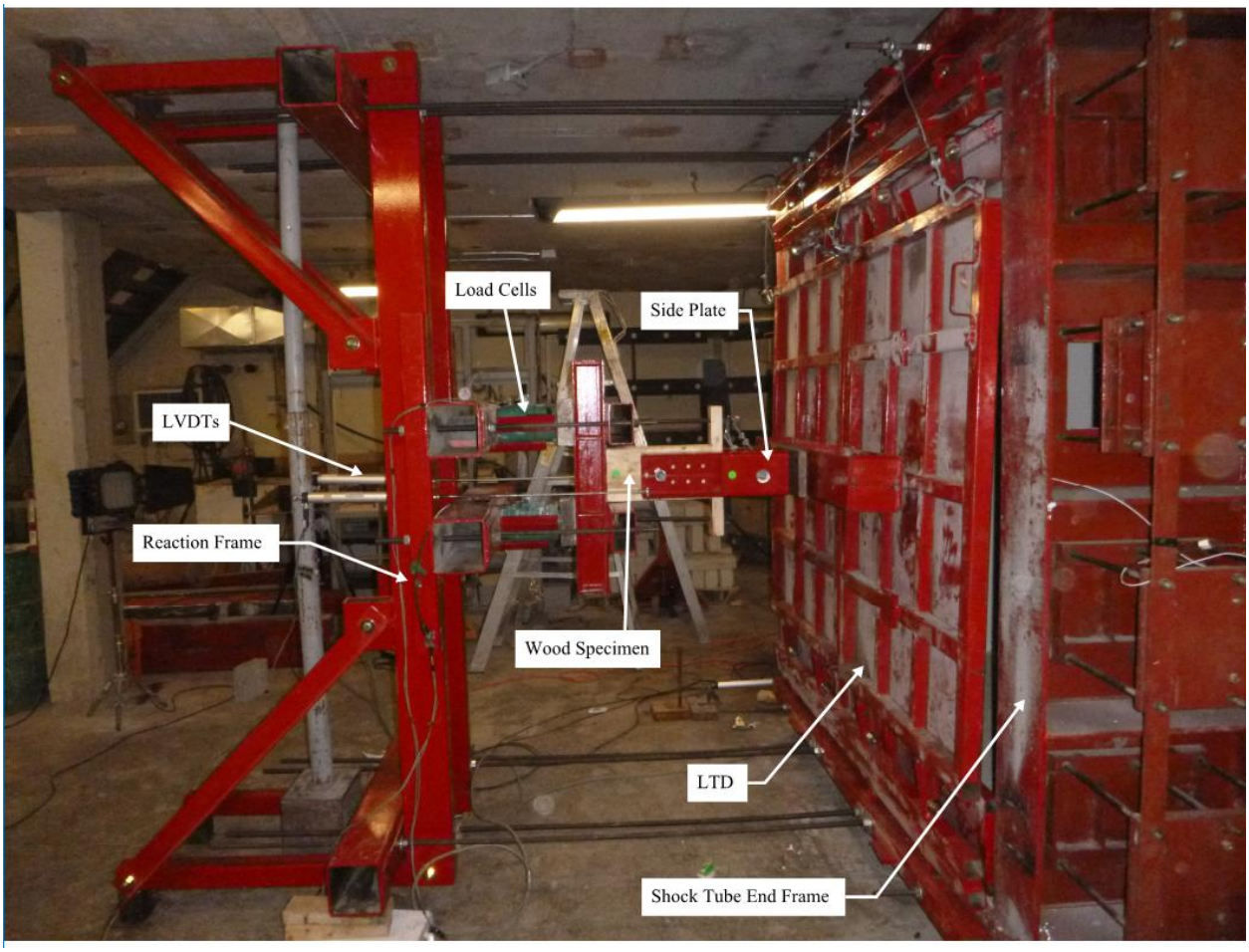

Figure 3.13: Dynamic test setup

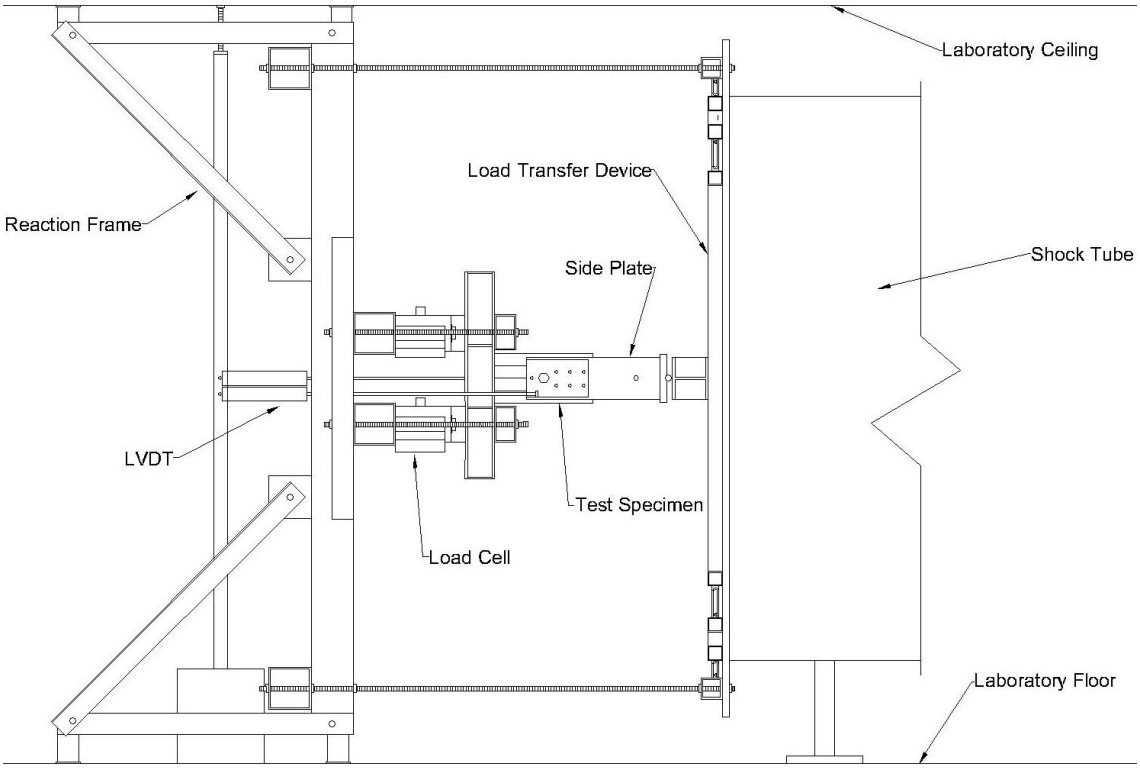

(a) Side View

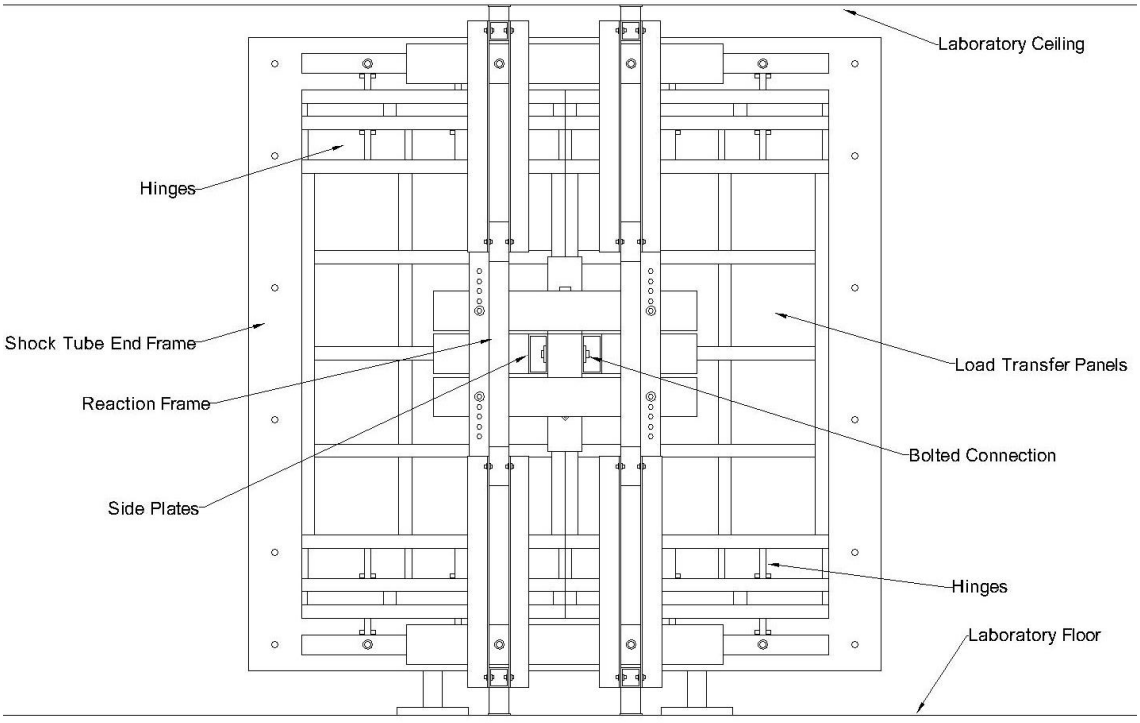

(b) Front View

Figure 3.14: Dynamic experimental setup

(a) Parallel to the grain connection designed to fail in Mode I

(b) Perpendicular to the grain connection designed to fail in Mode I

(c) Parallel to the grain connection designed to fail in Mode III

(d) Perpendicular to the grain connection designed to fail in Mode III

Figure 3.15: Typical dynamic test specimens

CHAPTER 4 – Experimental Results

4.1 General

This chapter presents the experimental results from the static and dynamic connection testing of all four connection configurations, as well as the bolt bending tests. The presented results include initial stiffness, yield load, displacement at yielding, ultimate strength, displacement at failure, and ductility. The yield load is defined differently depending on the connection configuration. Ultimate strength is defined as the maximum load recorded in the connection. Ultimate failure is considered to have occurred in the connection at a sudden complete loss of resistance. Ductility of the connection is defined as the ratio of the displacement when the resistance of the connection has degraded to 80% of the yield load or the displacement at failure to the displacement at yielding. The shock wave parameters are also provided for the dynamic tests. Additional details on the results of the static and dynamic tests can be found in Appendix A and B, respectively.

4.2 Bolt bending test results

A total of ten bending tests of individual A307 12.7 mm bolts were conducted to characterize the material behaviour. The force displacement response was characterized by linear elastic behaviour followed by a plastic yield plateau, as seen in Figure 4.1. The tests were conducted until the bolts bent to an angle of 45°. No ultimate failures occurred in any of the bolts, indicating they are capable of undergoing significant deformation without failing, or losing strength. This behaviour makes these slender bolts ideal for energy dissipative connections.

According to the ASTM F1575 – 17 standard (2017), the yield load was determined by fitting a straight line to the initial linear portion of the force displacement curve, and then offsetting this line along the displacement axis by an amount equal to 5% of the bolt diameter. The yield load is defined as the intersection between the offset line and the force displacement curve, as seen in Figure 4.1. Using the plastic section modulus of the bolt and the span of the test set-up, the average yield strength was calculated to 412.8 MPa with a COV of 0.042. Figure 4.2 displays the yield strength of each bolt bending test along with the experimental average.

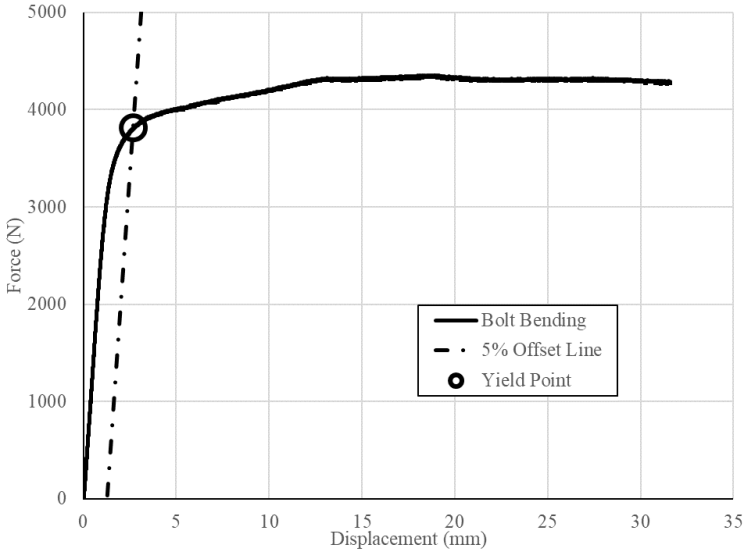

Figure 4.1: Typical force displacement response of 12.7 mm bolt in bending

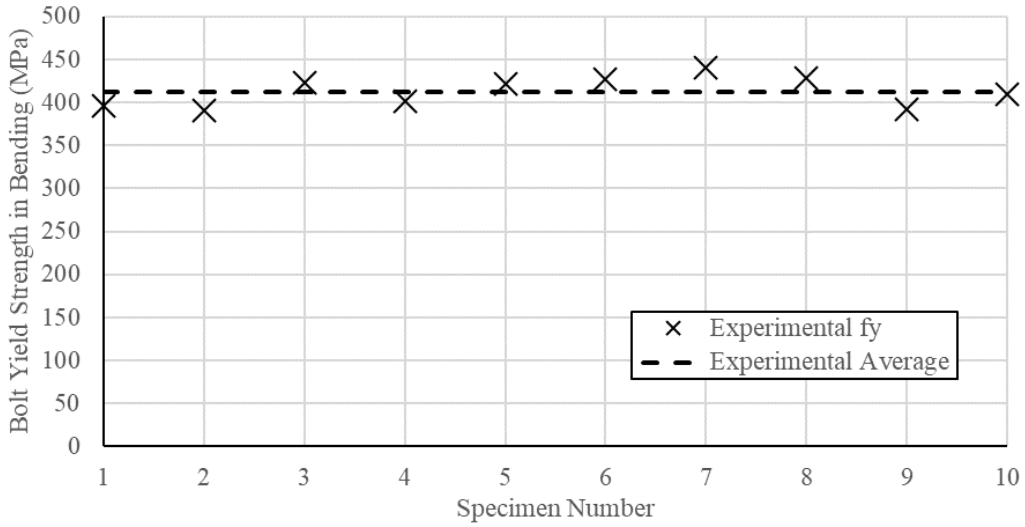

Figure 4.2: Experimental yield strength in bending for 12.7 mm bolts

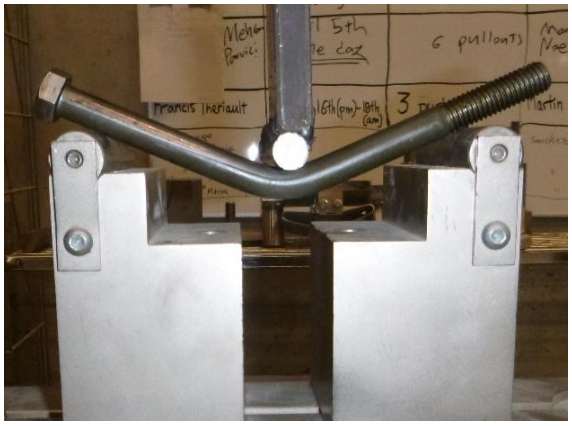

Figure 4.3: 12.7 mm bolt after testing

4.3 Static test results

The following section summarises the test results of the fourteen connections tested under static loading. For each connection the initial stiffness, yield load, displacement at yielding, ultimate strength, displacement at failure, and ductility are presented. Representative force displacement curves are provided in this section for each connection configuration. Complete details for each test can be found in Appendix A.

4.3.1 Parallel to the grain connections designed to fail in Mode I

Five parallel to the grain connections designed to fail in Mode I were tested under static loading. A small amount of initial slip occurred in the connections before the bolt was fully engaged. The connections then behaved in a linear elastic manner until yielding was reached. Post peak behaviour consisted of a sustained yielding (crushing) plateau with some strength degradation, as seen in Figure 4.4. Ultimate failure consisted of wood splitting initiated at the bolt hole. There was a small amount of permanent bending deformation in the 25.4 mm bolts. Figure 4.5 shows the typical failure mode of the specimen. The yield load for this connection configuration was determined in accordance with ASTM D5652 (2015) by fitting a straight line to the initial linear portion of the force displacement curve, and then offsetting this line along the displacement axis by an amount equal to 5 % of the bolt diameter. The yield load was defined as the intersection between the offset line and the force displacement curve. The average yield load and initial stiffness were 91.4 kN and 34,600 N/mm with a COV of 0.11 and 0.15, respectively. The average displacement at failure was 12.2 mm with a COV of 0.48. The ductility of the connections ranged from 1.8 – 5.4. The results of all tests are presented in Table 4.1.

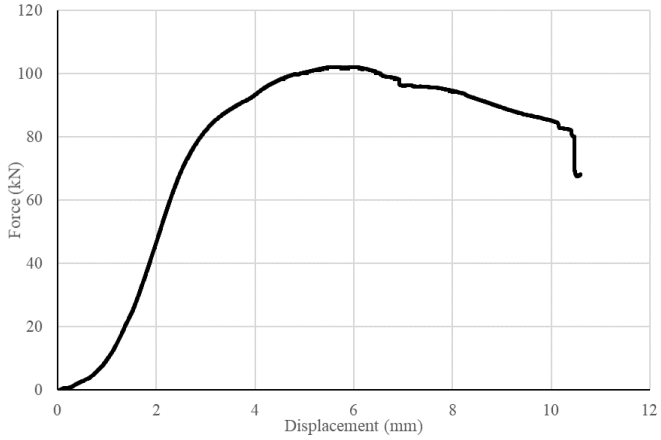

Figure 4.4: Representative static force displacement response for parallel to the grain connections designed to fail in Mode I

Table 4.1: Summary of parallel to the grain static test results for connections designed to fail in Mode I

Test Name	K[a] (N/mm)	F_y[b] (kN)	d_y[c] (mm)	F_u[d] (kN)	d_u[e] (mm)	μ[f]
E0S[1]	35,200	99.7	4.1	102.1	9.7	2.4
E0S[2]	38,000	101.0	3.9	102.1	7.2	1.8
E0S[3]	40,800	89.8	3.5	99.9	11.5	3.3
E0S[4]	32.400	90.3	4.1	100.9	10.3	2.5
E0S[5]	26,800	76.3	4.1	78.5	22.1	5.4

[a] Initial Stiffness [b] Yield load [c] Displacement at yield
[d] Ultimate strength [e] Displacement at failure [f] Ductility

(a) Splitting failure

(b) Crushing in bolt hole

(c) 25.4 mm bolt after testing

Figure 4.5: Representative failure of parallel to the grain static tests designed to fail in Mode I

4.3.2 Perpendicular to the grain connections designed to fail in Mode I

Three perpendicular to the grain connections designed to fail in Mode I were tested under static loading. A small amount of initial slip occurred in the connections before the bolt was fully engaged. The connections then behaved in a linear elastic manner until the yield point was reached. After yielding, the resistance of the connections continued to increase but with a lower stiffness compared to the initial stiffness, as seen in Figure 4.6. At significantly large displacements,

splitting was observed at the depth of the bolt hole. No ultimate failure was observed for these connections. There was a small amount of permanent bending deformation in the 25.4 mm bolts, however this occurred at large displacements where the wood under the bolt had densified significantly. Figure 4.7 shows a typical specimen after testing. The yield load for these tests were determined in accordance with EN 12512: Timber Structures - Test Methods - Cyclic Testing of Joints Made with Mechanical Fasteners (CEN, 2001). This method was chosen because of its suitability to adequately describe force displacement curves that have two well defined linear portions. The yield load was determined as the intersection between these two linear parts. The initial stiffness was taken as the slope of a line fitted to the data between 10% and 40% of the yield load. The average yield load and initial stiffness were 53.8 kN and 16,100 N/mm with a COV of 0.13 and 0.15, respectively. The results of all tests are presented in Table 4.2.

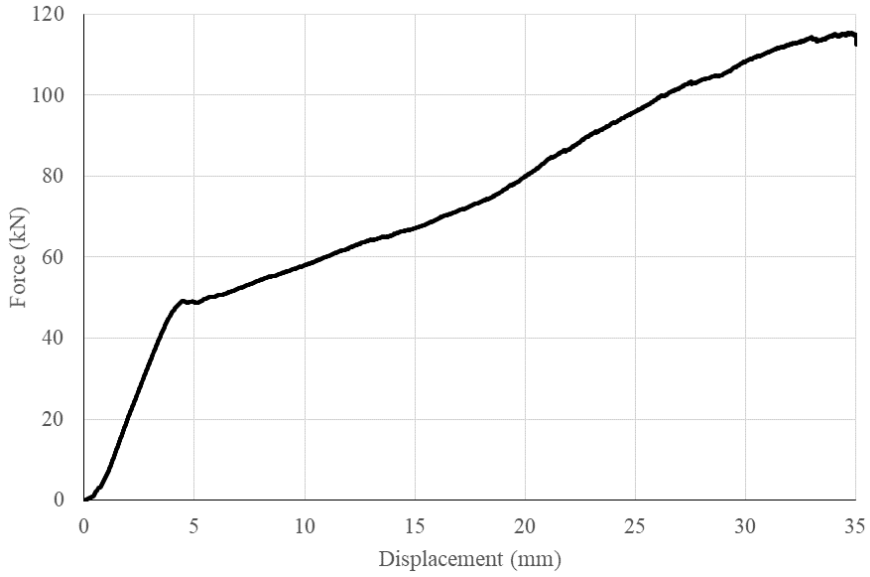

Figure 4.6: Representative static force displacement response for perpendicular to the grain connections designed to fail in Mode I

(a) Extensive crushing

(b) 25.4 mm bolt after testing

Figure 4.7: Representative failure of perpendicular to the grain static tests designed to fail in Mode I

Table 4.2: Summary of perpendicular to the grain static test results for connections designed to fail in Mode I

Test Name	K^a (N/mm)	$F_y{}^b$ (kN)	$d_y{}^c$ (mm)	$F_u{}^d$ (kN)	$d_u{}^e$ (mm)	μ^f
E90S[1]	19,000	59.8	3.2			
E90S[2]	14,500	46.0	3.2	No ultimate failure		
E90S[3]	14,800	55.5	3.7			

[a] Initial Stiffness [b] Yield load [c] Displacement at yield
[d] Ultimate strength [e] Displacement at failure [f] Ductility

4.3.3 Parallel to the grain connections designed to fail in Mode III

Three parallel to the grain connections designed to fail in Mode III were tested under static loading. A small amount of initial slip occurred in the connections before the bolt was fully engaged. The connections then behaved in a linear elastic manner until the bolt yielded in bending. Due to the restraint of the bolt head and nut, two plastic hinges developed at each shear plane, one at the side plate and one inside the wood specimen. The resistance of the connections then continued to increase with a lower stiffness than the initial stiffness, as seen in Figure 4.8. The connections ultimately failed due to a shear failure in the bolt. Figure 4.9 shows a typical failure in the specimen and the bending in the 12.7 mm bolt. The same method of determining the yield point as for the perpendicular to the grain connections designed to fail in Mode I was used for these connections.

The average yield load and initial stiffness were 20.3 kN and 12,800 N/mm with a COV of 0.03 and 0.06, respectively. The average displacement at failure was 33.0 mm with a COV of 0.03. The ductility of the connections ranged from 20.0 – 21.9. The results of all tests are presented in Table 4.3.

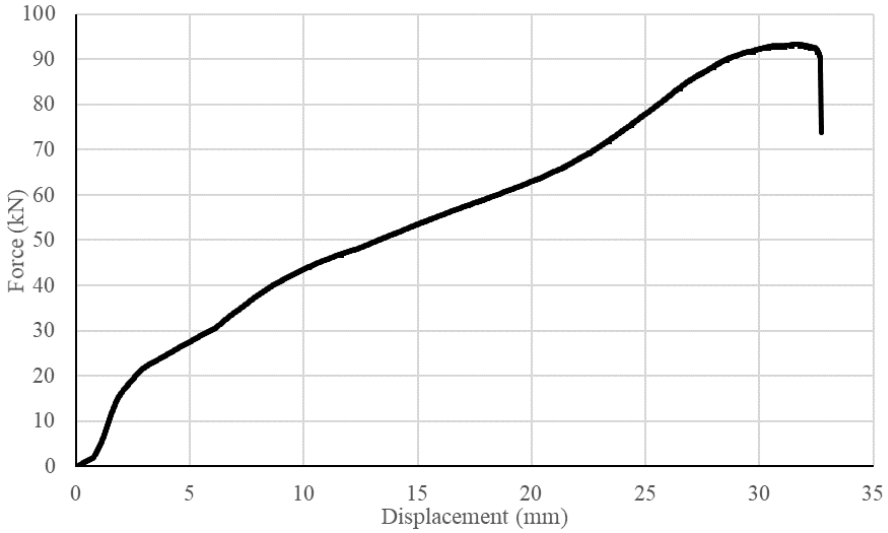

Figure 4.8: Representative static force displacement response for parallel to the grain connections designed to fail in Mode III

(a) Specimen cut open to show deformed shape of bolt

(b) Sheared off bolt

Figure 4.9: Representative failure of parallel to the grain static tests designed to fail in Mode III

Table 4.3: Summary of parallel to the grain static test results for connections designed to fail in Mode III

Test Name	K[a] (N/mm)	F_y[b] (kN)	d_y[c] (mm)	F_u[d] (kN)	d_u[e] (mm)	μ[f]
Y0S[1]	12,200	20.1	1.7	102.3	34.2	20.1
Y0S[2]	13,600	21.0	1.5	96.4	32.8	21.9
Y0S[3]	12,700	19.8	1.6	93.3	32.0	20.0

[a] Initial Stiffness [b] Yield load [c] Displacement at yield
[d] Ultimate strength [e] Displacement at failure [f] Ductility

4.3.4 Perpendicular to the grain connections designed to fail in Mode III

Three perpendicular to the grain connections designed to fail in Mode III were tested under static loading. The force displacement response of these three connections, as seen in Figure 4.10, was similar to the behaviour observed in the parallel to the grain connections designed to fail in Mode III, however, as expected, the yield load and stiffness were lower. The ultimate strength for these connections was similar to the parallel to the grain connections due to the ultimate failure mode of both types of connections being in bolt shear. Figure 4.11 shows a typical failed specimen and presents the bending in the 12.7 mm bolt. The average yield load and initial stiffness were 13.3 kN and 7,800 N/mm with a COV of 0.04 and 0.08, respectively. The average displacement at failure was 35.2 mm with a COV of 0.12. The ductility of the connections ranged from 17.2 – 25.0. The results of all tests are presented in Table 4.4.

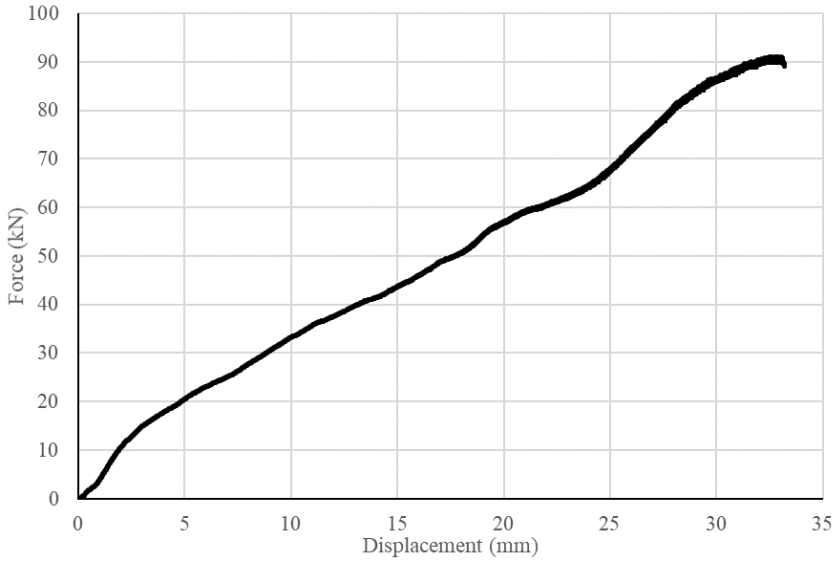

Figure 4.10: Representative static force displacement response for perpendicular to the grain connections designed to fail in Mode III

(a) Shape of bent bolt (b) Sheared off bolt

Figure 4.11: Representative failure of perpendicular to the grain static tests designed to fail in Mode III

Table 4.4: Summary of perpendicular to the grain static test results for connections designed to fail in Mode III

Test Name	K[a] (N/mm)	F_y[b] (kN)	d_y[c] (mm)	F_u[d] (kN)	d_u[e] (mm)	μ[f]
Y0S[1]	7,900	12.9	1.6	97.3	40.0	25.0
Y0S[2]	7,200	13.9	1.9	91.1	32.7	17.2
Y0S[3]	8,400	13.1	1.6	91.0	32.9	20.6

[a] Initial Stiffness [b] Yield load [c] Displacement at yield
[d] Ultimate strength [e] Displacement at failure [f] Ductility

4.4 Dynamic test results

The following section summarises the test results of the twenty-one connections tested dynamically. For each connection test the driver pressure, reflected pressure, reflected impulse, positive phase duration, initial stiffness, yield load, displacement at yielding, displacement at failure, and ductility are presented. The connection behaviour and failure mode are also described. Figure 4.12 shows a typical pressure and impulse-time history. Complete details for each test are presented in Appendix B.

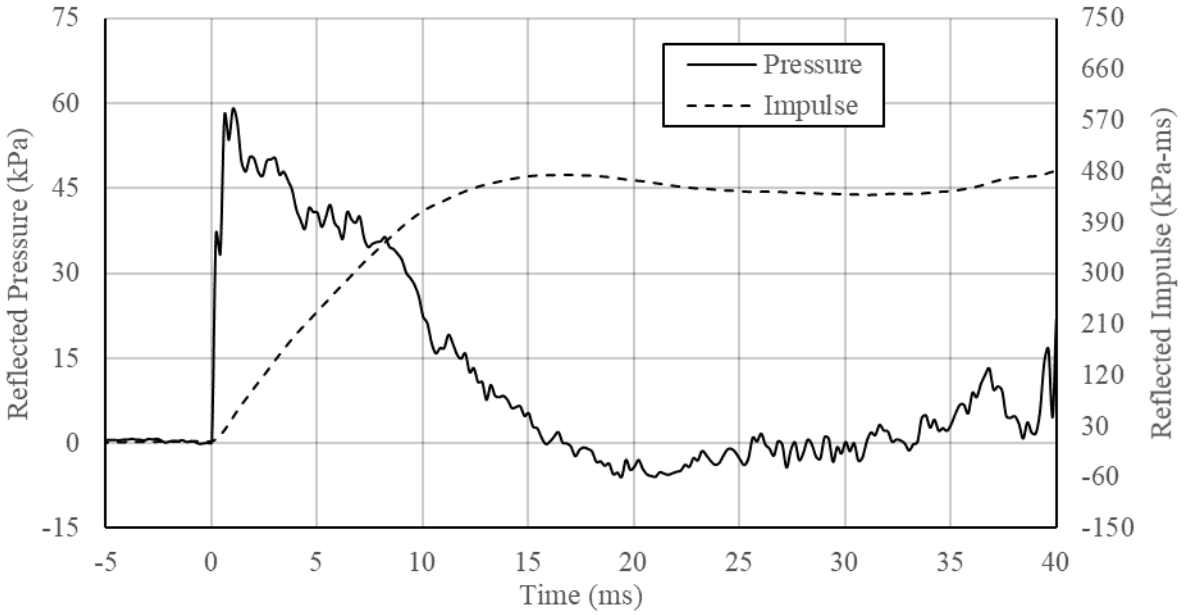

Figure 4.12: Reflected pressure-impulse-time history for test E0D[4]

4.4.1 Parallel to the grain connections designed to fail in Mode I

Nine parallel to the grain connections designed to fail in Mode I were tested under dynamic loading. The yield point was determined using the same 5% offset method used for the static tests. For specimens E0D[1] – E0D[6] the shock tube driver length was set at 1829 mm, while for specimens E0D[7] – E0D[9] it was increased to 2743 mm. The increased driver length was required to provide enough energy to overcome the increased resistance of the reinforced specimens. The blast wave parameters and results of all tests can be found in Table 4.5. Photos of the tested specimens are shown in Figure 4.16.

Specimens E0D[1] and E0D[2] showed similar behaviour. Specimen E0D[1] was subjected to a reflected pressure of 32.2 kPa and impulse of 255.5 kPa-ms. Specimen E0D[2] was subjected to a reflected pressure of 38.9 kPa and impulse of 366.3 kPa-ms. Both specimens remained in the linear elastic range and no permanent deformation was observed in either connection. Due to the connections not reaching their yield points, only the initial stiffness could be determined. E0D[1] and E0D[2] had an initial stiffness of 35,500 N/mm and 28,700 N/mm, respectively. Figure 4.13 shows the force displacement response of specimens E0D[1] and E0D[2].

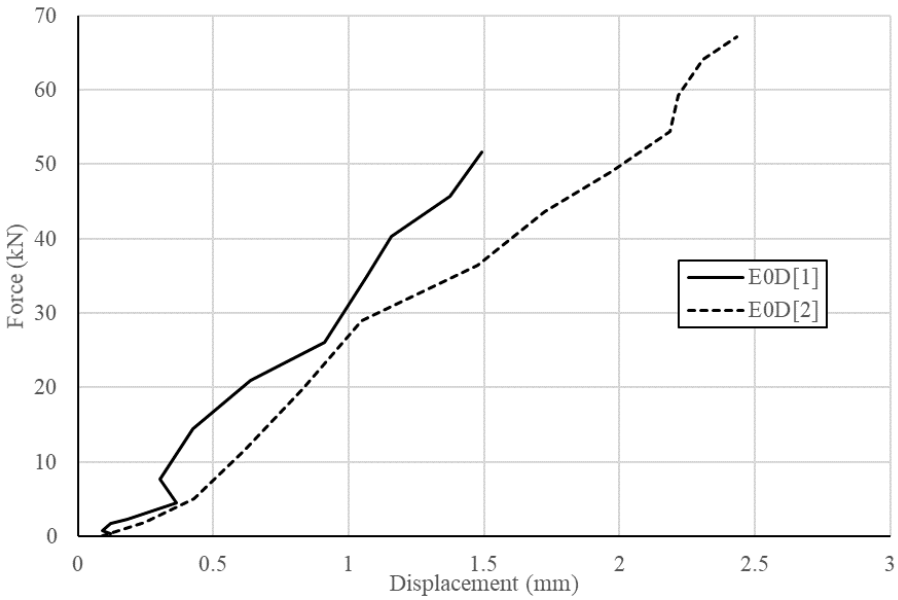

Figure 4.13: Force displacement response for E0D[1] & E0D[2]

Specimens E0D[3], E0D[4], and E0D[5] were tested with higher combinations of reflected pressure and impulse than E0D[1] and E0D[2]. These three specimens all exhibited a similar response of initial linear elastic behaviour, followed by a small amount of plastic deformation, and ultimately failing due to splitting. The displacements that were observed before splitting were almost entirely from wood crushing, with some minor bending in the bolt. Specimen E0D[3] was exposed to a reflected pressure of 59.8 kPa and impulse of 488.1 kPa-ms. The connection had an initial stiffness of 57,400 N/mm, yielded at 117.2 kN and failed at an ultimate displacement of 5.9 mm. Specimen E0D[4] was exposed to a reflected pressure of 59.0 kPa and impulse of 473.7 kPa-ms. The connection had an initial stiffness of 47,400 N/mm, yielded at 92.8 kN and failed at an ultimate displacement of 3.2 mm. Specimen E0D[5] was exposed to a reflected pressure of 56.5 kPa and impulse of 491.3 kPa-ms. The connection had an initial stiffness of 55,200 N/mm, yielded at 103.2 kN and failed at an ultimate displacement of 5.9 mm. These connections all exhibited relatively low ductility ratios ranging from 1.0 to 2.0. Figure 4.14 shows the force displacement response of specimens E0D[3], E0D[4] and E0D[5].

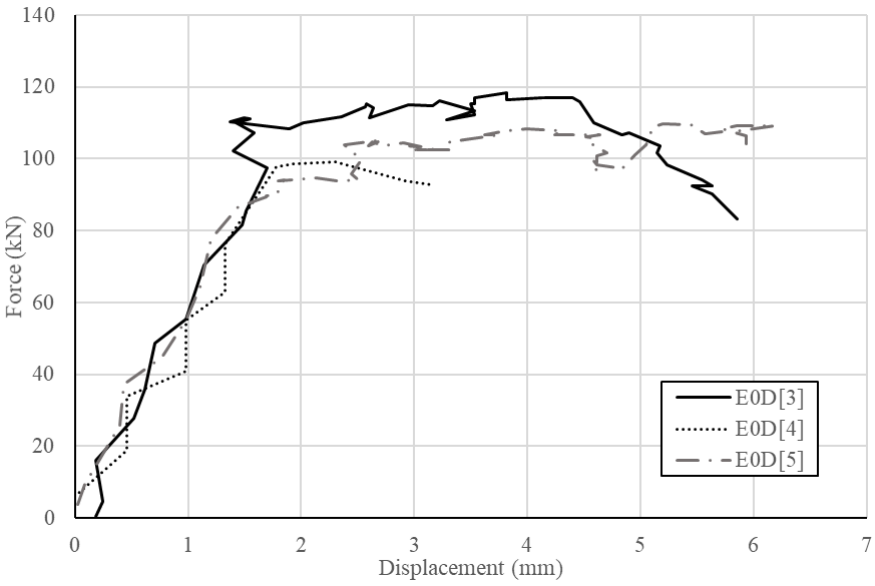

Figure 4.14: Force displacement response for E0D[3], E0D[4] & E0D[5]

Tests E0D[6] – E0D[9] were reinforced with self-tapping screws in an attempt to prevent splitting failure, and to improve the ductility of the connection. Specimen E0D[6] was exposed to a reflected pressure of 59.5 kPa and impulse of 452.3 kPa-ms. The connection had an initial stiffness of 58,700 N/mm, yielded at 108.5 kN and reached a displacement of 5.1 mm. The self-tapping screws were successful in preventing the splitting failure, but there was not enough energy in the shockwave to develop significant plastic deformation.

Due to the blast wave not having enough energy to fail E0D[6], the driver length was increased to 2743 mm for specimen E0D[7] and all subsequent specimens. E0D[7] was exposed to a reflected pressure of 54.6 kPa and impulse of 621.1 kPa-ms. The connection had an initial stiffness of 34,700 N/mm and yielded at 97.8 kN. The self-tapping screws improved the performance of the connection by allowing it to deform up to 28.1 mm, with some strength degradation, before the screws failed in withdrawal resulting in splitting failure in the wood specimen.

Specimen E0D[8] was exposed to a reflected pressure of 59.8 kPa and impulse of 659.0 kPa-ms. The connection had an initial stiffness of 40,500 N/mm and yielded at 121.2 kN. The self-tapping screws improved the performance of the connection by allowing it to deform up to 41.5 mm with some strength degradation and no ultimate failure. Significant cracking was observed in the specimen, but the screws did not fail in withdrawal.

Specimen E0D[9] was subjected to a reflected pressure of 81.7 kPa and impulse of 724.4 kPa-ms. The connection had an initial stiffness of 112,800 N/mm and yielded at 112.2 kN. The self-tapping screws improved the performance of the connection by allowing it to deform up to 26.7 mm, without any loss in resistance, before the screws failed in withdrawal resulting in splitting failure in the wood specimen. Figure 4.15 shows the force displacement response of specimens E0D[6], E0D[7], E0D[8] and E0D[9].

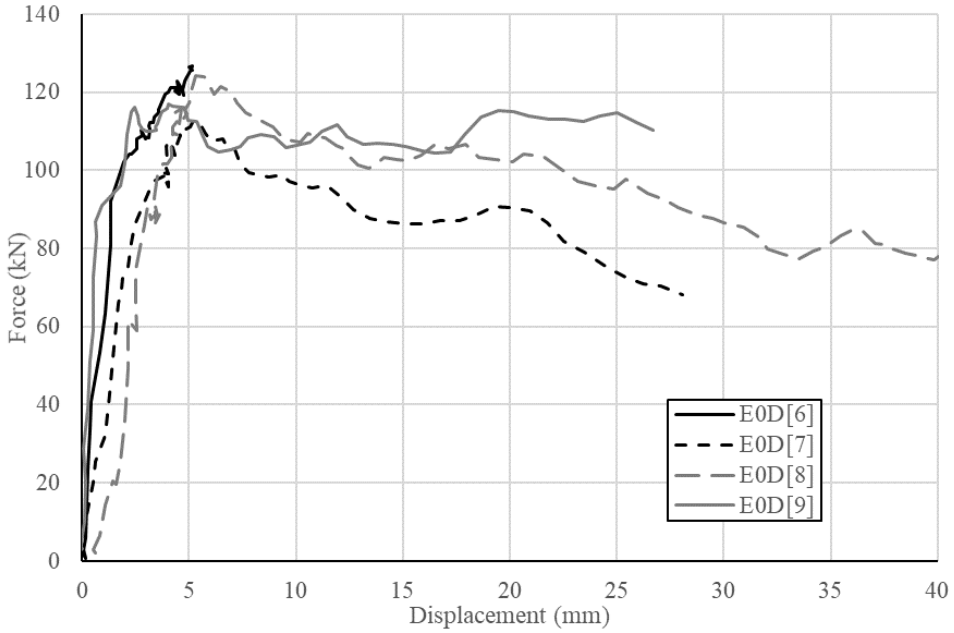

Figure 4.15: Force displacement response for E0D[6], E0D[7], E0D[8] & E0D[9]

The average yield load for all parallel to the grain dynamic connections designed to fail in Mode I was 107.4 kN with a COV of 0.095. The average initial stiffness was 52,300 N/mm with a COV of 0.48. Without reinforcing, the average displacement at failure was 5.0 mm with a COV of 0.32, while with reinforcing the average displacement for the two specimens that failed was 27.4 mm and one specimen displaced 41.5 mm without a failure. This represents an average ductility of 1.6 for the unreinforced connections and 7.8 for the reinforced connections.

(a) E0D[2] (E0D[1] similar)

(b) E0D[4] (E0D[3] & E0D[5] similar)

(c) E0D[6]

(d) E0D[7] (E0D[9] similar)

(e) E0D[8]

Figure 4.16: Parallel to the grain dynamic connections designed to fail in Mode I after testing

Table 4.5: Summary of dynamic test results for parallel to the grain connections designed to fail in Mode I

Test Name	P_D[a] (kPa)	P_R[b] (kPa)	I_R[c] (kPa-ms)	t_d[d] (ms)	K[e] (N/mm)	F_y[f] (kN)	d_y[g] (mm)	F_u[h] (kN)	d_u[i] (mm)	μ[j]
E0D[1]	243.4	32.2	255.5	15.4	35,500	No yielding				
E0D[2]	277.9	38.9	366.3	15.0	28,700					
E0D[3]	485.4	59.8	488.1	15.8	57,400	117.2	3.3	118.2	5.9	1.7
E0D[4]	481.9	59.0	473.7	16.6	47,400	92.8	3.1	99.2	3.2	1.0
E0D[5]	446.1	56.5	491.3	20.8	55,200	103.2	3.0	109.8	5.9	2.0
E0D[6]	455.1	59.5	452.3	14.8	58,700	108.5	3.0	No ultimate failure		
E0D[7]	450.9	54.6	621.1	23.8	34,700	97.8	4.0	112.6	28.1	5.9
E0D[8]	451.6	59.8	659.0	24.0	40,500	121.2	4.3	124.2	No ultimate failure	5.3
E0D[9]	499.2	81.7	724.4	22.0	112,800	111.2	2.2	116.9	26.7	12.1

[a] Driver pressure [b] Reflected pressure [c] Reflected impulse [d] Positive phase duration
[e] Initial Stiffness [f] Yield load [g] Displacement at yield [h] Ultimate strength
[i] Displacement at failure [j] Ductility

4.4.2 Perpendicular to the grain connections designed to fail in Mode I

Three perpendicular to the grain connections designed to fail in Mode I were tested under dynamic loading. The yield point was determined using the same stiffness intersection method as was used in the static tests. For all specimens the shock tube driver length was 2743 mm. The blast wave parameters and results of all tests can be found in Table 4.6. Photos of the tested specimens are shown in Figure 4.18.

All three specimens showed similar behaviour. The connections exhibited linear elastic response until yielding, after which the resistance of the connections continued to increase, but with a lower stiffness than the initial linear elastic behaviour. Similar to the static testing, at significantly large displacements splitting was observed at the depth of the bolt hole. No ultimate failure was observed for these connections.

Specimen E90D[1] was subjected to a reflected pressure of 54.4 kPa and impulse of 549.8 kPa-ms. The connection had an initial stiffness of 28,700 N/mm and yielded at 62.3 kN. Specimen E90D[2] was subjected to a reflected pressure of 52.4 kPa and impulse of 533.0 kPa-ms. The connection had an initial stiffness of 28,300 N/mm and yielded at 71.2 kN. Specimen E0D[3] was subjected to a reflected pressure of 55.6 kPa and impulse of 555.9 kPa-ms. The connection had an

initial stiffness of 35,900 N/mm and yielded at 60.6 kN. Figure 4.17 shows the force displacement response of specimens E90D[1], E90D[2] and E90D[3].

The average yield load for all perpendicular to the grain dynamic connections designed to fail in Mode I was 64.7 kN with a COV of 0.088. The average initial stiffness was 31,000 N/mm with a COV of 0.14.

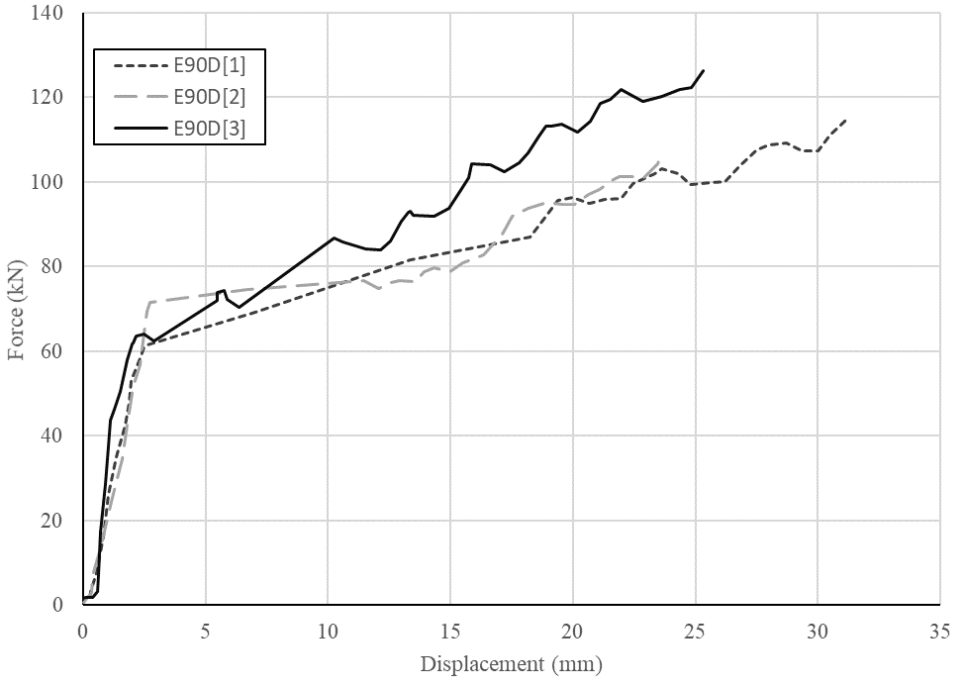

Figure 4.17: Force displacement response for E90D[1], E90D[2] & E90D[3]

Table 4.6: Summary of dynamic test results for perpendicular to the grain connections designed to fail in Mode I

Test Name	P_D[a] (kPa)	P_R[b] (kPa)	I_R[c] (kPa-ms)	t_d[d] (ms)	K[e] (N/mm)	F_y[f] (kN)	d_y[g] (mm)	F_u[h] (kN)	d_u[i] (mm)	μ[j]
E90D[1]	435.7	54.4	549.8	23.4	28,700	62.3	1.7			
E90D[2]	435.7	52.4	533.0	23.4	28,300	71.2	2.2	No ultimate failure		
E90D[3]	435.7	55.6	555.9	21.4	35,900	60.6	2.5			

[a] Driver pressure [b] Reflected pressure [c] Reflected impulse [d] Positive phase duration
[e] Initial Stiffness [f] Yield load [g] Displacement at yield [h] Ultimate strength
[i] Displacement at failure [j] Ductility

(a) E90D[1]

(b) E90D[2]

(c) E90D[3]

Figure 4.18: Perpendicular to the grain dynamic connections designed to fail in Mode I after testing

4.4.3 Parallel to the grain connections designed to fail in Mode III

Six parallel to the grain connections designed to fail in Mode III were tested under dynamic loading. Three of the connections were reinforced with self-tapping screws. The yield point was determined using the same stiffness intersection method as that used for static tests. For all specimens the shock tube driver length was 2743 mm. The blast wave parameters and results of all tests can be found in Table 4.7. Photos of tested specimens are shown in Figure 4.21.

Specimens Y0D[1], Y0D[2], and Y0D[3] were tested without reinforcement and similar behaviour for all three specimens was observed. The response was linear elastic until the bolt yielded in bending. Similar to the observations made in the static tests, two plastic hinges formed for each shear plane. After the bolt yielded, the connections' resistance continued to increase with increased displacement, but with a lower stiffness. Specimen Y0D[1] was subjected to a reflected pressure of 36.9 kPa and impulse of 425.5 kPa-ms. The connection had an initial stiffness of 20,400 N/mm and yielded at 26.1 kN. Y0D[1] ultimately failed when the specimen split at a displacement of 25.3 mm. Specimen Y0D[2] was subjected to a reflected pressure of 39.9 kPa and impulse of 355.6 kPa-ms. The connection had an initial stiffness of 16,000 N/mm and yielded at 22.2 kN. Y0D[2] displaced 29.6 mm without failure. Specimen Y0D[3] was subjected to a reflected pressure of 43.6 kPa and impulse of 402.1 kPa-ms. The connection had an initial stiffness of 15,100 N/mm and yielded at 25.6 kN. Y0D[3] ultimately failed when the specimen split at a displacement of 27.7 mm. These unreinforced specimens exhibited ductility ratios in the range of 17.3 to 19.5. Figure 4.19 shows the force displacement response of specimens Y0D[1], Y0D[2] and Y0D[3].

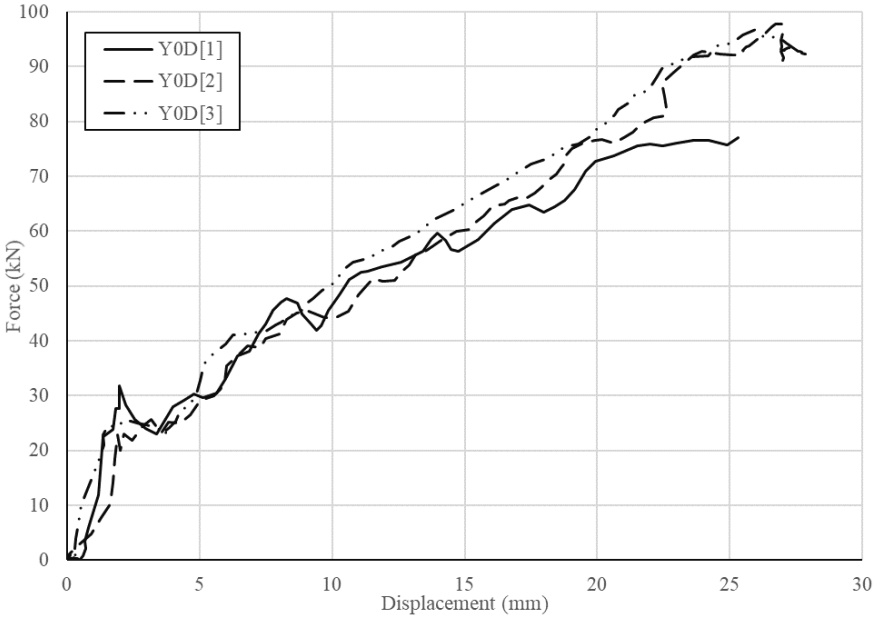

Figure 4.19: Force displacement response for Y0D[1], Y0D[2] & Y0D[3]

Specimens Y0D[4], Y0D[5], and Y0D[6] were reinforced with self-tapping screws prior to testing. These reinforced specimens exhibited a similar behaviour as the unreinforced specimens, except for their ultimate failure mode. The self-tapping screws were successful in preventing the specimens from splitting and changed the ultimate failure mode to a shear failure in the bolt.

Specimen Y0D[4] was subjected to a reflected pressure of 44.6 kPa and impulse of 387.6 kPa-ms. The connection had an initial stiffness of 38,300 N/mm, yielded at 23.1 kN and ultimately failed at a displacement of 30.5 mm. Specimen Y0D[5] was subjected to a reflected pressure of 45.4 kPa and impulse of 396.9 kPa-ms. The connection had an initial stiffness of 14,400 N/mm, yielded at 24.1 kN and ultimately failed at a displacement of 29.2 mm. Specimen Y0D[6] was subjected to a reflected pressure of 45.1 kPa and impulse of 419.6 kPa-ms. The connection had an initial stiffness of 15,100 N/mm, yielded at 23.7 kN and ultimately failed at a displacement of 34.3 mm. These reinforced specimens exhibited ductility ratios in the range of 21.4 to 50.8. Figure 4.20 shows the force displacement response of specimens Y0D[4], Y0D[5] and Y0D[6].

The average yield load for all parallel to the grain dynamic connections designed to fail in Mode III was 24.1 kN with a COV of 0.063. The average initial stiffness was 19,900 N/mm with a COV of 0.47. Without reinforcing, splitting was the ultimate failure and the average displacement at failure was 27.5 mm. With reinforcing, bolt shear was the ultimate failure and the average displacement was 31.2 mm with a COV of 0.11.

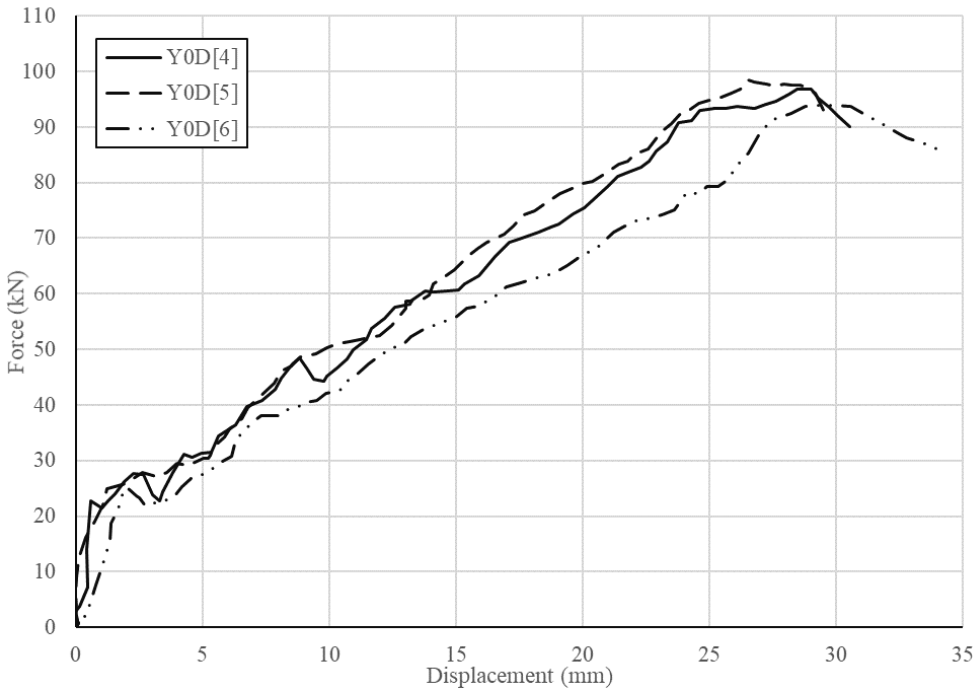

Figure 4.20: Force displacement response for Y0D[4], Y0D[5] & Y0D[6]

(a) Bolt deformed shape (b) Deformation in bolt hole

Figure 4.21: Parallel to the grain dynamic connections designed to fail in Mode III after testing

Table 4.7: Summary of dynamic test results for parallel to the grain connections designed to fail in Mode III

Test Name	P_D[a] (kPa)	P_R[b] (kPa)	I_R[c] (kPa-ms)	t_d[d] (ms)	K[e] (N/mm)	F_y[f] (kN)	d_y[g] (mm)	F_u[h] (kN)	d_u[i] (mm)	μ[j]
Y0D[1]	312.3	36.9	425.5	23.6	20,400	26.1	1.3	77.0	25.3	19.5
Y0D[2]	277.9	39.9	355.6	21.0	16,000	22.2	1.4	No ultimate failure		
Y0D[3]	313.0	43.6	402.1	20.8	15,100	25.6	1.6	96.8	27.7	17.3
Y0D[4]	333.0	44.6	387.6	21.0	38,300	23.1	0.6	93.7	30.5	50.8
Y0D[5]	319.2	45.4	396.9	20.8	14,400	24.1	1.1	96.8	29.2	26.5
Y0D[6]	322.0	45.1	419.6	20.8	15,100	23.7	1.6	93.7	34.3	21.4

[a] Driver pressure [b] Reflected pressure [c] Reflected impulse [d] Positive phase duration
[e] Initial Stiffness [f] Yield load [g] Displacement at yield [h] Ultimate strength
[i] Displacement at failure [j] Ductility

4.4.4 Perpendicular to the grain connections designed to fail in Mode III

Three perpendicular to the grain connections designed to fail in Mode III were tested under dynamic loading. The yield point was determined using the same stiffness intersection method as that used for static tests. For all specimens the shock tube driver length was 2743 mm. All specimens were observed to have similar behaviour as the static tests, with linear elastic behaviour before yielding, a reduced stiffness after yielding, and an ultimate failure of the bolt in shear. The deformed shape of the bolt was the same as for the static specimens. The blast wave parameters and results of all tests can be found in Table 4.8.

For specimens Y90D[1] and Y90D[2] an error in the test set-up prevented accurate load cell readings from being recorded. The specimens were not tightly secured to the support frame, causing them to impact the frame when the shock wave arrived. This produced readings in the load cells that were unassociated with the force in the connection. Specimen Y90D[1] was subjected to a reflected pressure of 43.5 kPa and impulse of 403.8 kPa-ms. Specimen Y90D[2] was subjected to a reflected pressure of 44.3 kPa and impulse of 396.6 kPa-ms. The connection stiffness and yield load could not be determined for these specimens due to the lack of load cell data. The connections failed in the bolt in shear at a displacement of 31.9 mm and 31.8 mm for Y90D[1] and Y90D[2], respectively.

Load cell data was recorded for specimen Y90D[3] which was exposed to a reflected pressure of 39.5 kPa and impulse of 403.7 kPa-ms. The connection had an initial stiffness of 20,400 N/mm, yielded at 16.2 kN and ultimately failed in the bolt in shear at a displacement of 30.8 mm. This represents a ductility ratio of 38.5. Figure 4.22 shows the force displacement response of specimen Y90D[3].

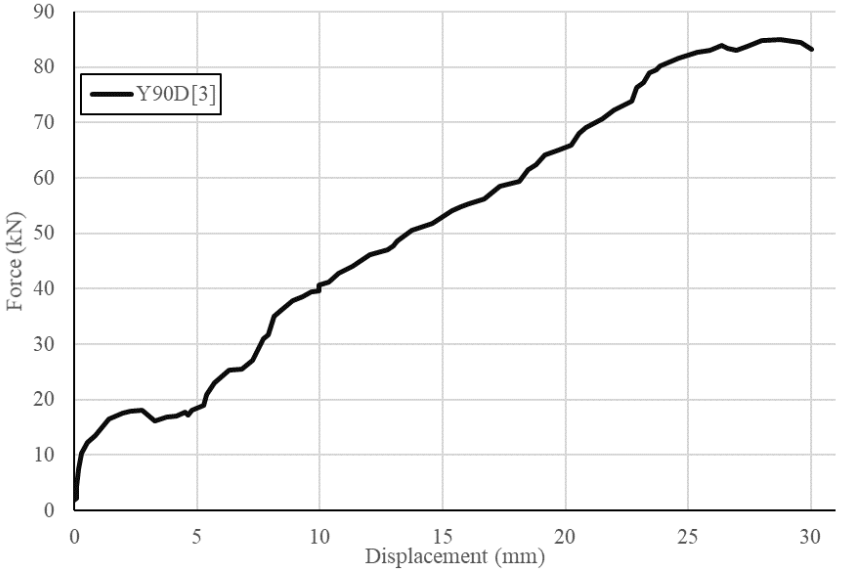

Figure 4.22: Force displacement response for Y90D[3]

Table 4.8: Summary of dynamic test results for perpendicular to the grain connections designed to fail in Mode III

Test Name	P_D[a] (kPa)	P_R[b] (kPa)	I_R[c] (kPa-ms)	t_d[d] (ms)	K[e] (N/mm)	F_y[f] (kN)	d_y[g] (mm)	F_u[h] (kN)	d_u[i] (mm)	μ[j]
Y90D[1]	314.4	43.5	403.8	20.4	-	-	-	99.8	31.9	-
Y90D[2]	312.3	44.3	396.6	20.2	-	-	-	94.6	31.8	-
Y90D[3]	312.3	39.5	403.7	21.2	20,400	16.2	0.8	85.1	30.8	38.5

[a] Driver pressure [b] Reflected pressure [c] Reflected impulse [d] Positive phase duration
[e] Initial Stiffness [f] Yield load [g] Displacement at yield [h] Ultimate strength
[i] Displacement at failure [j] Ductility

CHAPTER 5 – Analytical Modelling and Results

5.1 General

This chapter presents the analytical modelling approach and results. Both single degree of freedom (SDOF) and two-degrees of freedom (TDOF) models were investigated. Preliminary assessment of the supporting frame showed that it was very difficult to provide rigid support during the testing, especially for the large capacity connections. The displacement of the supporting frame was therefore measured for each test. A SDOF model representing only the connection specimen was not capable of accurately predicting the joint response. This was attributed to the energy dissipated through the deformation in the support frame. A TDOF model was deemed necessary to represent the experimental setup. The mass and stiffness properties of the frame needed as inputs into the TDOF model are described in Section 5.2.

5.2 Determining frame properties

The stiffness of the support frame was determined through an iterative SDOF approach. A SDOF system is based on solving the equation of motion seen in Equation 5.1, where all the terms are as described in Section 1.4.1.

$$K_{LM} m \ddot{y}(t) + R(y(t)) = F(t) \tag{5.1}$$

The blast analysis software *RCBlast*® was used to solve the equation of motion for displacement (Jacques, 2014). This analysis software has been shown to provide accurate results for various structural components including reinforced concrete (Burrell, 2012; Jacques, et al., 2013), light frame wood stud walls (Lacroix, 2013; Viau, 2016), and CLT panels (Poulin, 2019).

SDOF modelling requires the structural element to be idealized as a lumped mass and spring at a single point where the displacement is to be determined. As seen in Equation 5.1, a load-mass factor is required to convert the support frame into a lumped mass-spring system. The procedure to determine the load-mass factors is presented in Section 1.4.2. For typical structural arrangements load-mass factors are readily available in the literature (Biggs, 1964; USACE, 2008). For this SDOF model the load mass factor of the frame was based on the assumption that the main vertical members exhibited a deflected shape of a simply supported beam subjected to a mid-span point load. This resulted in a load mass factor of 0.49 being applied to the 140.1 kg distributed mass of the vertical members. No load-mass factor was required for the mass of the load cells and

supporting HSS members as they were attached at the mid-span of the frame. Combined, the two supporting HSS and load cells weighed 111.2 kg. Adding the two masses together yields an effective mass of 179.8 kg for the support frame.

The forcing function used as an input to the SDOF model was the sum of the recorded force in the two reaction load cells. This measurement represented the dynamically applied load on the support frame.

The output of the SDOF model was the displacement-time history at the mid-span of the support frame. The model was run up to the time when a failure in the specimen occurred or the forcing function became negative. The procedure consisted of iteratively changing the stiffness of the frame until the predicted maximum displacement, time-to-maximum displacement, and the overall shape of the displacement-time history best matched that from the experimental program. This procedure was performed for each individual connection test. The determined stiffness of the frame for each test can be seen in Table 5.1. Figure 5.1 compares representative displacement-time histories of the frame from the SDOF model to the experimentally measured displacements for the four different connection configurations.

As can be seen from Figure 5.1, relatively good agreement between the SDOF results and experimentally recorded displacement-time histories was achieved. The stiffness of the frame varied slightly between each test with a coefficient of variation of 0.13. This is to be expected because the frame was re-secured to the shock tube for each test and some minor adjustments were made to the frame to accommodate the different sizes of test specimens. Due to the slight differences between each test, when running the TDOF model the frame stiffness from the individual test being investigated was used, rather than an average frame stiffness.

Table 5.1: Frame stiffness determined through SDOF model

Test Name	Stiffness (N/mm)	Test Name	Stiffness (N/mm)
E0D[1]	15,500	**Y0D[1]**	24,000
E0D[2]	17,000	**Y0D[2]**	24,500
E0D[3]	21,000	**Y0D[3]**	18,500
E0D[4]	22,500	**Y0D[4]**	23,500
E0D[5]	22,000	**Y0D[5]**	21,500
E0D[6]	21,500	**Y0D[6]**	20,000
E0D[7]	22,000	**Y90D[1]**	22,500
E0D[8]	20,000	**Y90D[2]**	23,500
E0D[9]	21,000	**Y90D[3]**	17,000
E90D[1]	17,000	**Average**	20,450
E90D[2]	17,000	**Standard Deviation**	2,640
E90D[3]	18,000	**COV**	0.13

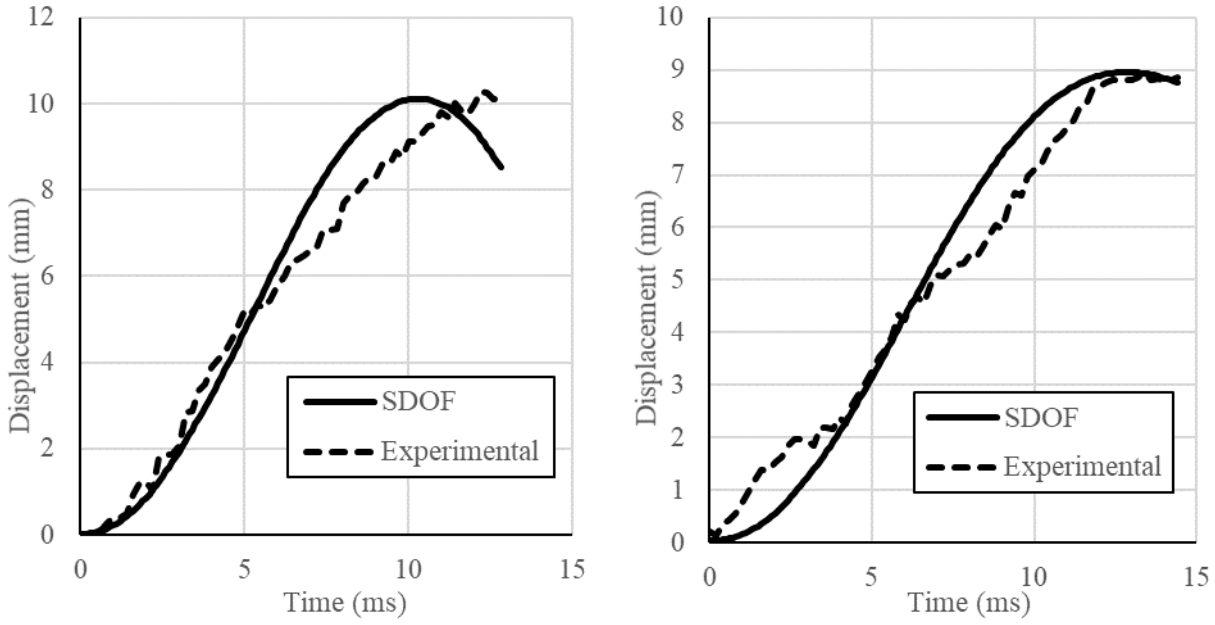

(a) E0D[3] (b) E90D[2]

Figure 5.1: Comparison between SDOF and experimental displacement-time histories for the frame

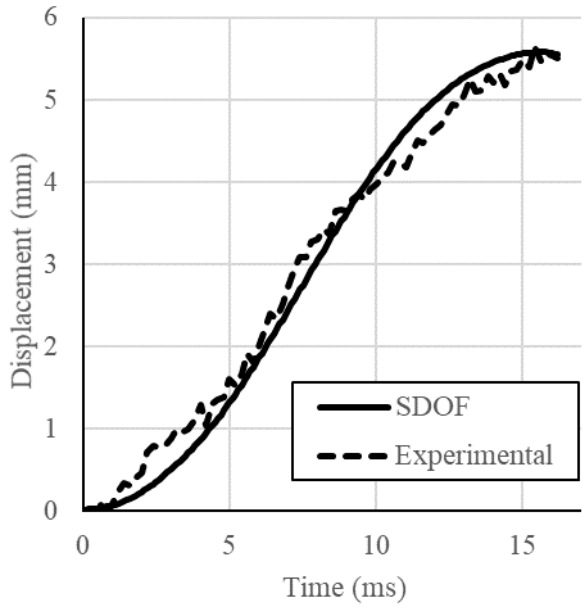

(c) Y0D[5]

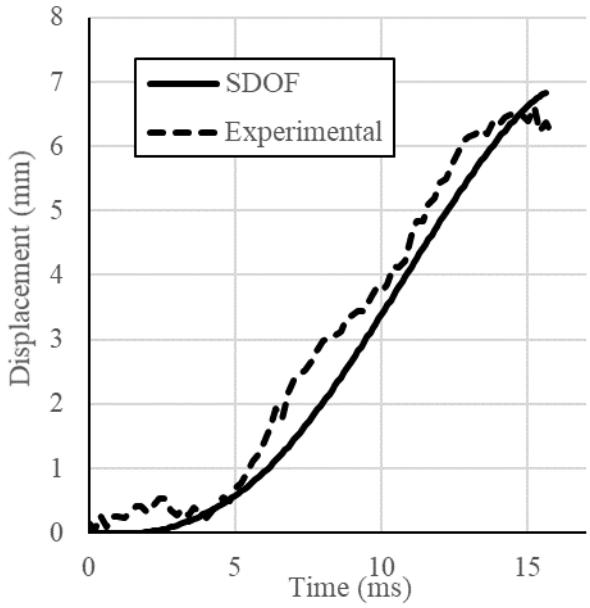

(d) Y90D[3]

Figure 5.1 cont.: Comparison between SDOF and experimental displacement-time histories for the frame

5.3 TDOF model

A TDOF model was used to conduct dynamic analysis on each connection specimen. A TDOF model is based on simultaneously solving the equations of motion for the joint system and the support frame, respectively, as presented in Equations 5.2 and 5.3 (terms are as described in Section 1.4.3).

$$m_1\ddot{y}_1(t) + R_1(y_1(t) - y_2(t)) = F(t) \tag{5.2}$$

$$K_{LM2}m_2\ddot{y}_2(t) + R_2\big(y_2(t)\big) - R_1(y_1(t) - y_2(t)) = 0 \tag{5.3}$$

The TDOF modelling software *BlasTDOF* developed by Viau (2019) was used to perform the dynamic analysis. This software uses the Newmark-beta numerical integration method with the constant average acceleration (Newmark, 1959) to solve the above equations. *BlasTDOF* has been shown to accurately predict the displacements of two degree of freedom systems, namely, CLT panels with various end connections (Viau & Doudak, 2019).

5.3.1 Model inputs

In Equation 5.2 no load-mass factor is used because both the mass and resistance associated with this degree of freedom act through a single point, namely, the connection specimen. The mass of

this degree of freedom (m_1) was the mass of the LTD and the loading arms, for a total mass of 258 kg. The effective mass of the frame ($K_{LM2}m_2$) was 180 kg as described in Section 5.2.

The forcing function input into Equation 5.2 was the recorded reflected pressure-time history multiplied by the effective area of the LDT, 3.55 m^2. Figure 5.2 shows a reflected pressure-time history from test E0D[4]

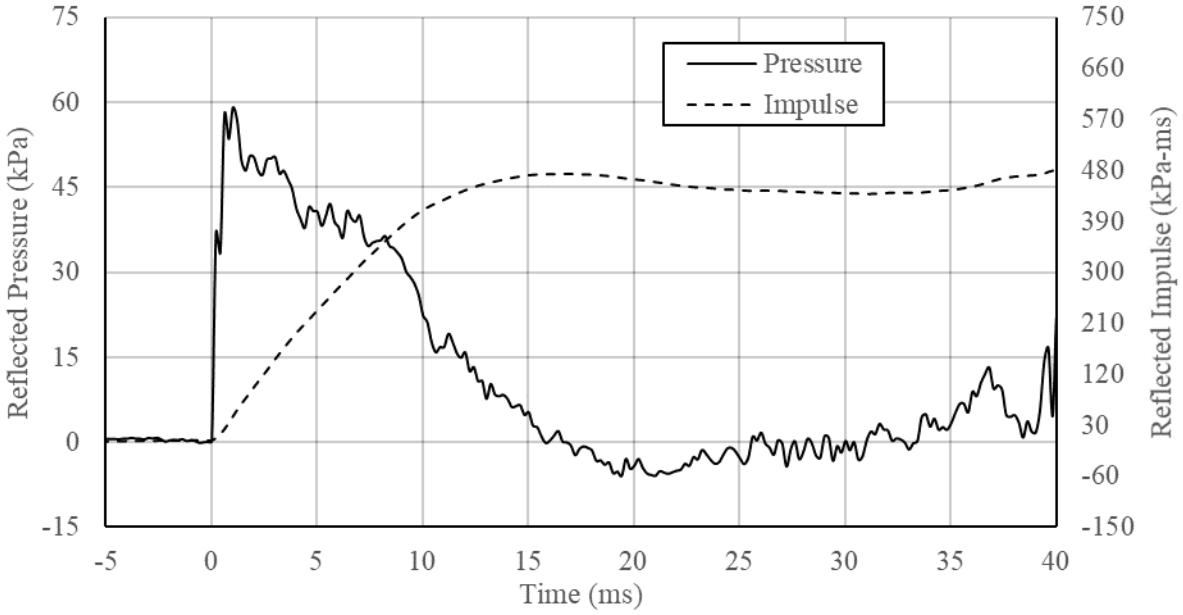

Figure 5.2: Reflected pressure-time history for test E0D[4]

The resistance function of the connection ($R_1(y_1(t) - y_2(t))$) was taken as the experimentally measured force displacement relationship for the connection being modelled. The force displacement relationships for all dynamic connections are presented in Section 4.4. The support frame was modelled as a linear spring, therefore the resistance of the frame ($R_2(y_2(t))$) was simply the stiffness multiplied by the displacement. The frame stiffness used in the TDOF model was the stiffness determined from the individual test. The measured resistance curves and the determined frame stiffness were used as inputs in order to validate the procedure of using a TDOF model to model the connection behaviour.

5.3.2 Model results

For each connection, the TDOF model was run until the maximum recorded displacement in the connection was reached. The time-to-maximum displacement of the connection was used to compare the model results to the experimental measurements. The predicted displacement-time

histories were compared to the experimental data for a representative connection from each connection group in Figure 5.3. Figure 5.4 shows the predicted time-to-maximum displacement for each connection configuration compared to the experimental result. Quantification of the relative accuracy of the TDOF model can be found in Table 5.2. These results show that the TDOF model under predicts the time-to-maximum displacement by 10% for the parallel to the grain connections designed to fail in Mode I. For all other connection groups, the model provides accurate results, within 4% of the time-to-maximum displacement. The lower accuracy in predicting the parallel to grain connections designed to fail in Mode I can be attributed to the fact that average stiffness in those specimens was high compared to estimated stiffness of the frame, and thus the results were dominated by deformation in the frame. It is recommended that future studies of this kind used a significantly stiffer support frame in order to minimize the effect of the support flexibility on the results.

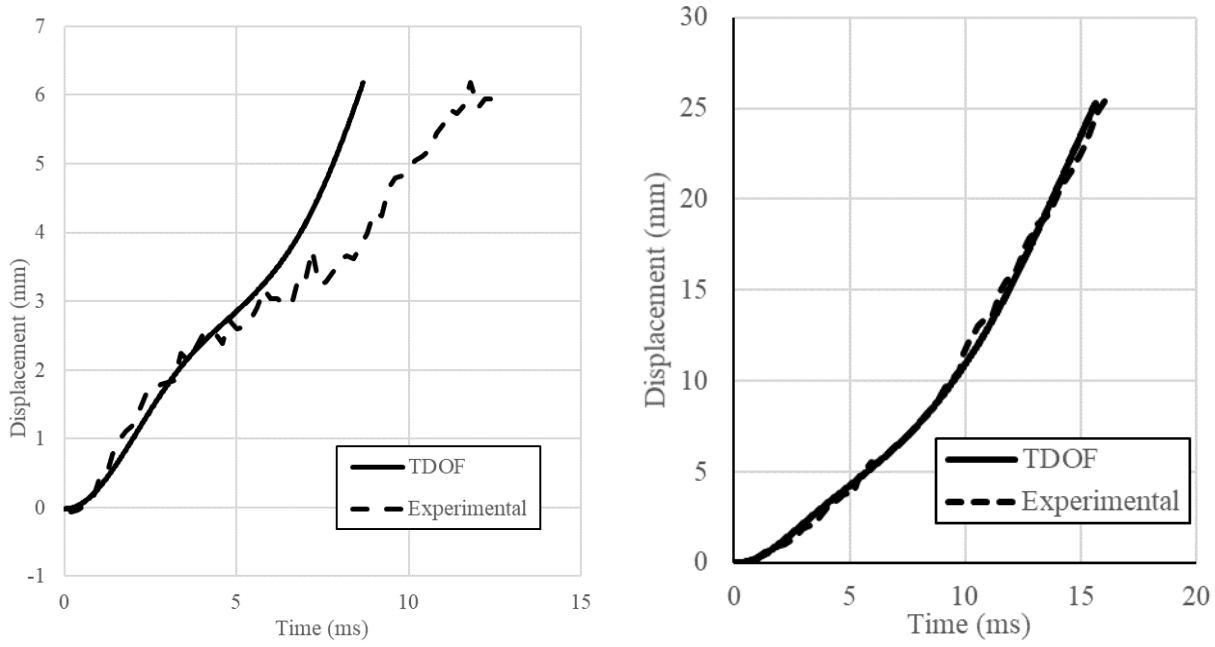

(a) E0D[5] (b) E90D[1]

Figure 5.3: Comparison between TDOF and experimental displacement-time histories

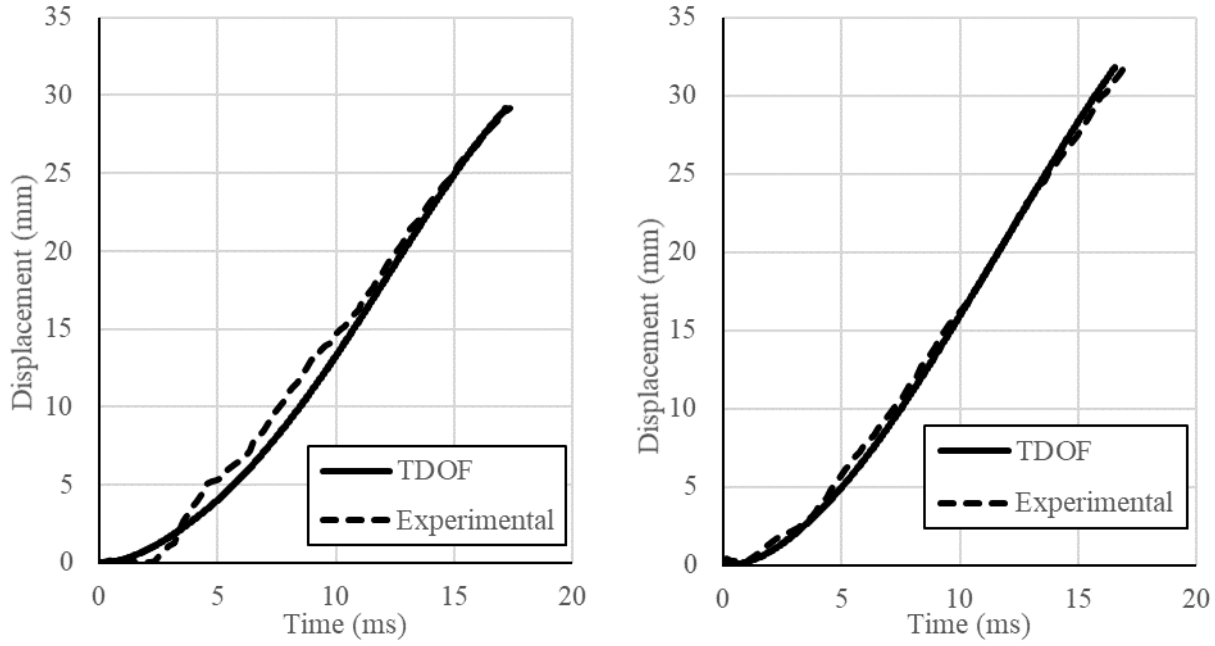

(c) Y0D[4] (d) Y90D[1]

Figure 5.3 cont.: Comparison between TDOF and experimental displacement-time histories

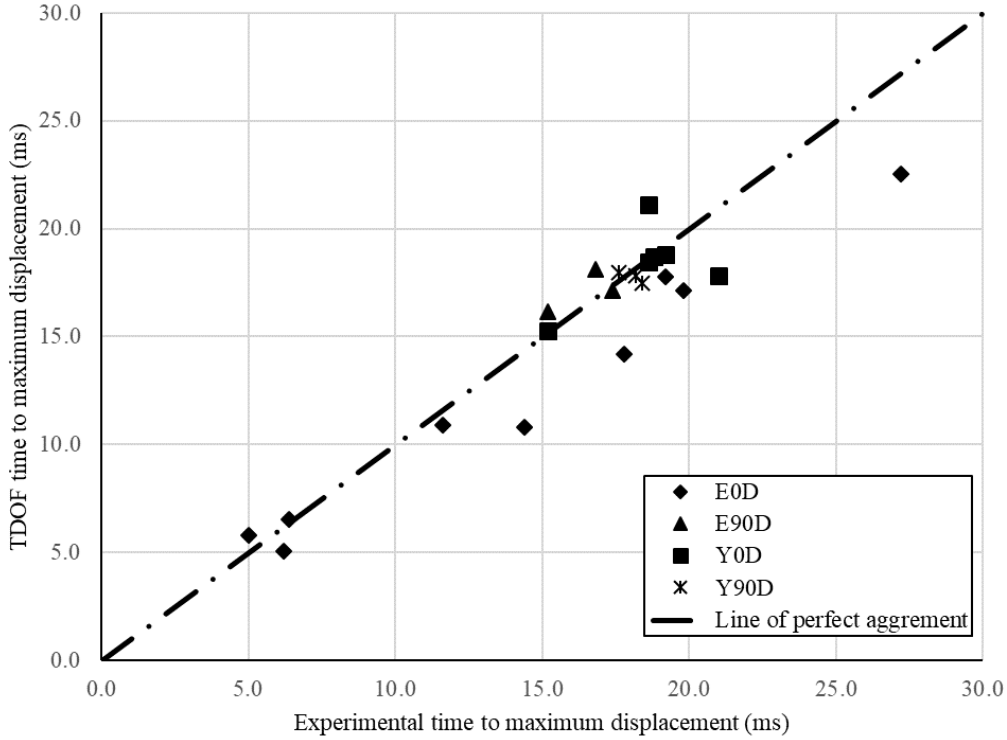

Figure 5.4: TDOF predicted results compared to experimental results

Table 5.2: Summary of experimental-TDOF response

Test Name	Number of tests	Time-to-maximum displacement ratio, $\frac{t_{TDOF}}{t_{exp}}$	
		Mean	Std. dev
All connections	21	0.96	0.11
Mode I Parallel to the Grain	9	0.90	0.13
Mode I Perpendicular to the Grain	3	1.04	0.05
Mode III Parallel to the Grain	6	0.99	0.09
Mode III Perpendicular to the Grain	3	0.98	0.04

CHAPTER 6 – Discussion

6.1 General

The current study investigates the response of bolted wood connections when subjected to simulated blast loads. A comparison between the connections' behaviour when subjected to static and dynamic loads is presented in this section. This includes determining the dynamic increase in resistance and stiffness as well as a discussion of the observed differences in post peak behaviour. The ability of reinforcement to improve connection performance by preventing brittle failure is also discussed. The effects of grain direction and failure mode on the connection performance are presented. The TDOF modelling of beam-connection assemblies and the associated findings and recommendations are also presented.

Throughout the following section the terminology "connections designed to fail in Mode I" refers to connections whose behaviour is dominated by wood crushing under the bolt, and "connections designed to fail in Mode III" refers to connections whose behaviour is dominated by bending in the bolt with minimal wood crushing.

6.2 Effects of dynamic loading

It is well-documented that wood experiences a dynamic increase in strength, similar to other structural materials, such as concrete and steel. This increase has been demonstrated in lumber (Jacques et al., 2014), glulam (Lacroix & Doudak, 2018), and CLT (Poulin et al., 2018). However, systematic investigation of the dynamic strength of wood connections has not yet been undertaken. The dynamic increase is defined as the ratio of the dynamic strength or stiffness relative to that obtained during static testing. In the current study four connection configurations, including those designed to fail in Mode I or Mode III, in the direction parallel or perpendicular to the wood grain are investigated.

For the parallel to the grain connections designed to fail in Mode I, a dynamic increase of 1.2 and 1.5 has been observed on the yield load and stiffness, respectively. It was also observed that this connection configuration exhibited a significant decrease in ductility under dynamic loading. The static tests had an average ductility ratio of 3.1, while the unreinforced dynamic tests had an average of 1.6. The ultimate failure was the same in both loading regimes and consisted of a

splitting (perpendicular to grain) failure. This increase in resistance, and stiffness as well as the loss of ductility can be seen in Figure 6.1.

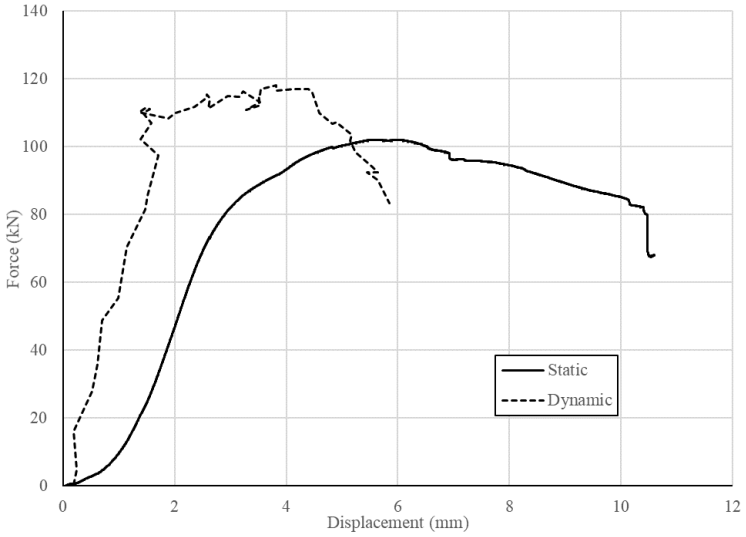

Figure 6.1: Comparison between representative force displacement response for static and dynamic parallel to the grain connections designed to fail in Mode I

For the perpendicular to the grain connections designed to fail in Mode I, a dynamic increase of 1.2 and 1.9 has been observed on the yield load and stiffness, respectively. This increase in resistance and stiffness can be seen in Figure 6.2. No ultimate failure was observed for this connection configuration in either the static or the dynamic tests. This was due to the connection specimens being fully supported along the bottom edge.

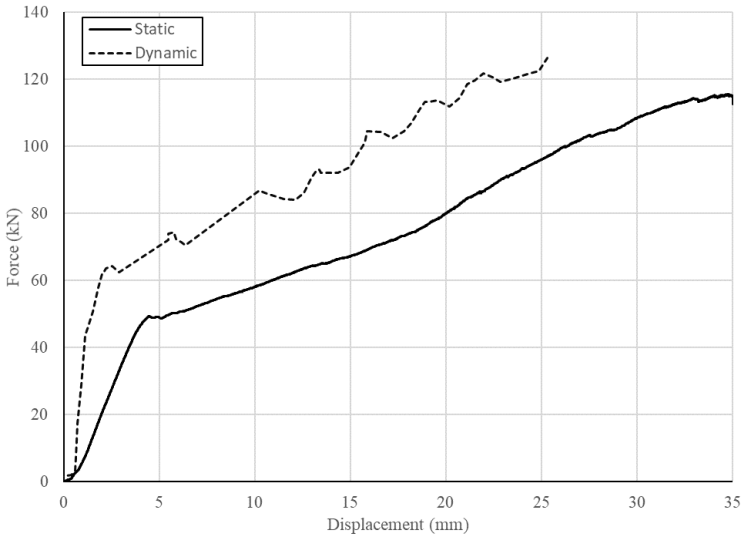

Figure 6.2: Comparison between representative force displacement response for static and dynamic perpendicular to the grain connections designed to fail in Mode I

For the parallel to the grain connections designed to fail in Mode III, no dynamic increase was observed for the yield load or stiffness. This can be seen in Figure 6.3, where no clear increase in resistance or stiffness is observed for the dynamic specimens, and significant overlap between the static and dynamic response is observed. In addition, for the dynamic tests of this connection configuration the yield point was reached quickly and at relatively low displacements. This created difficulties in defining the initial stiffness of the connections as there was a limited amount of data before the yield point. This resulted in high variability in the measured stiffness. The ultimate failure observed during the static and dynamic tests was different; static tests were dominated by bolt shear failure and the dynamic tests by wood splitting, as seen in Figure 6.4. This change in ultimate failure resulted in a small decrease in deformation at ultimate failure of 19% under dynamic loading. However, this had a minimal impact on the overall connection behaviour because all ultimate failures occurred after significant displacement of more than 25 mm.

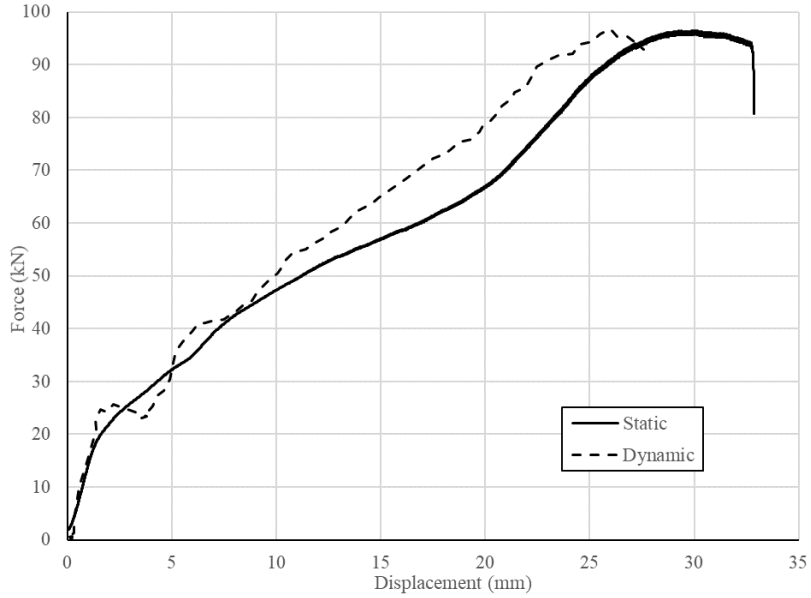

Figure 6.3: Comparison between representative force displacement response for static and dynamic parallel to the grain connections designed to fail in Mode III

(a) Static test – bolt shear failure (b) Dynamic test – splitting failure

Figure 6.4: Ultimate failure for parallel to the grain connections designed to fail in Mode III

For the perpendicular to the grain connections designed to fail in Mode III, no dynamic increase can be recommended for the yield load or stiffness. This is because only one dynamic test could be compared to the static results due to experimental error in the other two dynamic tests. In addition, for the dynamic tests, the yield point was reached quickly and at relatively low displacements. This created difficulties in defining the initial stiffness of the connections as there was a limited amount of data before the yield point. Figure 6.5 shows a comparison between static and dynamic force displacement curves where overlap between the static and dynamic response can be observed. All connections of this configuration ultimately failed in bolt shear and no change in ductility was observed under dynamic loading.

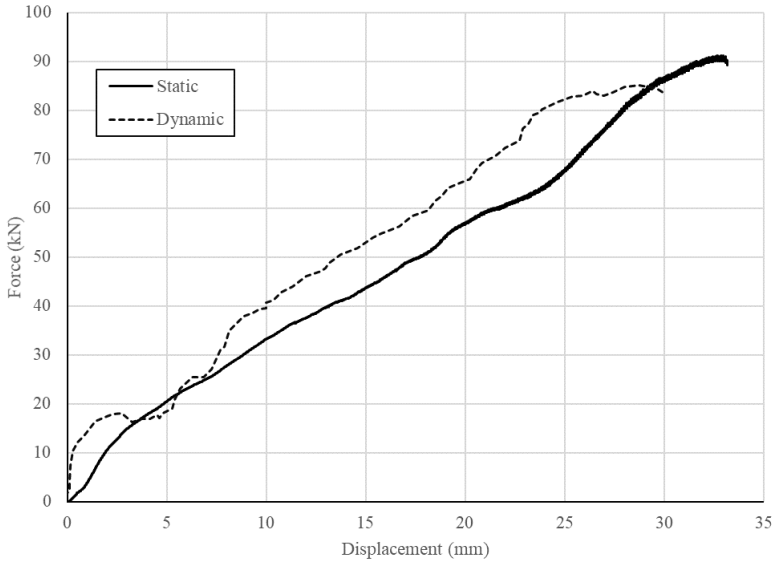

Figure 6.5: Comparison between representative force displacement response for static and dynamic perpendicular to the grain connections designed to fail in Mode III

6.3 Effects of reinforcing

Seven parallel to the grain dynamic connections were reinforced with self-tapping screws to investigate the ability of reinforcement to prevent the observed splitting failures. The details of the reinforcing used are described in Section 3.1. Four of those connections were designed to fail in Mode I and three were designed to fail in Mode III. It was observed that the reinforcement had no effect on the stiffness or yield load of the connections, however it significantly affected the post yielding behaviour.

For the connections designed to fail in Mode I, the reinforcing was effective in preventing the early splitting failure observed in the unreinforced specimens. Although splitting failure did occur in two of the specimens at relatively large displacements, where the screws failed in withdrawal. The average ductility significantly improved, where a ductility ratio of 7.8 was observed in the reinforced specimens compared to a ratio of 1.6 for specimens with no reinforcement. The results underline that self-tapping screw reinforcement can be used effectively to suppress brittle failure, prevent splitting and significantly enhance the post peak performance of a joint. Figure 6.6 shows the increased ductility observed in the reinforced specimens compared to the unreinforced specimens, and Figure 6.7 shows the corresponding ultimate failure modes.

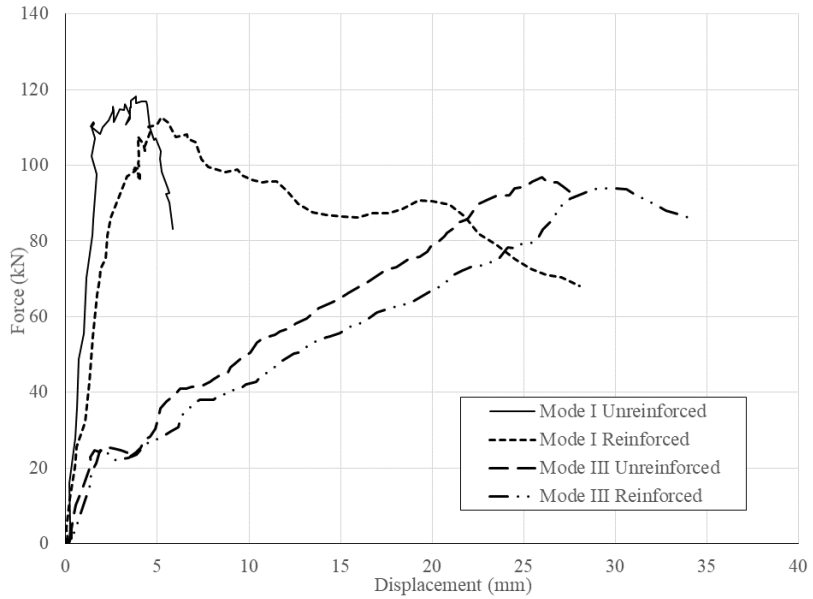

Figure 6.6: Comparison between representative force displacement response for both reinforced and unreinforced parallel to the grain connections designed to fail in Mode I and Mode III

(a) Unreinforced – splitting failure

(b) Reinforced – plastic deformation

Figure 6.7: Effect of reinforcement - parallel to the grain dynamic connections designed to fail in Mode I

For the connections designed to fail in Mode III, the reinforcement prevented the splitting failure observed in the unreinforced connections and changed the ultimate failure to shear in the bolt. The average displacement at failure slightly improved from 26.5 mm without the reinforcement to 31.3 mm with the reinforcement (an increase of 18%). The relatively small benefit of reinforcement in this case was expected since splitting in the unreinforced specimens occurred at loads only slightly lower than the load required to fail the bolt in shear, and hence this provided less room for the reinforcement to improve the capacity. Figure 6.6 shows the force displacement response for both the reinforced and unreinforced connections. Figure 6.8 shows the differences in the ultimate failure between the reinforced and reinforced specimens.

(a) Unreinforced – splitting failure

(b) Reinforced – bolt shear failure

(c) Reinforced - sheared off bolt

Figure 6.8: Effect of reinforcement - parallel to the grain dynamic connections designed to fail in Mode III

6.4 Effects of grain direction

The grain direction of the wood is known to have an impact on the behaviour of connections. It is for example well established that the embedment strength in the perpendicular to grain direction is approximately half of that in the parallel to the grain direction (CSA, 2014). The design standard does not, however, address stiffness and ductility in the connections. Based on the testing conducted in the current study, it was observed that for the connections designed to fail in Mode I, the force displacement behaviour in the parallel and perpendicular to the grain directions were significantly different. Connections loaded parallel to the grain exhibited linear-elastic behaviour followed by a relatively short yield plateau. While the perpendicular to the grain connections exhibited linear-elastic behaviour until yielding, after which the resistance of the connections continued to increase. The parallel and perpendicular to the grain connections also differed in their average stiffness and yield load. For both yield load and stiffness, the ratio of parallel to perpendicular to the grain for the dynamic connections was 1.7. This is slightly less than the ratio of 2.3 that is specified in the standard (CSA, 2014) for the specified strength. A comparison between representative parallel and perpendicular to the grain dynamic results can be seen in Figure 6.9.

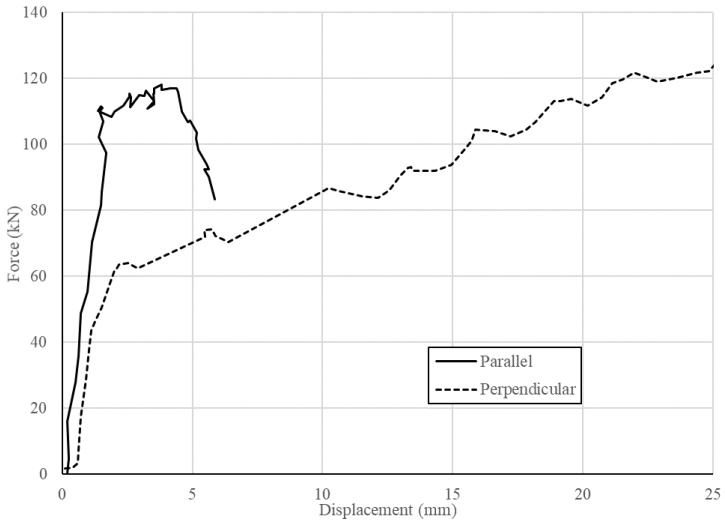

Figure 6.9: Comparison between force displacement response for parallel and perpendicular to the grain connections designed to fail in Mode I

For the connections designed to fail in Mode III, the force displacement behaviour in the parallel and perpendicular to the grain directions was similar. Both parallel and perpendicular to the grain connections exhibited linear-elastic behaviour until yielding, after which the resistance of the connections continued to increase. The ultimate failure of bolt shear was observed for both the parallel and perpendicular to the grain connections. Under dynamic loading, the stiffness was similar for the parallel and perpendicular to the grain directions, but the yield load was higher for the parallel to the grain connections (a ratio of 1.5). A comparison between representative parallel and perpendicular to the grain dynamic results can be seen in Figure 6.10.

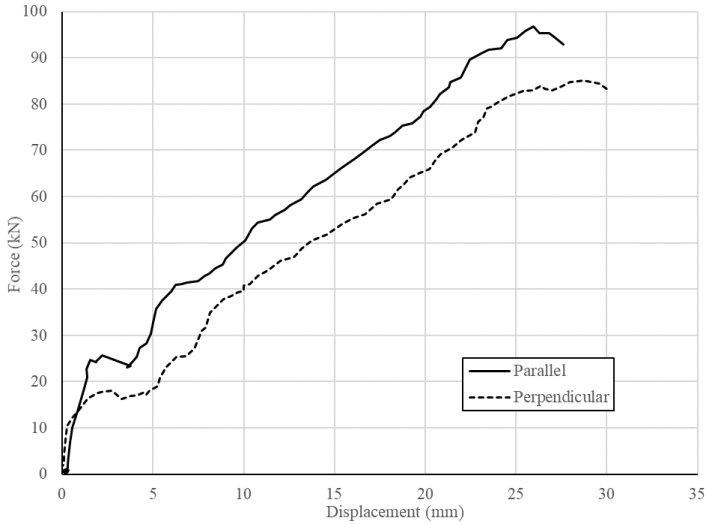

Figure 6.10: Comparison between force displacement response for parallel and perpendicular to the grain connections designed to fail in Mode III

6.5 Effects of failure mode

As expected, the behaviour of the connections designed to fail in Mode I and Mode III were significantly different. Both connection configurations yielded in the failure mode they were designed for. Figure 6.11 shows the difference in the deformed shapes of the bolts after testing.

In the parallel to the grain direction, the post yielding behaviour of the connections designed to fail in Mode I and Mode III were different. The connections designed to fail in Mode I had a short yield plateau and an ultimate failure in splitting, while the resistance of the connections designed to fail in Mode III continued to increase after yielding and the ultimate failure was in bolt shear. This difference in ultimate failure mode resulted in the connections designed to fail in Mode III having a ductility ratio more than six times greater than the ductility ratio of the connections designed to fail in Mode I. This higher level of ductility is ideal for blast loading because a large amount of energy can be dissipated and shows that Mode III failures are more suitable for blast loading than Mode I failures. A comparison between the dynamic results of these connections is shown in Figure 6.6.

In the perpendicular to the grain direction, the post yielding behaviour of the connections designed to fail in Mode I and Mode III were similar, with both connection configurations exhibiting an increase in resistance after yielding. No ultimate failure was observed in the connections designed to fail in Mode I while an ultimate failure of bolt shear was observed for the connections designed to fail in Mode III. A comparison between the dynamic results of these connections is shown in Figure 6.12.

(a) Connections designed to fail in Mode I: slight deformation in 25.4 mm bolt

(b) Connections designed to fail in Mode III: bending in 12.7 mm bolt

Figure 6.11: Bolts after dynamic testing

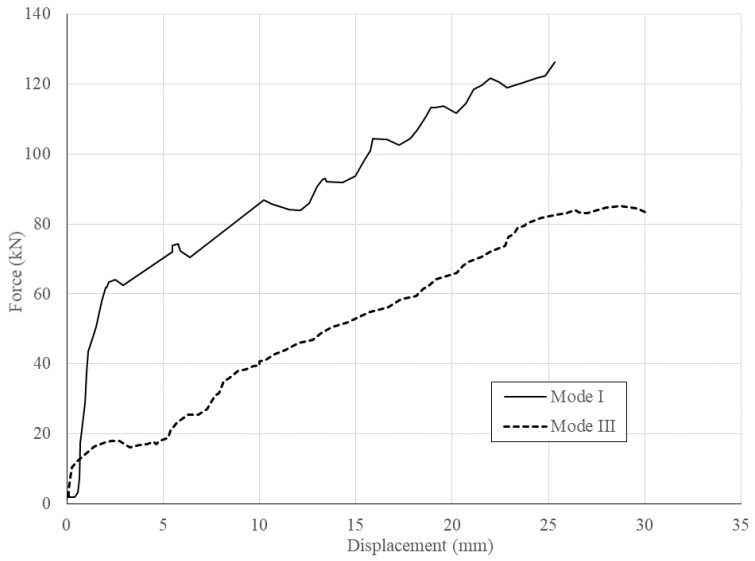

Figure 6.12: Comparison between force displacement response for perpendicular to the grain connections designed to fail in Mode I and Mode III

6.6 TDOF model of beam-connection assemblies

Wood in flexure fails in a brittle manner with limited post-peak resistance as reported by Jacques et al. (2014) and Lacroix (2017) for dimensioned lumber and glulam, respectively. This results in all of the energy dissipation of a simply supported wood beam being provided through linear-elastic deformation. A method of improving the energy dissipation and dynamic performance of brittle flexure members is to include the properties of the connections in the analysis. To investigate the benefit of including connections in the analysis, a beam-connection assembly was modeled using a TDOF model. The performance of this assembly was compared to the performance of a simply supported beam.

The resistance curve for glulam beams tested by Lacroix (2017) was used for this investigation, and is given in Figure 6.13. These beams were 137 mm wide by 222 mm deep and had a clear span of 2235 mm. They were loaded at the third points through a load transfer device and were assumed to have all the mass concentrated at these points, resulting in the load mass factor of 0.87. To determine the performance of this beam without considering the connections, the SDOF modelling software *RCBlast*® (Jacques, 2014) was used. In this model, the mass of the system was 321 kg, the loaded area was 3.55 m^2, and the loading function was a triangular load where the positive phase duration was set at 20 ms. The resulting pressure-impulse combination to fail the beam was determined to be 42.4 kPa and 424 kPa-ms.

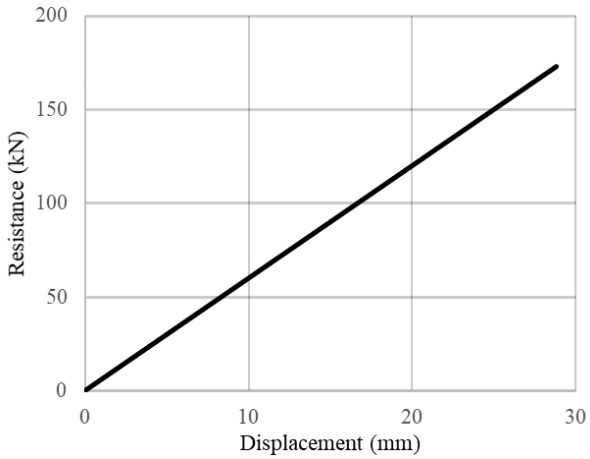

Figure 6.13: Resistance curve for glulam beam (Lacroix, 2017)

A beam-connection assembly was modelled using the TDOF software *BlasTDOF* (Viau, 2019). The same mass, loaded area, and positive phase duration were uses as for the SDOF model. The mass of the connections was neglected in this analysis by using the software's minimum connection mass of 1 kg. A beam has a connection on each of its ends, but for the purpose of TDOF modelling the properties of the two connection, which act in parallel, are summed together to provide the total properties of the connection degree-of-freedom. The connection portion of this assembly was modelled using the properties of the perpendicular to the grain connections designed to fail in Mode III. This connection configuration was chosen because connections at the ends of a beam are loaded in the perpendicular to the grain direction. The width of the beam used for these models is the same as the thickness of the wood specimens in the connections designed to fail in Mode III, therefore the experimentally determined properties of the connection can be used directly. No dynamic increase on either yield load or stiffness was recommended for this connection configuration so the static test data was used to create an idealized resistance curve for the connection. The assembly was modelled with two bolts at each end of the beam, for a total of four bolts connecting the full beam. The connection resistance curve compared to the beam's resistance curve can be seen in Figure 6.14. The ratio of the properties of the connection degree of freedom to that of the beam is presented in Table 6.1. Because the connection's ultimate resistance was greater than that of the beam, the failure of this assembly was governed by the flexural failure in the beam. This is a desirable failure mode because it allows the connections to dissipate energy and it removes the potential for failures where the member becomes completely detached from its supports. The pressure-impulse combination required to fail this beam-connection assembly was

49.7 kPa and 497 kPa-ms. This represents a 17% increase in the pressure-impulse combination over the beam by itself. This relatively small increase in performance can be attributed to the fact that even after yielding the connections had a secondary stiffness of 1.7 times the beams stiffness. If the connections had a distinct yield plateau or a significantly smaller secondary stiffness a greater increase in performance would be expected.

Based on the above analysis the following recommendations can be made:

- Ductile connections that have a yield load less than the connected member's ultimate load should be used to improve the blast performance of wood in flexure;
- To prevent premature failure of the assembly at the connection, the ultimate resistance of the connections should be at least 1.2 times the ultimate load of the connected member;

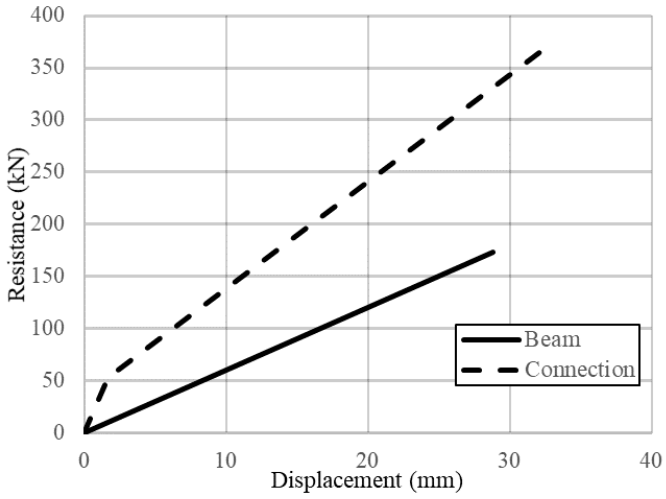

Figure 6.14: Resistance curves for bolted connection and glulam beam

Table 6.1: TDOF connection properties

Property	Value for connection	Connection / Beam
K_1[a] (kN/mm)	31.4	5.2
R_Y[b] (kN)	53.2	0.31
K_2[c] (kN/mm)	10.2	1.7
R_U[d] (kN)	372.4	2.15

[a] Initial stiffness [b] Yield Load

[c] Secondary stiffness [d] Ultimate load

6.7 Design considerations

The design philosophy of Canadian blast design standard (CSA, 2012) is to over design the connections such that the connected structural members fail before the joints. This is achieved by applying a DIF and a strength increase factor (SIF) on the static capacity of the member and requiring the connections to be designed for forces corresponding to 1.2 times the capacity of the connected members. In addition, the code provides a DIF and SIF equal to unity for wood connections. The connections are also required to fail in a ductile manner. For the design of wood structures, this approach means all the energy dissipation must come from the structural members because the connections are over designed and will not yield before the members fail. With this design approach, energy dissipation may be difficult to develop because wood in flexure is relatively brittle and possess limited ductility. As shown in the present work, wood connections, if detailed appropriately, have the potential to fail in a ductile manner and undergo large amounts of deformation before reaching their ultimate failure. If this ductility and energy dissipation is utilized in the analysis and design of the structure, the forces in structural members will be less, due to the addition of a significant source of energy dissipation. This section provides recommendations to designers to ensure that wood connections fail in a predictable manner, with sufficient ductility such that the energy dissipation in the connections can be utilized in design.

Based on the wood design standard (CSA, 2014) ductile failure modes include the crushing (failure Mode I) and yielding (failure Mode III) connections tested in this study. From the results of this work, there is a clear distinction in the level of ductility achieved between these connection configurations. The parallel to the grain connections designed to fail in Mode I had a relatively low ductility ratio (1.6) under dynamic loading. This was due to the connections being susceptible to splitting failure at relatively low displacements, despite the fact that an end distance of seven times the fastener diameter, which is greater than the minimum requirement in CSA O86 (CSA, 2014) of five times the fastener diameter, was provided. The connections designed to fail in Mode III showed more favourable behaviour when compared to the connections designed to fail in Mode I. The average ductility ratio under blast loading was 18.4, more than ten times that obtained for the connections designed to fail in Mode I. This high level of ductility was due to bending and yielding of the steel bolts. It is therefore recommended that design requirements include provisions specifically promoting yielding in the bolts by using slender fasteners (high length to diameter aspect ratio) for the purpose of blast design. This will provide more desirable

behaviour, including energy dissipation, than that allowing connections to only engage in wood crushing.

This experimental work has also shown that reinforcing parallel to the grain connections with self-tapping screws can significantly improve connection performance under blast loading. This reinforcing would be suitable for reinforcing existing connections and could be a preferred method of adding ductility to the structure rather than significantly retrofitting the structural members. Similarly, this experimental work has shown that perpendicular to the grain connections are able to develop significant ductility when the splitting failure mode was suppressed.

CHAPTER 7 – Conclusions

The following conclusions can be drawn from the current research study:

- A shock tube with a load transfer device and a support frame can be effectively used to generate high loading rates in bolted wood connections.
- An average dynamic increase of 1.2 was observed on the yield load of connections designed to fail in Mode I (i.e. wood crushing failure). For this failure mode, an average dynamic increase of 1.5 and 1.9 was observed on the initial stiffness for parallel and perpendicular to the grain connections, respectively. No significant dynamic increase on the yield load or stiffness was found for connections designed to fail in Mode III.
- A loss of ductility was observed under dynamic loading for the parallel to the grain connections designed to fail in Mode I. This was due to splitting failures occurring at lower displacements under dynamic loading than static loading. Self-tapping screw reinforcement was shown to be an effective method of preventing premature splitting failures and enhancing the performance of a connection.
- A two degree-of-freedom model was capable of modelling the connections even when the support frame had some flexibility. Lesser accuracy was found when the connection stiffness was higher than the stiffness of the supporting frame. The validated model was used to investigate cases where the connection could contribute to the energy dissipation. It was found that ductile connections that have a yield and ultimate capacities that are respectively lower and higher than the member's ultimate strength can be used to improve the blast performance of wood in flexure.
- Due to the higher level of ductility obtained in connections designed to fail in Mode III, it is recommended that the standard's design requirements include provisions specifically promoting yielding in the bolts by using slender fasteners for the purpose of blast design.

7.1 Recommendation for future work

Based on the work that has been completed to date, the following research areas and topics have been identified for future work:

- This work was limited to single bolts, while typical connections contain a group of fasteners. The introduction of group effects and the brittle failure modes of row shear,

group tear out, net tension, and splitting could have a significant impact on the behaviour of connection subjected to blast load.

- The connections designed to fail in Mode III tested in this work were limited to deformations of approximately 30 mm due to the strength of the bolts. Connections capable of deforming significantly more while still maintaining their capacity would be ideal for blast loading and should be investigated.
- This study was limited to the investigations of connections and did not consider the interaction between flexure members and the connections. Further research on this interaction could lead to the development of design procedures for flexure members with connections subjected to blast loading.

References

ASTM. (2014). *Standard Specification for Carbon Steel Bolts, Studs, and Threaded Rod 60 000 PSI Tensile Strength*. American Society for Testing and Materials.

ASTM. (2015). *ASTM D5652—Standard Test Methods for Single-Bolt Connections in Wood and Wood-Based Products*. American Society for Testing and Materials.

ASTM. (2017). *ASTM F1575-17 Standard Test Method for Determining Bending Yield Moment of Nails*. American Society for Testing and Materials.

Biggs, J. M. (1964). *Introduction to Structural Dynamics*. McGraw-Hill Inc.

Burrell, R. (2012). *Performance of Steel Fiber Reinforced Concrete Columns Under Shock Tube Induced Shock Wave Loading* (MASc). University of Ottawa, Ottawa.

CEN. (2001). *EN 12512—Timber structures—Test methods—Cyclic testing of joints made with mechanical fasteners*.

Cormie, D., Mays, G., & Smith, P. (2009). *Blast Effects on Buildings* (Second Edition). Thomas Telford Limited.

Cote, D. (2017). *Effect of Realistic Boundary Conditions on the Behaviour of Cross-Laminated Timber Elements Subjected to Simulated Blast Loads*. University of Ottawa, Ottawa.

Côté, D., & Doudak, G. (2019). Experimental Investigation of Cross-Laminated Timber Panels With Realistic Boundary Conditions Subjected to Simulated Blast Loads. *Engineering Structures*, *187*(15), 444–456.

CSA. (2012). *CSA S850—Design and Assessment of Buildings Subjected to Blast Loads*. Canadian Standards Association.

CSA. (2014). *CSA O86—Engineering Design in Wood*. Canadian Standards Association.

DHS. (2011). *Reference Manual to Mitigate Potential Terrorist Attacks Against Buildings FEMA-426*. Department of Homeland Security.

Dusenberry, D. O. (2010). *Handbook for Blast-Resistant Design of Buildings*. Hoboken, New Jersey: John Wiley & Sons, Inc.

Gilbertson, C. G., & Bulleit, W. M. (2013). Load Duration Effects in Wood at High Strain Rates. *Journal of Materials in Civil Engineering*, *25*(11), 1647–1654.

Girhammar, U. A., & Andersson, H. (1988). Effect of Loading Rate on Nailed Timber Joint Capacity. *Journal of Structural Engineering*, *114*(11), 2439–2456.

Jacques, E. (2014). RCBlast (Version 0.5.1). Retrieved from http://www.rcblast.ca/

Jacques, E., Lloyd, A., Braimah, A., Saatcioglu, M., Doudak, G., & Abdelalim, O. (2014). Influence of High Strain-Rates on the Dynamic Flexural Material Properties of Spruce–Pine–Fir Wood Studs. *Canadian Journal of Civil Engineering*, *41*(1), 56–64.

Jacques, E., Lloyd, A., & Saatcioglu, M. (2013). Predicting Reinforced Concrete Response to Blast Loads. *Canadian Journal of Civil Engineering*, *40*(5), 427–444.

Johansen, K. W. (1949). Theory of Timber Connectors. *Publications of the International Association of Bridge and Structural Engineering*, *9*, 249–262.

Krauthammer, T. (2008). *Modern Protective Structures*. Boca aton, FL: CRC Press.

Krishnappa, N., Bruneau, M., & Warn, G. P. (2014). Weak-Axis Behavior of Wide Flange Columns Subjected to Blast. *Journal of Structural Engineering*, *140*(5).

Lacroix, D. (2013). *Behaviour of Light-Frame Wood Stud Walls Subjected to Blast Loading* (MASc). University of Ottawa, Ottawa.

Lacroix, D. (2017). *Investigating the Behaviour of Glulam Beams and Columns Subjected to Simulated Blast Loading*. University of Ottawa, Ottawa.

Lacroix, D., & Doudak, G. (2015). Investigation of Dynamic Increase Factors in Light-Frame Wood Stud Walls Subjected to Out-of-Plane Blast Loading. *Journal of Structural Engineering*, *141*(6).

Lacroix, D., & Doudak, G. (2018a). Determining the Dynamic Increase Factor for Glued-Laminated Timber Beams. *Journal of Structural Engineering*, *144*(9).

Lacroix, D., & Doudak, G. (2018b). Effects of High Strain Rates on the Response of Glulam Beams and Columns. *Journal of Structural Engineering*, *144*(5).

Lacroix, D., & Doudak, G. (2018c). Experimental and Analytical Investigation of FRP Retrofitted Glued-Laminated Beams Subjected to Simulated Blast Loading. *Journal of Structural Engineering*, *144*(7).

Larsen, H. J. (1973). The Yield Load of Bolted and Nailed Joints. *Proceedings, International Union of Forestry Research Organization Meeting - 5th Congress*. Presented at the South Africa. South Africa.

Larsen, H. J. (1979). Design of Bolted Joints. *International Council for Building Research Studies and Documentation, Working Commission W 18—Timber Structures*. Presented at the Bordeaux, France. Bordeaux, France.

Markwardt, L. J., & Liska, J. A. (1956). *The Influence of Rate of Loading on the Strength of Wood and Wood-Base Materials*. *185*, 3–18. Atlantic City, N.J., USA: ASTM International.

Mays, C. G., Heterington, J. G., & Rose, T. A. (1999). Response to Blast Loading of Concrete Wall Panels with Openings. *Journal of Structural Engineering*, *125*(12), 1448–1450.

Möller, T. (1950). En ny Metod För Beräkning av Spikförband: New Method of Estimating the Bearing Strength of Nailed Wood Connections (in Swedish and English translation). *Chalmers Tekniska Högskolas Handlingar, No. 117*.

Nadeau, J. S., Bennett, R., & Fuller, E. R. (1982). An Explanation of the Rate-of-Loading and the Duration-of-Load Effects in Wood in Terms of Fracture Mechanics. *Journal of Materials Science*, *17*(10), 2831–2840.

Nassr, A. A., Razaqpur, A. G., Tait, M., Campidelli, M., & Foo, S. (2014). Dynamic Response of Steel Columns Subjected to Blast Loading. *Journal of Structural Engineering*, *140*(7).

Newmark, N. (1959). A Method of Computation for Structural Dynamics. *Journal of the Engineering Mechanics Division, 85*, 67–94.

Paultre, P. (2011). *Dynamics of Structures*. ISTE Ltd.

Poulin, M. (2019). *Behaviour of Cross-Laminated Timber Subjected to Blast Loading* (MASc). University of Ottawa.

Poulin, M., Viau, C., Lacroix, D., & Doudak, G. (2018). Experimental and Analytical Investigation of Cross-Laminated Timber Panels Subjected to Out-of-Plane Blast Loads. *Journal of Structural Engineering*, *144*(2).

Rosowsky, D. V., & Reinhold, T. A. (1999). Rate-of-Load and Duration-of-Load Effects for Wood Fasteners. *Journal of Structural Engineering*, *125*(7), 719–724.

Silva, P. F., & Lu, B. (2009). Blast Resistance Capacity of Reinforced Concrete Slabs. *Journal of Structural Engineering*, *135*(6), 708–716.

Soroushian, P., & Choi, K.-B. (1987). Steel Mechanical Properties at Different Strain Rates. *Journal of Structural Engineering*, *113*(4), 663–672.

Spencer, R. (1978). *Rate of Loading Effect in Bending for Douglas-Fir Lumber*. Presented at the 1st International Conference on Wood Fracture, Banff, Alberta, Canada.

Sukontasukkul, P., Lam, F., & Mindess, S. (2000). Fracture of Parallel Strand Lumber (PSL) Under Impact Loading. *Materials and Structures*, *33*(7), 445–449.

Syron, W. D. (2008). *Strain Rate Dependent Behavior of Laminated Strand Lumber*. The University of Maine, Maine.

USACE. (2008). *Methodology Manual for the Single-Degree-of-Freedom Blast Effects Design Spreadsheets (SBEDS)* (No. PDC TR-06-01 Rev 1). U.S. Army Corps of Engineers.

USADD. (2008). *Structures to Resist the Effects of Accidental Explosions* (No. UFC 3-340-02). Department of Defence.

USADD. (2009). *Design of Buildings to Resist Progressive Collapse* (No. UFC 4-023-03). Department of Defence.

Viau, C. (2016). *Investigating the Response of Light-Frame Wood Stud Walls With and Without Boundary Connections to Blast Loads*. University of Ottawa, Ottawa.

Viau, C. (2019). BlasTDOF (Version 0.1.3). Retrieved from https://www.cviau.ca/blastdof.html

Viau, C., & Doudak, G. (2016a). Investigating the Behavior of Light-Frame Wood Stud Walls Subjected to Severe Blast Loading. *Journal of Structural Engineering*, *142*(12).

Viau, C., & Doudak, G. (2016b). Investigating the Behaviour of Typical and Designed Wall-to-Floor Connections in Light-Frame Wood Stud Wall Structures Subjected to Blast Loading. *Canadian Journal of Civil Engineering*, *43*(6), 562–572.

Viau, C., & Doudak, G. (2019). Behaviour and Modelling of Cross-Laminated Timber Panels with Boundary Connections Subjected to Blast Loads. *Engineering Structures*, *197*, 1–17.

Warn, G. P., & Bruneau, M. (2009). Blast Resistance of Steel Plate Shear Walls Designed for Seismic Loading. *Journal of Structural Engineering*, *135*(10), 1222–1230.

Whale, L. R. J., Smith, I., & Larsen, H. J. (1987). Design of Nailed and Bolted Joints Proposals for the Revision of Existing Formulae in Draft Eurocode V and the CIB Code. *International Council for Building Research Studies and Documentation Working Commission W18A - Timber Structures*.

Widehammar, S. (2004). Stress–Strain Relationships for Spruce Wood: Influence of Strain Rate, Moisture Content and Loading Direction. *Experimental Mechanics*, *44*(1), 44–48.

Williams, G. D., & Williamson, E. B. (2011). Response of Reinforced Concrete Bridge Columns Subjected to Blast Loads. *Journal of Structural Engineering*, *137*(9), 903–913.

Yu, J., Rinder, T., Stolz, A., Tan, K.-H., & Riedel, W. (2014). Dynamic Progressive Collapse of an RC Assemblage Induced by Contact Detonation. *Journal of Structural Engineering*, *140*(6).

Appendix A – Static Test Results

Specimen: E0S[1]

Ultimate Failure Mode: Splitting

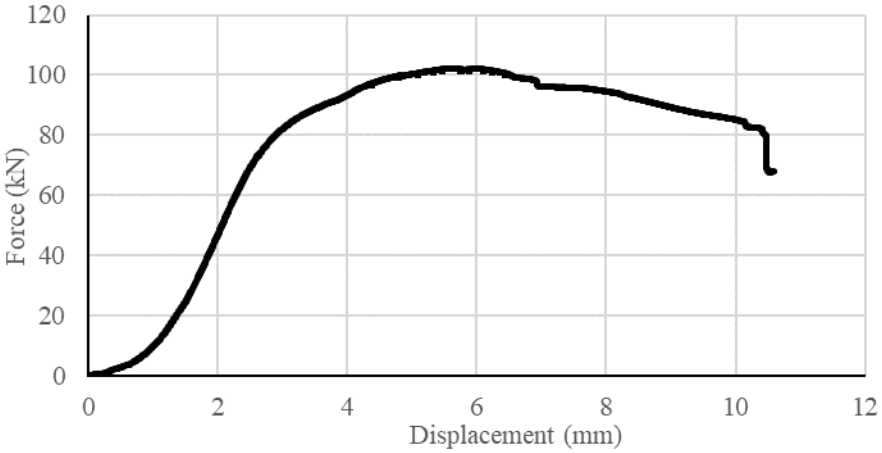

Figure A.1: Force displacement response for E0S[1]

(a) Splitting failure

(b) Crushing in bolt hole

(c) Slight bend in bolt

Figure A.2: Specimen E0S[1] after testing

Specimen: E0S[2]

Ultimate Failure Mode: Splitting

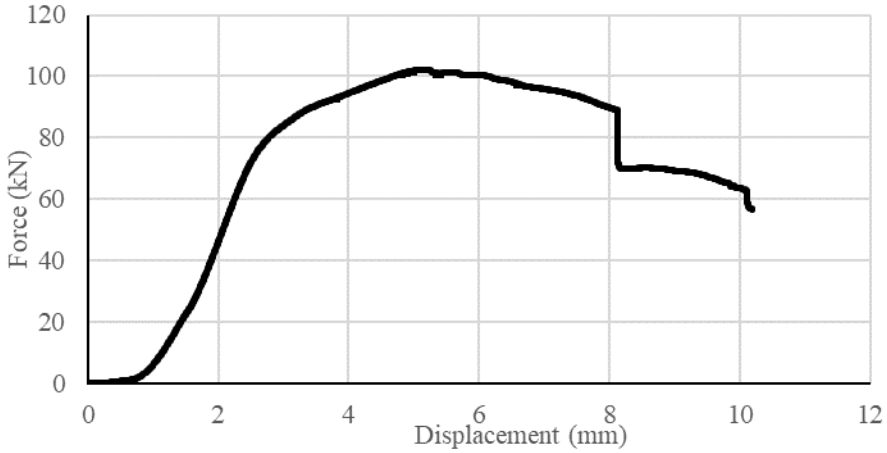

Figure A.3: Force displacement response for E0S[2]

(a) Splitting failure

(b) Crushing in bolt hole

(c) Slight bend in bolt

Figure A.4: Specimen E0S[2] after testing

Specimen: E0S[3]

Ultimate Failure Mode: Splitting

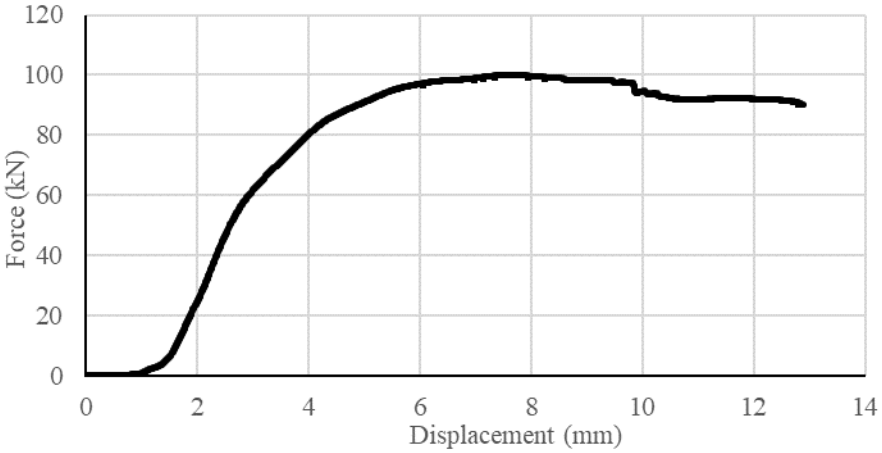

Figure A.5: Force displacement response for E0S[3]

(a) Splitting failure

(b) Crushing in bolt hole

(c) Slight bend in bolt

Figure A.6: Specimen E0S[3] after testing

Specimen: E0S[4]

Ultimate Failure Mode: Splitting

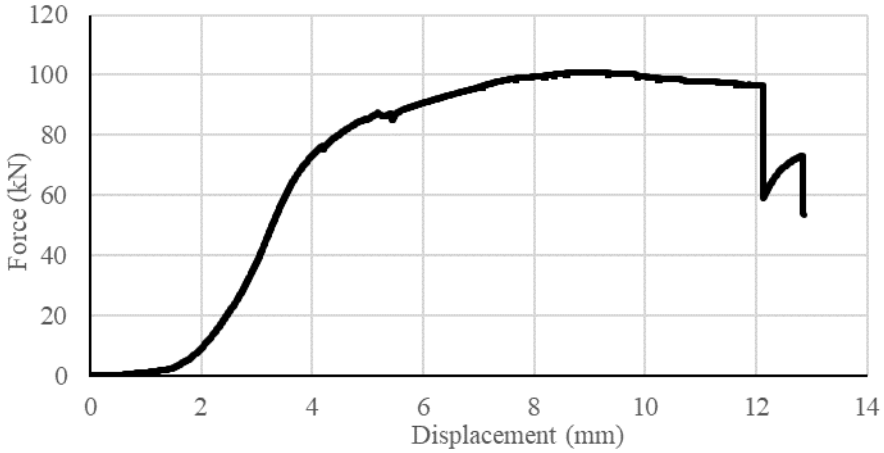

Figure A.7: Force displacement response for E0S[4]

(a) Splitting failure

(b) Crushing in bolt hole

(c) Slight bend in bolt

Figure A.8: Specimen E0S[4] after testing

Specimen: E0S[5]

Ultimate Failure Mode: Splitting

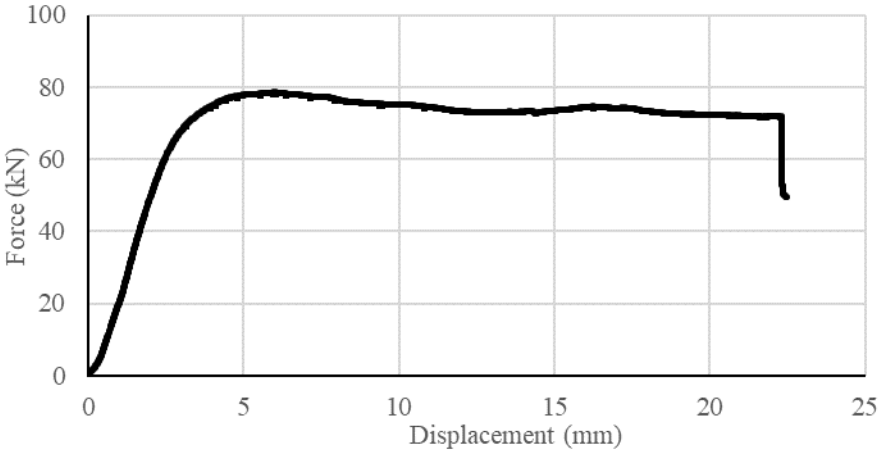

Figure A.9: Force displacement response for E0S[5]

(a) Splitting failure

(b) Crushing in bolt hole

(c) No bending in bolt

Figure A.10: Specimen E0S[5] after testing

Specimen: E90S[1]

No Ultimate Failure

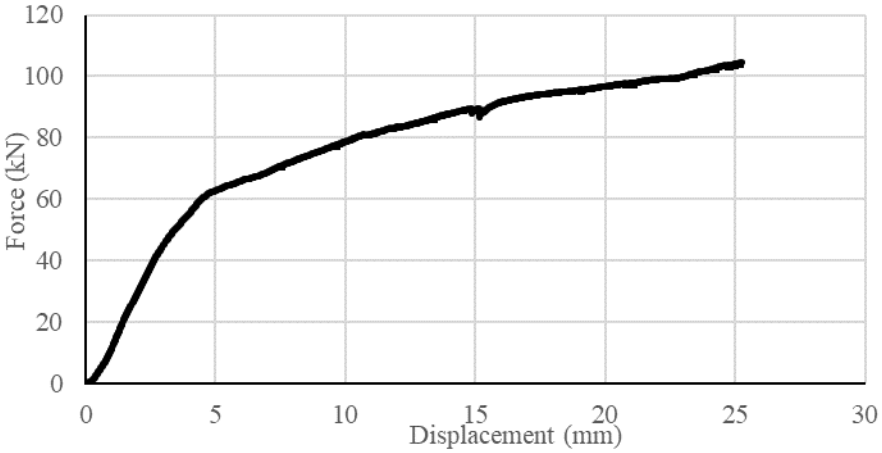

Figure A.11: Force displacement response for E90S[1]

(a) Specimen after testing

(b) Crushing in bolt hole

(c) No bending in bolt

Figure A.12: Specimen E90S[1] after testing

Specimen: E90S[2]

No Ultimate Failure

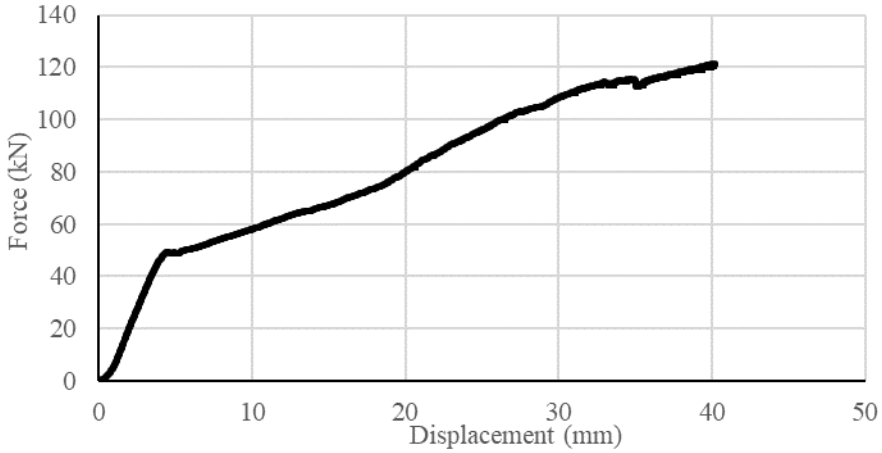

Figure A.13: Force displacement response for E90S[2]

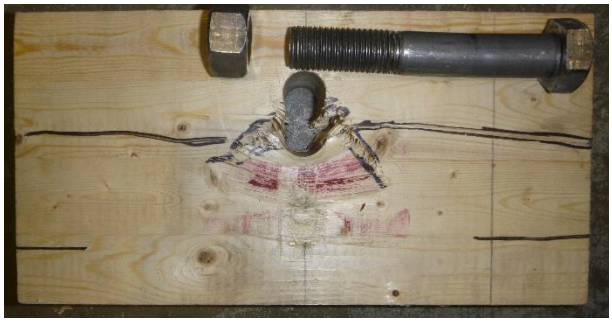

(a) Specimen after testing

(b) Crushing in bolt hole

(c) No bending in bolt

Figure A.14: Specimen E90S[2] after testing

Specimen: E90S[3]

No Ultimate Failure

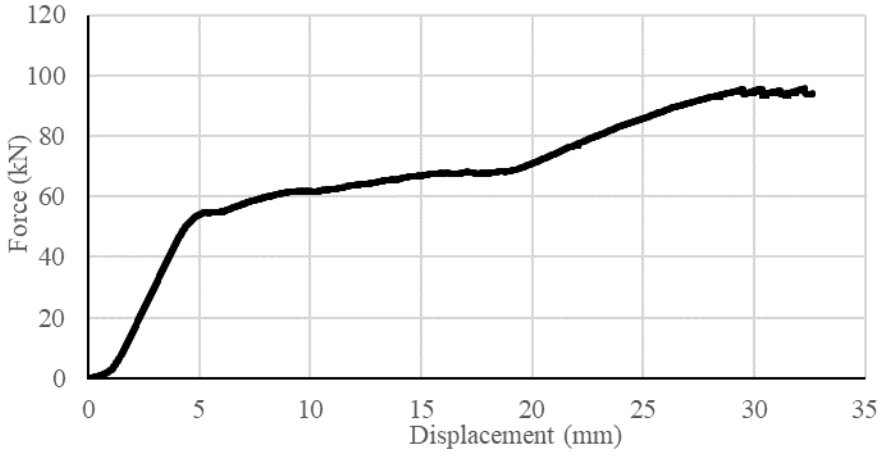

Figure A.15: Force displacement response for E90S[3]

(a) Specimen after testing

(b) Crushing in bolt hole

(c) No bending in bolt

Figure A.16: Specimen E90S[3] after testing

Specimen: Y0S[1]

Ultimate Failure Mode: Bolt shear

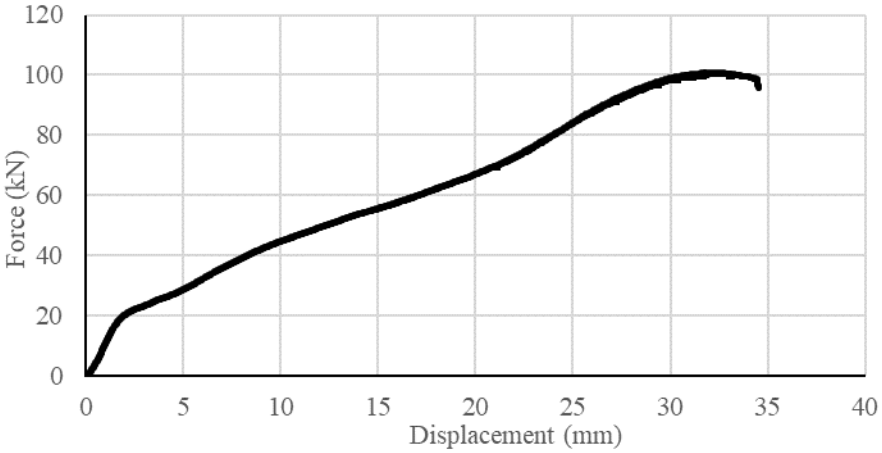

Figure A.17: Force displacement response for Y0S[1]

(a) Specimen cut open to observe crushing in wood

(b) Crushing at bolt hole edge

(c) Deformed shape of bolt and shear failure on nut side

Figure A.18: Specimen Y0S[1] after testing

Specimen: Y0S[2]

Ultimate Failure Mode: Bolt shear

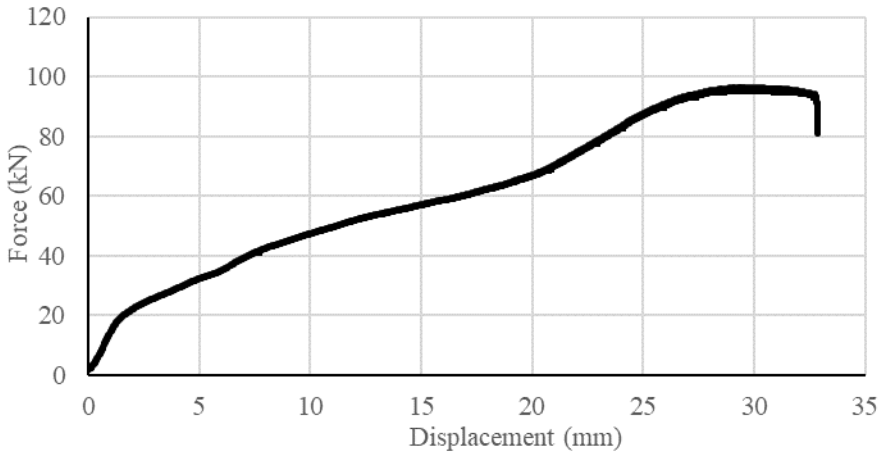

Figure A.19: Force displacement response for Y0S[2]

(a) Specimen after testing, bolt head side

(b) Specimen after testing, nut side

(c) Crushing at bolt hole edge

(d) Shear failure at bolt head

Figure A.20: Specimen Y0S[2] after testing

Specimen: Y0S[3]

Ultimate Failure Mode: Bolt shear

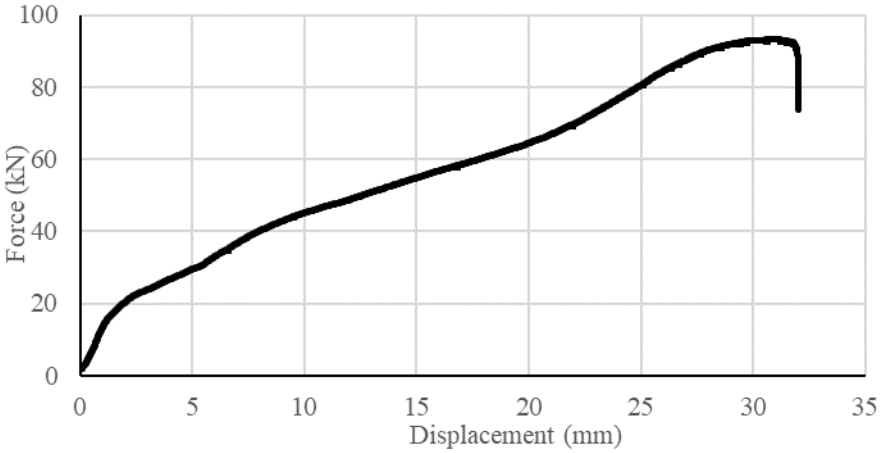

Figure A.21: Force displacement response for Y0S[3]

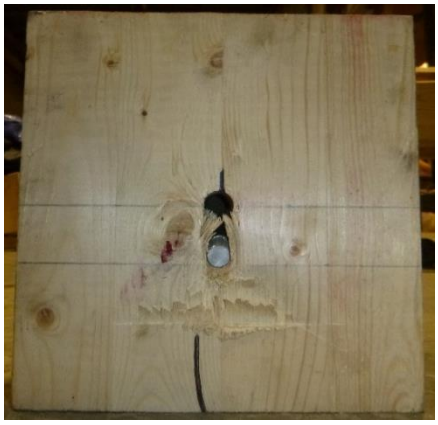

(a) Specimen after testing, bolt head side

(b) Specimen after testing, nut side

(c) Crushing at bolt hole edge

(d) Shear failure at bolt head

Figure A.22: Specimen Y0S[3] after testing

Specimen: Y90S[1]

Ultimate Failure Mode: Bolt shear

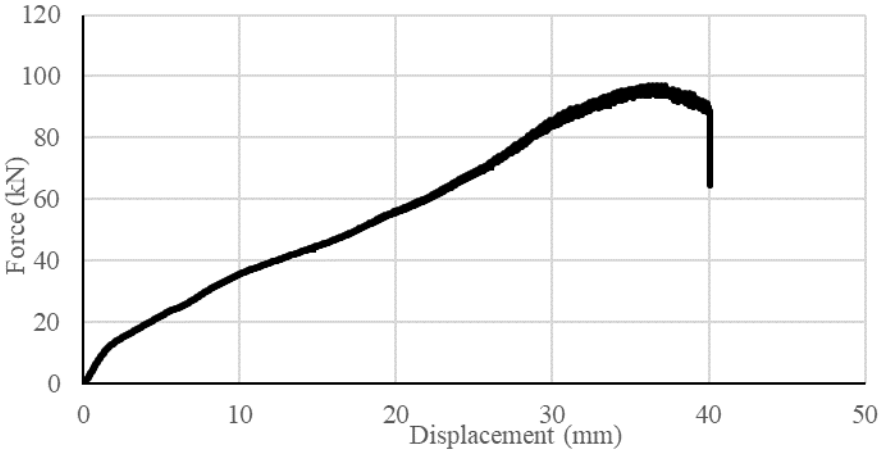

Figure A.23: Force displacement response for Y90S[1]

(a) Specimen after testing

(b) Crushing at bolt hole edge

(c) Deformed shape of bolt and shear failure on nut side

Figure A.24: Specimen Y90S[1] after testing

Specimen: Y90S[2]

Ultimate Failure Mode: Bolt shear

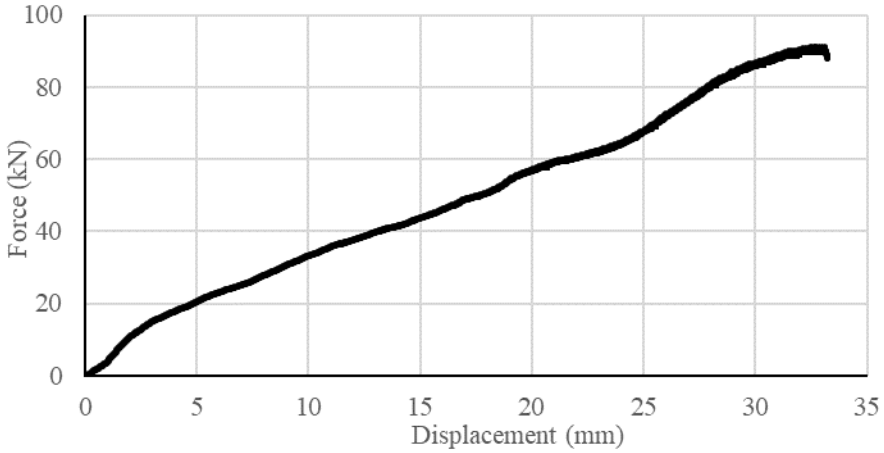

Figure A.25: Force displacement response for Y90S[2]

(a) Specimen after testing, bolt head side

(b) Specimen after testing, nut side

(c) Crushing at bolt hole edge

(d) Shear failure at bolt head

Figure A.26: Specimen Y90S[2] after testing

Specimen: Y90S[3]

Ultimate Failure Mode: Bolt shear

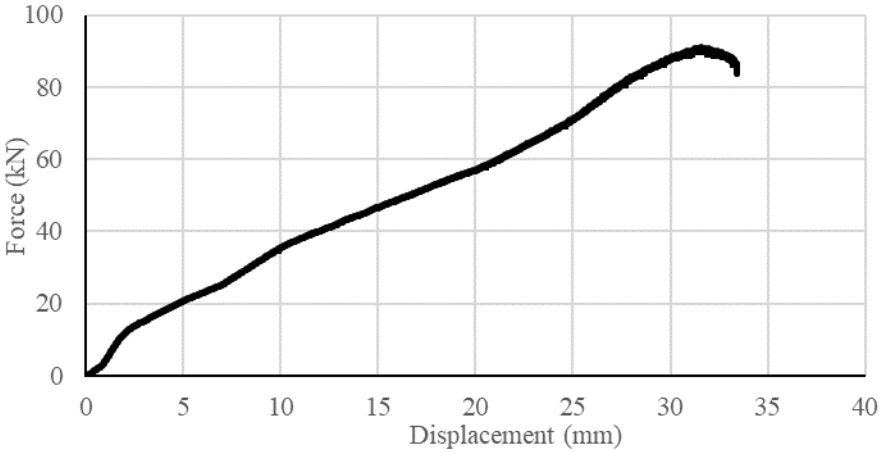

Figure A.27: Force displacement response for Y90S[3]

(a) Specimen after testing, bolt head side

(b) Specimen after testing, nut side

(c) Crushing at bolt hole edge

Figure A.28: Specimen Y90S[3] after testing

Appendix B – Dynamic Test Results

Table B.1: Dynamic connection test results

Test Name	P_D[a] (kPa)	P_R[b] (kPa)	I_R[c] (kPa-ms)	t_d[d] (ms)	K[e] (N/mm)	F_y[f] (kN)	d_y[g] (mm)	F_u[h] (kN)	d_u[i] (mm)	μ[j]
E0D[1]	243.4	32.2	255.5	15.4	35,500			No yielding		
E0D[2]	277.9	38.9	366.3	15.0	28,700					
E0D[3]	485.4	59.8	488.1	15.8	57,400	117.2	3.3	118.2	5.9	1.7
E0D[4]	481.9	59.0	473.7	16.6	47,400	92.8	3.1	99.2	3.2	1.0
E0D[5]	446.1	56.5	491.3	20.8	55,200	103.2	3.0	109.8	5.9	2.0
E0D[6]	455.1	59.5	452.3	14.8	58,700	108.5	3.0	No ultimate failure		
E0D[7]	450.9	54.6	621.1	23.8	34,700	97.8	4.0	112.6	28.1	5.9
E0D[8]	451.6	59.8	659.0	24.0	40,500	121.2	4.3	124.2	No ultimate failure	5.3
E0D[9]	499.2	81.7	724.4	22.0	112,800	111.2	2.2	116.9	26.7	12.1
E90D[1]	435.7	54.4	549.8	23.4	28,700	62.3	1.7			
E90D[2]	435.7	52.4	533.0	23.4	28,300	71.2	2.2	No ultimate failure		
E90D[3]	435.7	55.6	555.9	21.4	35,900	60.6	2.5			
Y0D[1]	312.3	36.9	425.5	23.6	20,400	26.1	1.3	77.0	25.3	19.5
Y0D[2]	277.9	39.9	355.6	21.0	16,000	22.2	1.4	No ultimate failure		
Y0D[3]	313.0	43.6	402.1	20.8	15,100	25.6	1.6	96.8	27.7	17.3
Y0D[4]	333.0	44.6	387.6	21.0	38,300	23.1	0.6	93.7	30.5	50.8
Y0D[5]	319.2	45.4	396.9	20.8	14,400	24.1	1.1	96.8	29.2	26.5
Y0D[6]	322.0	45.1	419.6	20.8	15,100	23.7	1.6	93.7	34.3	21.4
Y90D[1]	314.4	43.5	403.8	20.4	-	-	-	99.8	31.9	-
Y90D[2]	312.3	44.3	396.6	20.2	-	-	-	94.6	31.8	-
Y90D[3]	312.3	39.5	403.7	21.2	20,400	16.2	0.8	85.1	30.8	38.5

[a] Driver pressure [b] Reflected pressure [c] Reflected impulse [d] Positive phase duration

[e] Initial Stiffness [f] Yield strength [g] Displacement at yield [h] Ultimate strength

[i] Displacement at failure [j] Ductility

Specimen: E0D[1]

Comments: Specimen remained linear elastic

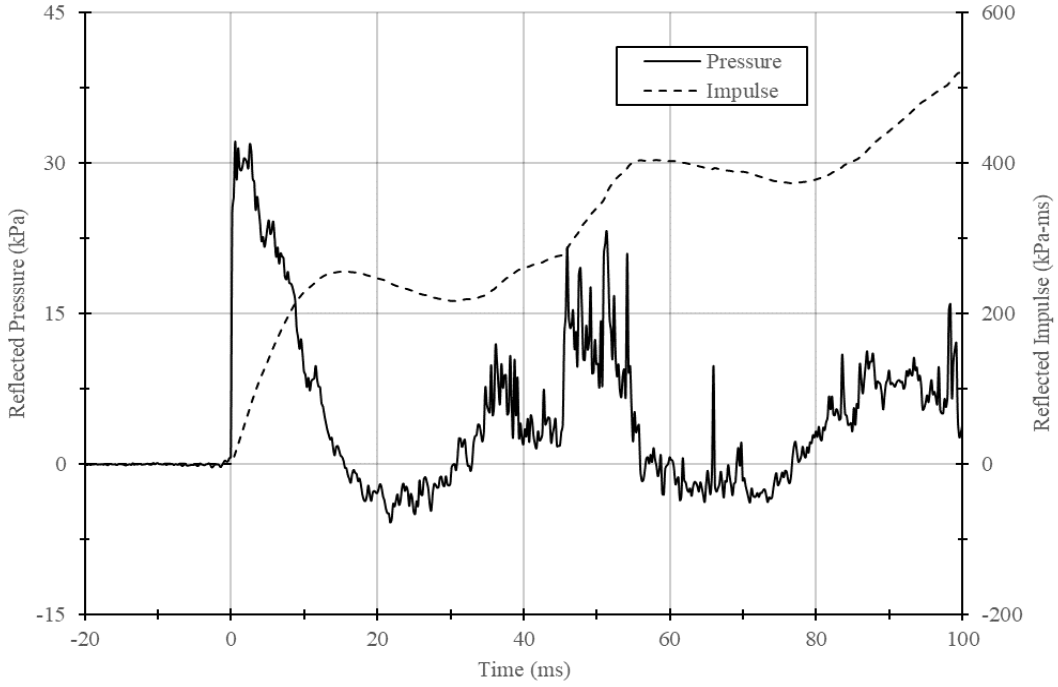

Figure B.1: Reflected pressure and impulse time histories for E0D[1]

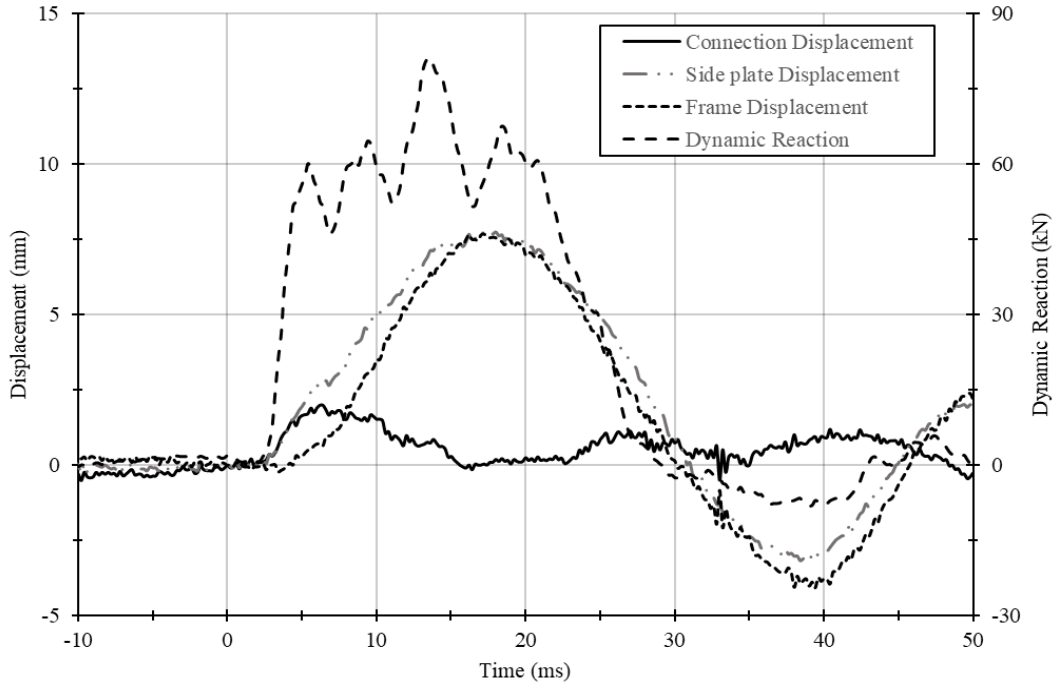

Figure B.2: Displacement and reaction time histories for E0D[1]

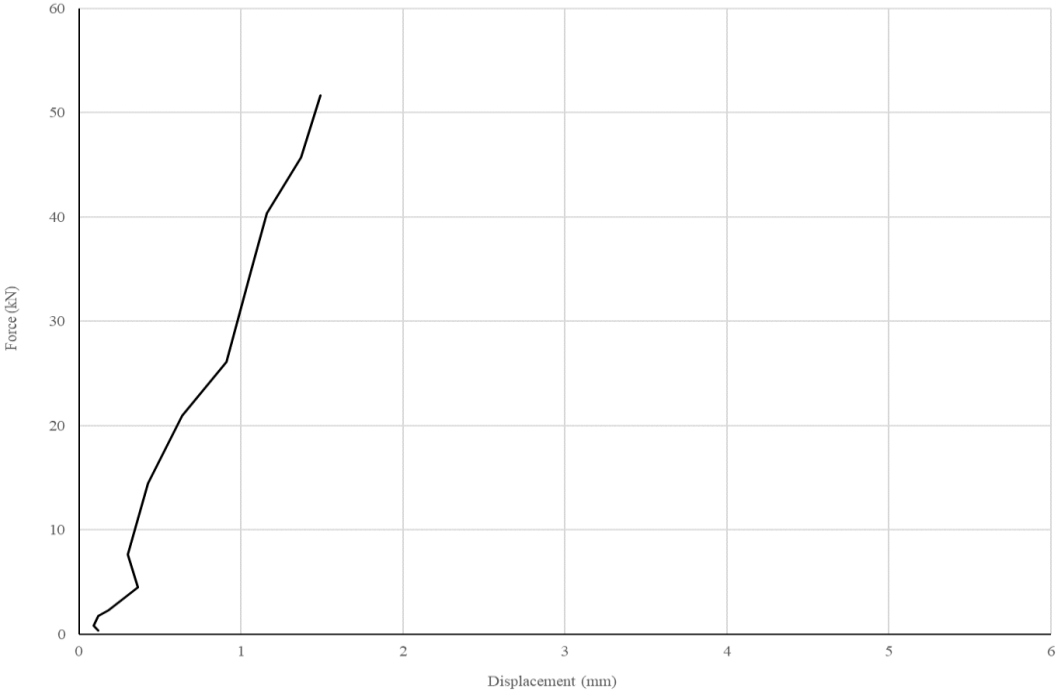

Figure B.3: Force displacement curve for E0D[1]

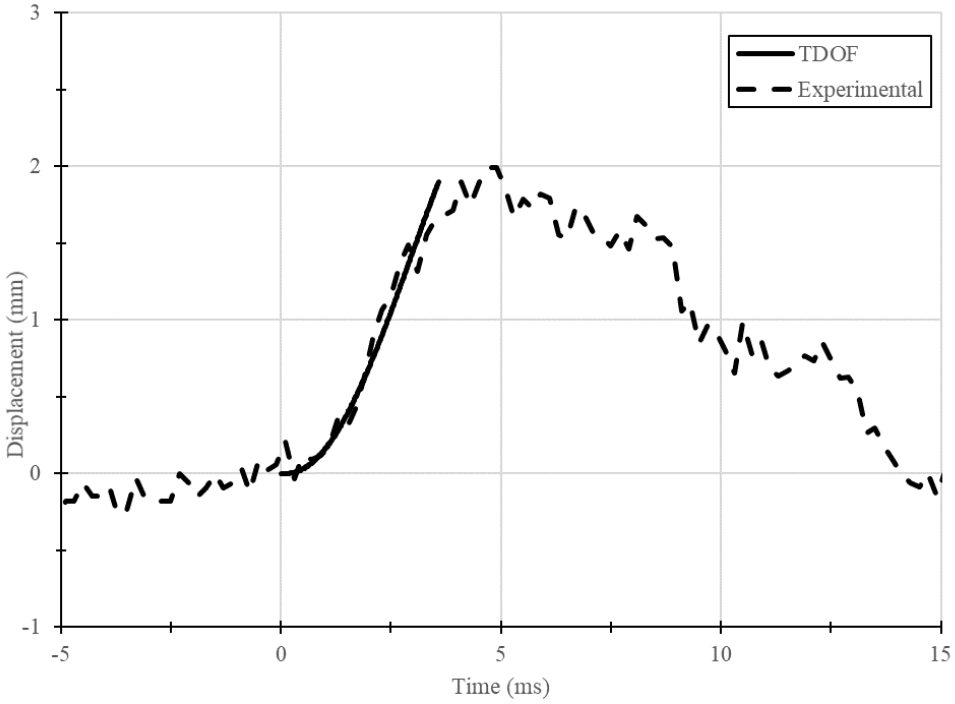

Figure B.4: TDOF prediction for E0D[1]

(a) Specimen after testing

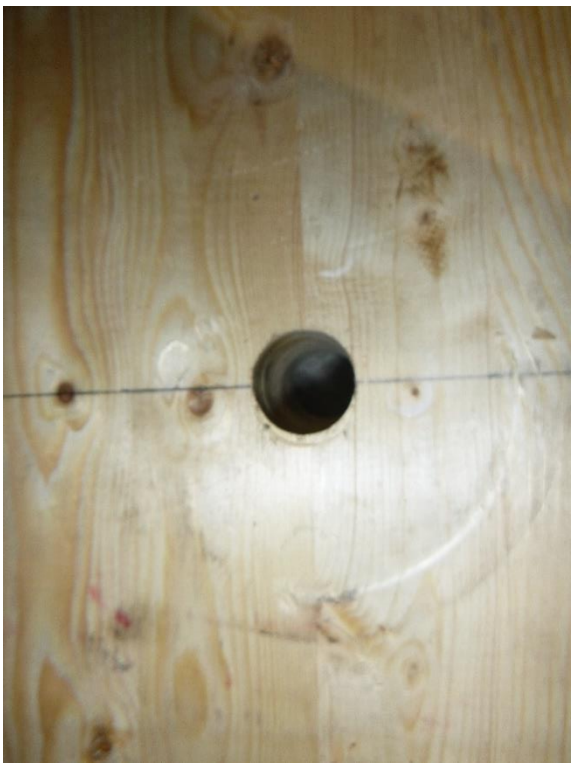

(b) Minimal crushing in bolt hole

(c) No bending in bolt

Figure B.5: Specimen E0D[1] after testing

Specimen: E0D[2]

Comments: Specimen remained linear elastic

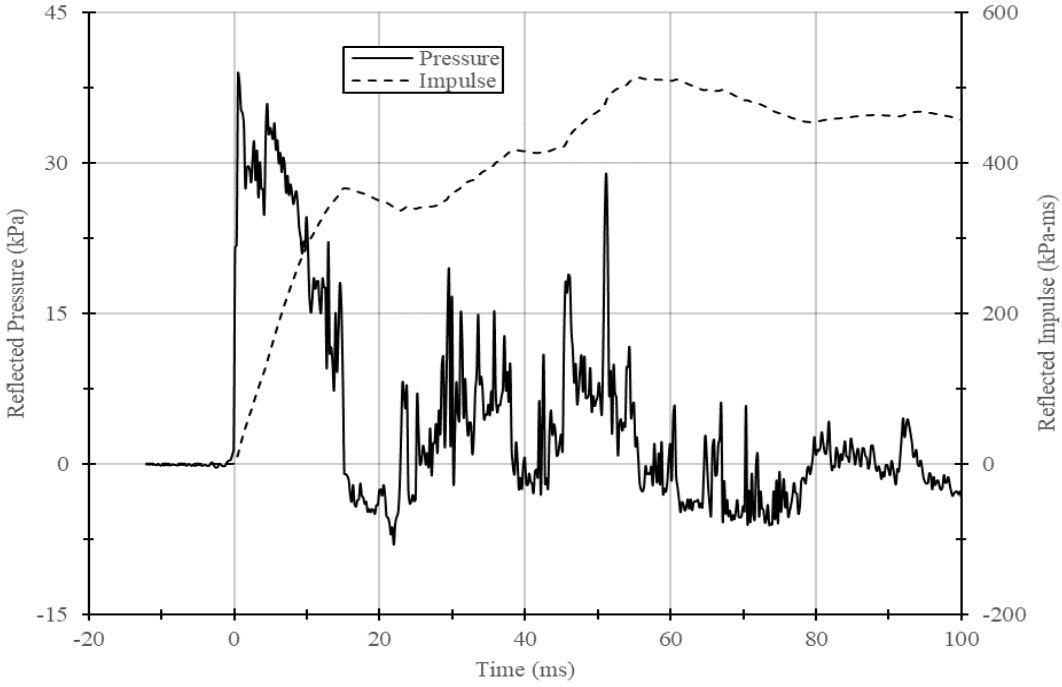

Figure B.6: Reflected pressure and impulse time histories for E0D[2]

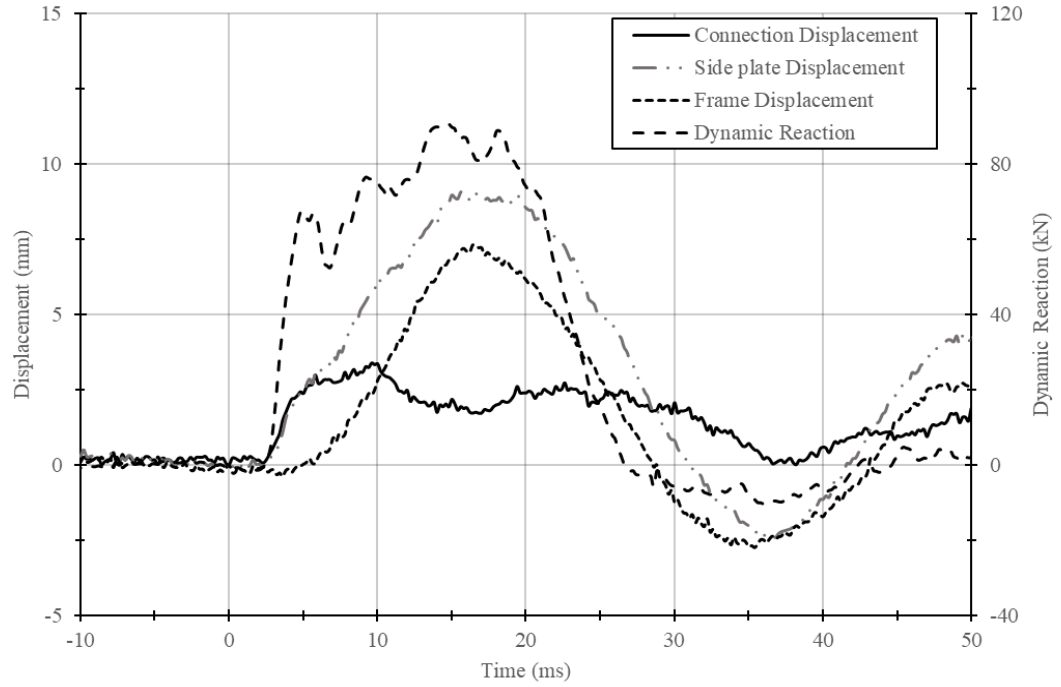

Figure B.7: Displacement and reaction time histories for E0D[2]

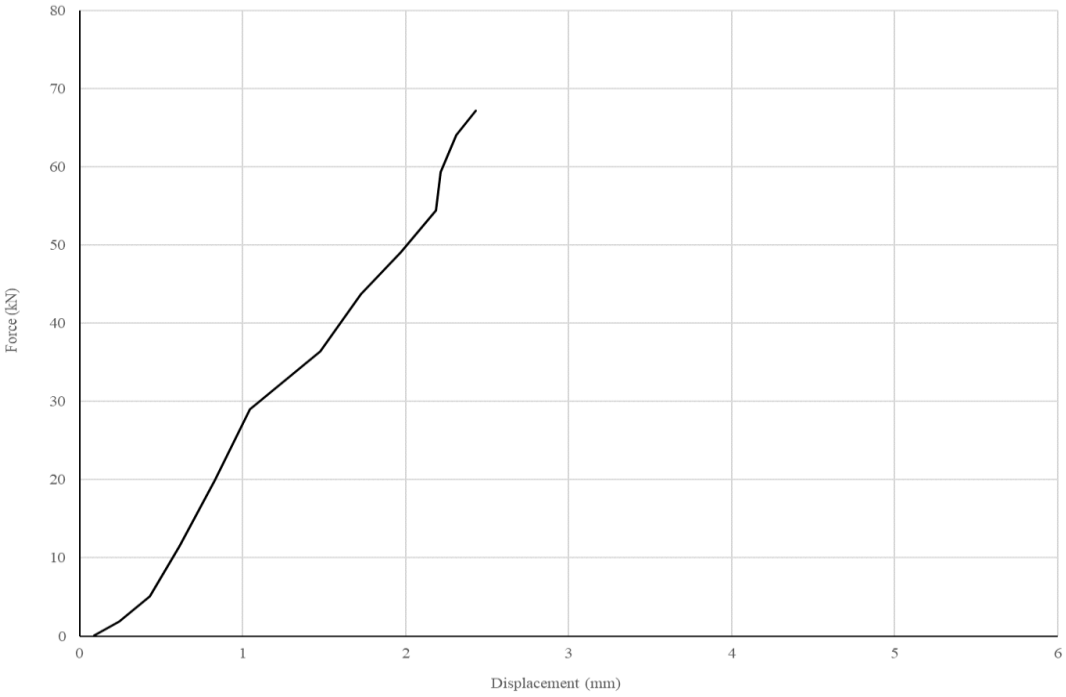

Figure B.8: Force displacement curve for E0D[2]

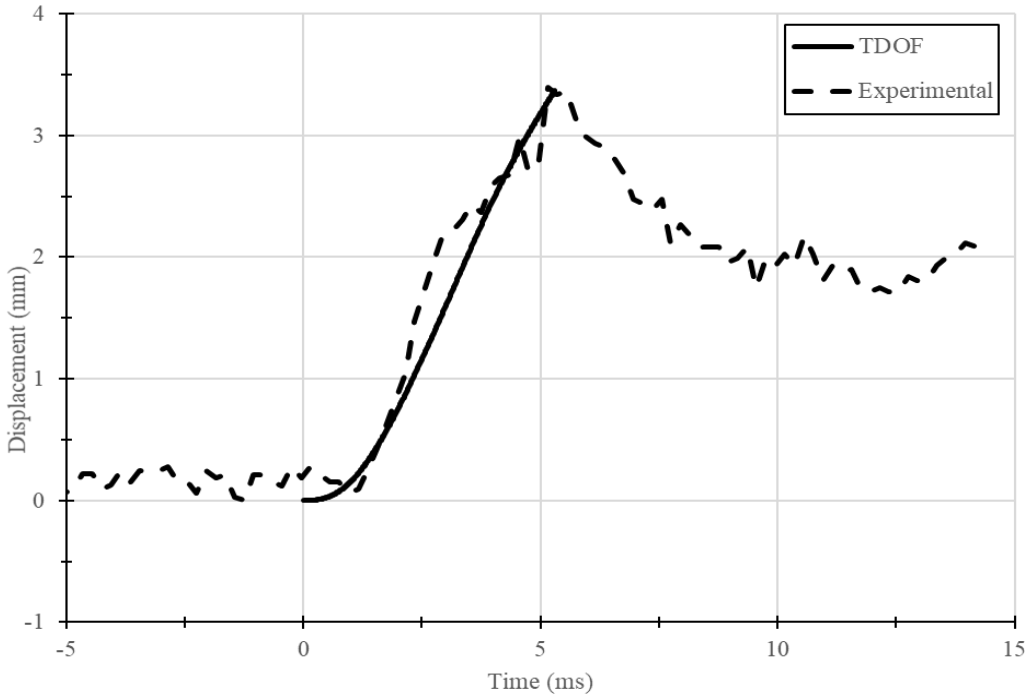

Figure B.9: TDOF prediction for E0D[2]

(a) Specimen after testing

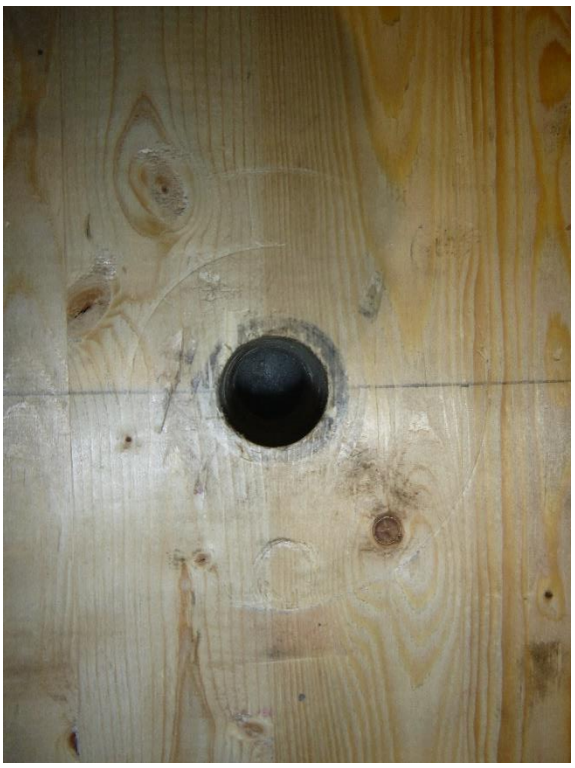

(b) Minimal crushing in bolt hole

(c) No bending in bolt

Figure B.10: Specimen E0D[2] after testing

Specimen: E0D[3]

Comments: Specimen failed in splitting

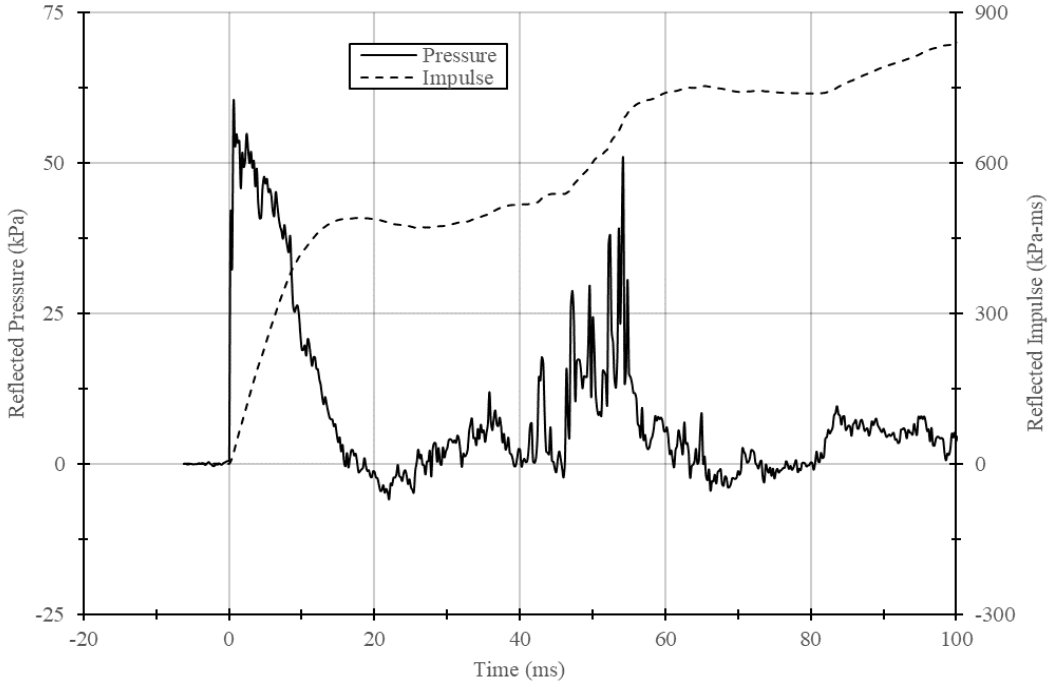

Figure B.11: Reflected pressure and impulse time histories for E0D[3]

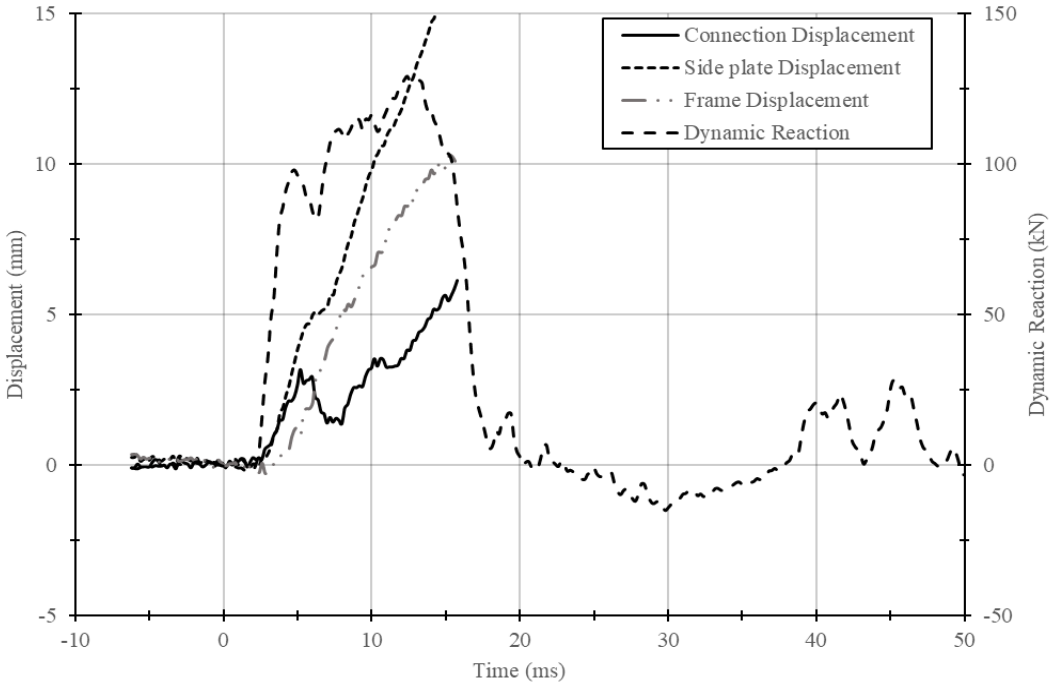

Figure B.12: Displacement and reaction time histories for E0D[3]

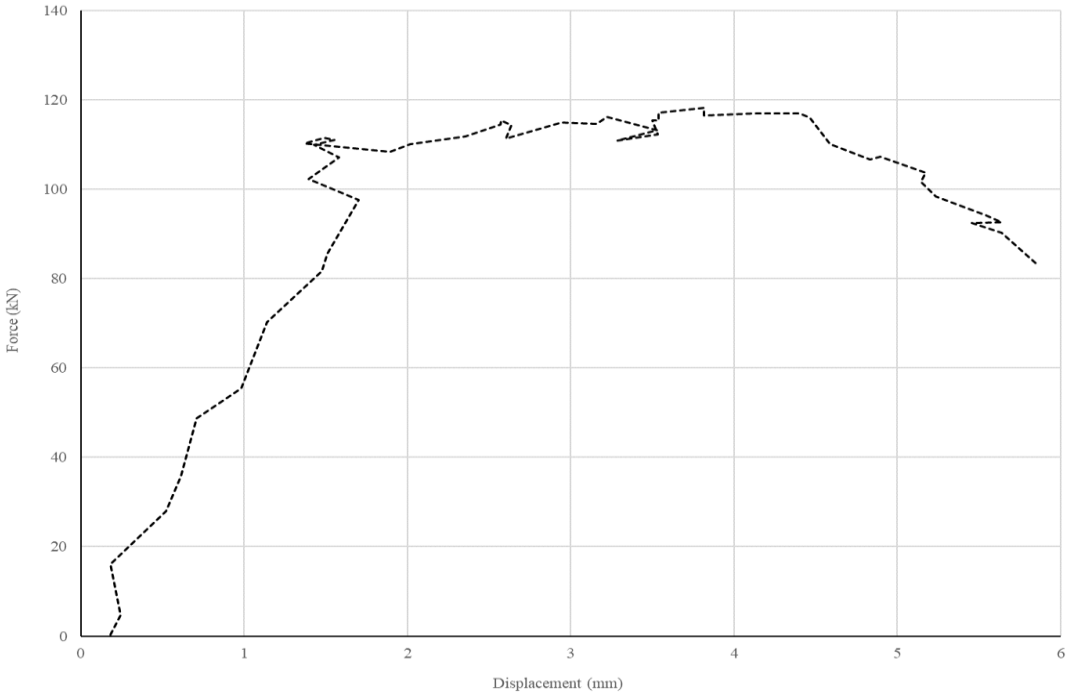

Figure B.13: Force displacement curve for E0D[3]

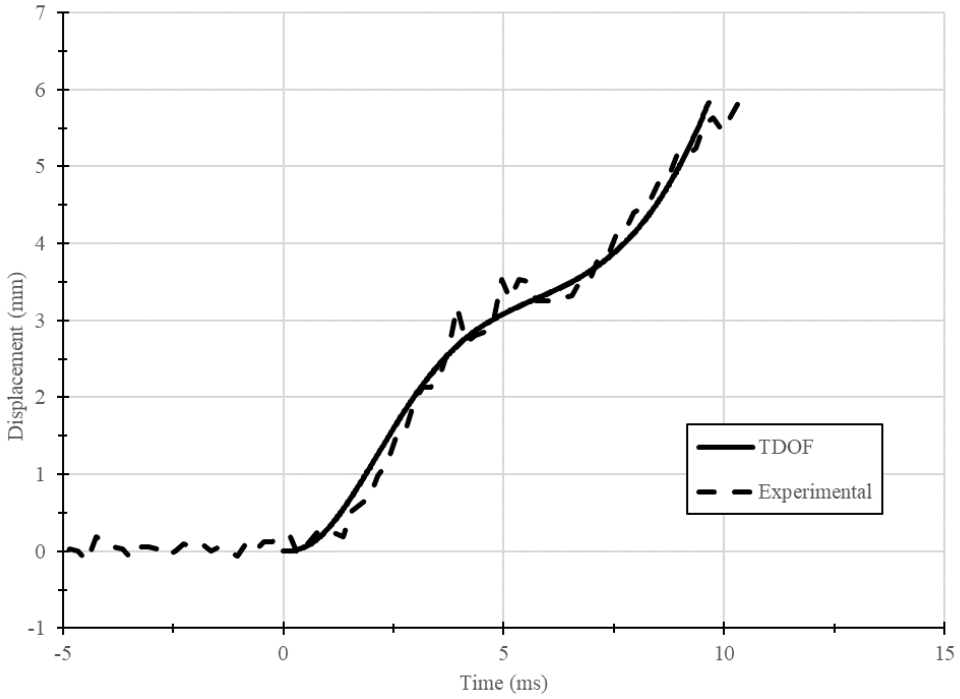

Figure B.14: TDOF prediction for E0D[3]

(a) Splitting failure

(b) Minimal crushing in bolt hole before splitting

(c) Slight bending in bolt

Figure B.15: Specimen E0D[3] after testing

Specimen: E0D[4]

Comments: Specimen failed in splitting

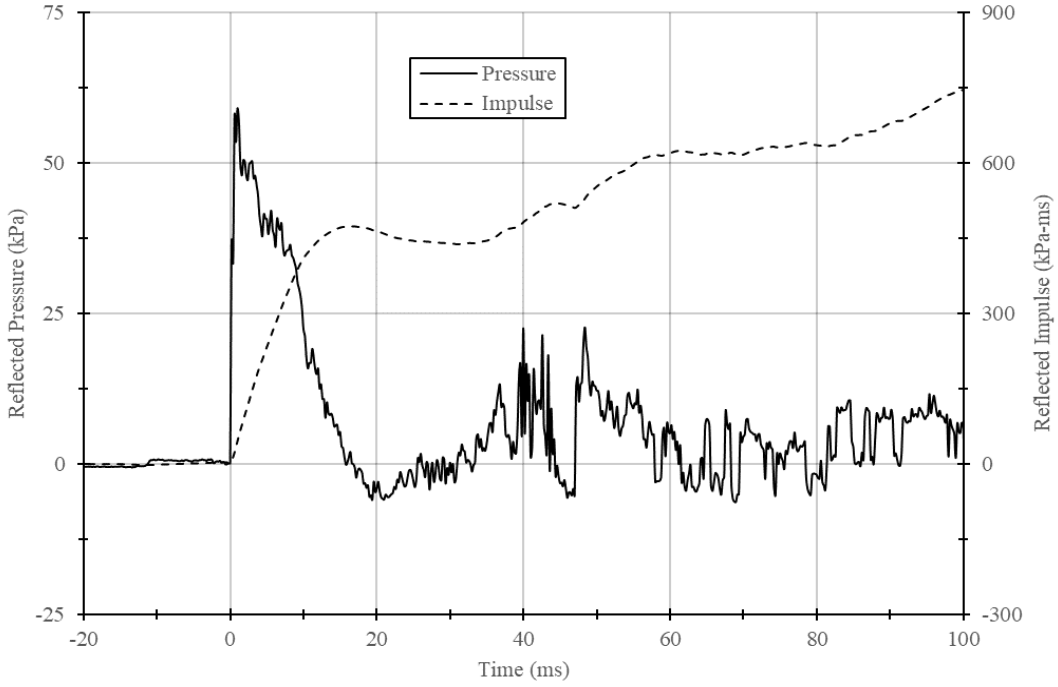

Figure B.16: Reflected pressure and impulse time histories for E0D[4]

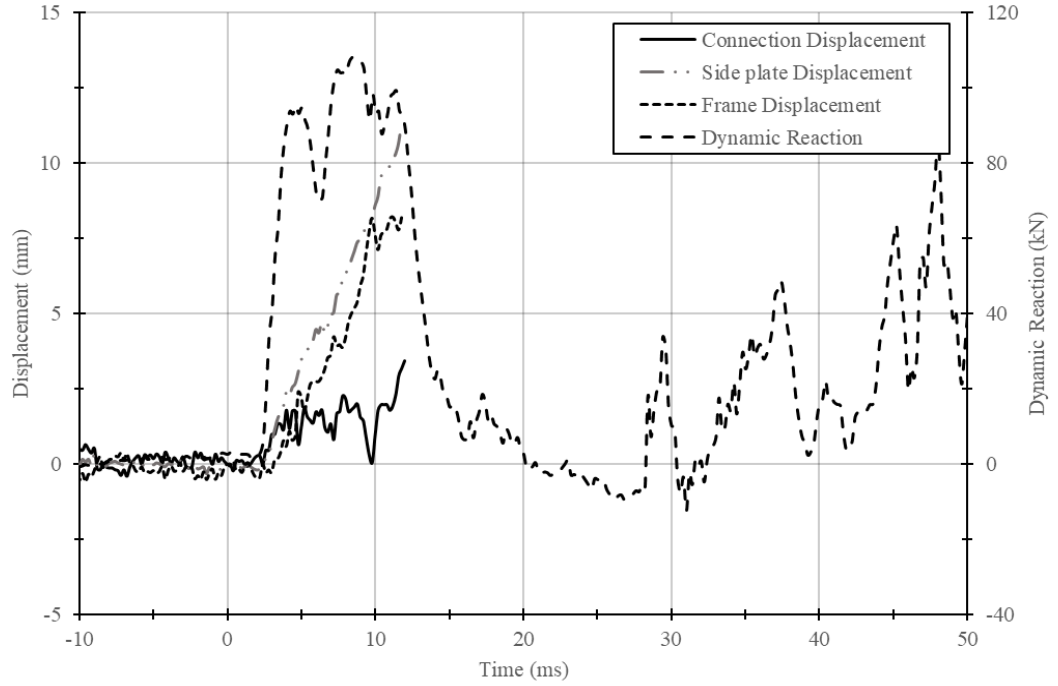

Figure B.17: Displacement and reaction time histories for E0D[4]

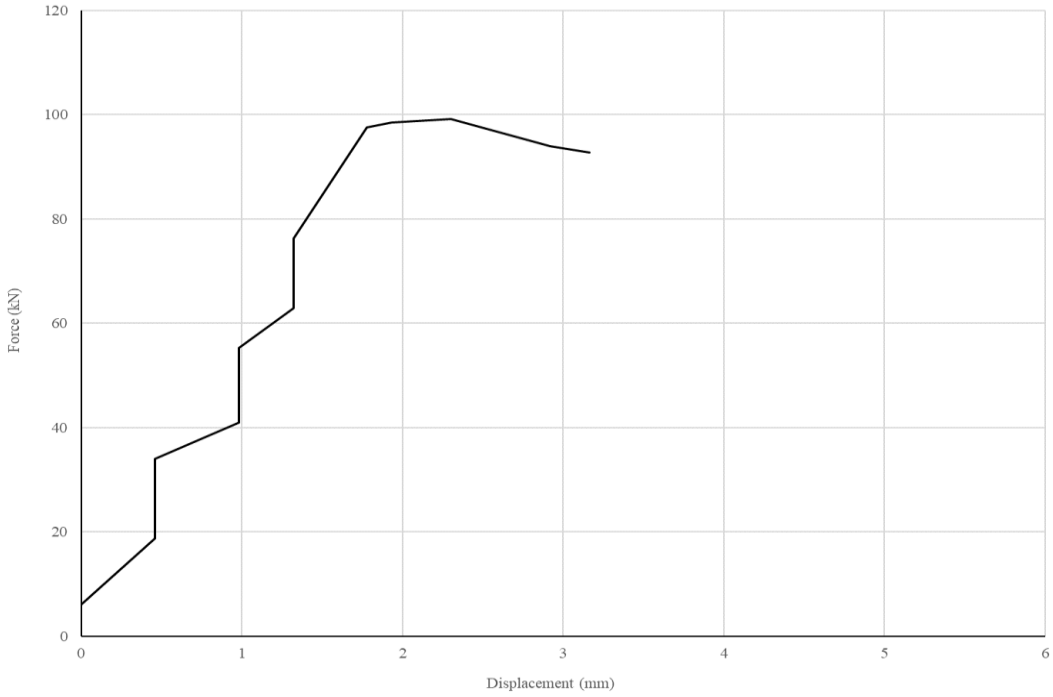

Figure B.18: Force displacement curve for E0D[4]

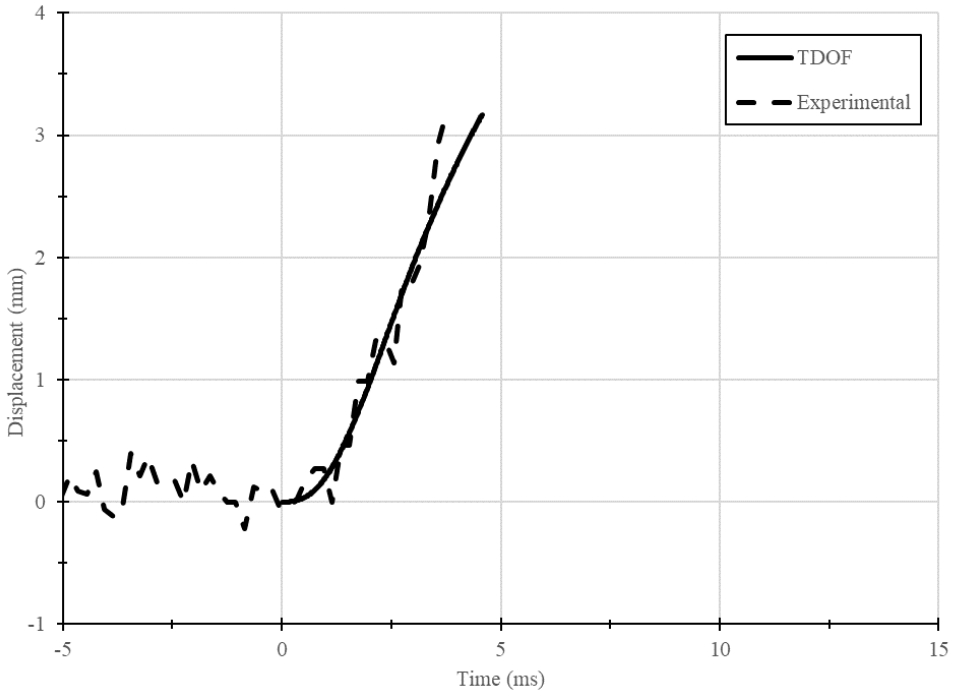

Figure B.19: TDOF prediction for E0D[4]

(a) Splitting failure

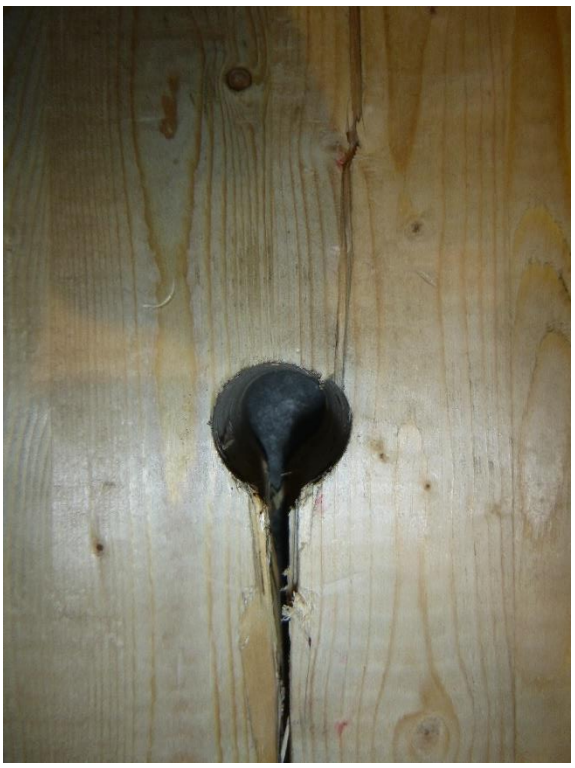

(b) Minimal crushing in bolt hole before splitting

(c) Slight bending in bolt

Figure B.20: Specimen E0D[4] after testing

Specimen: E0D[5]

Comments: Specimen failed in splitting

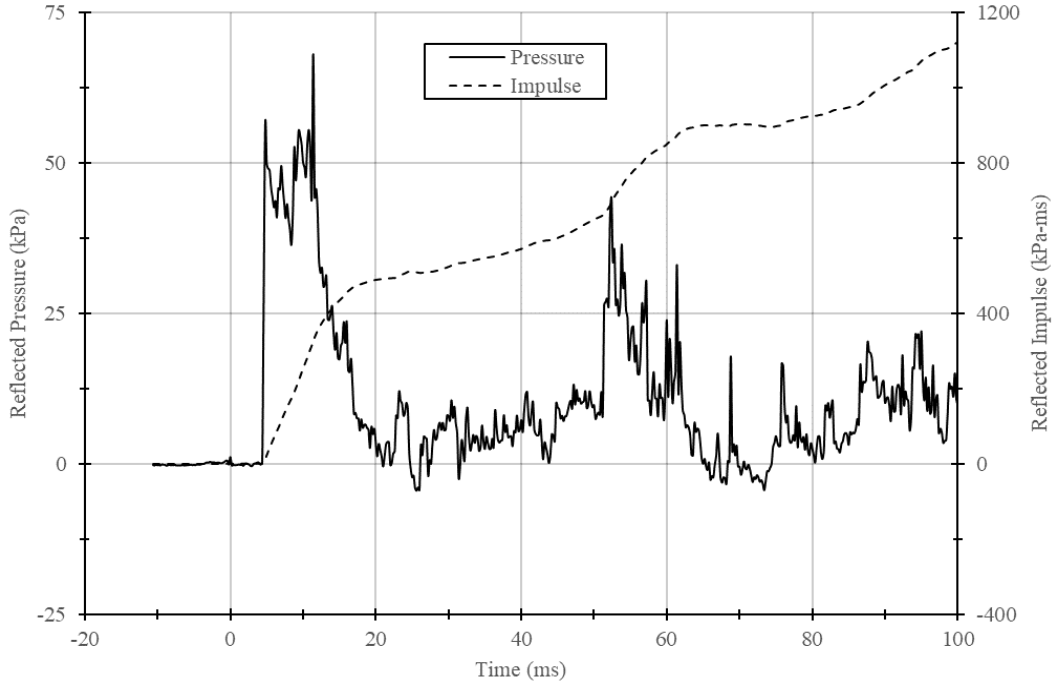

Figure B.21: Reflected pressure and impulse time histories for E0D[5]

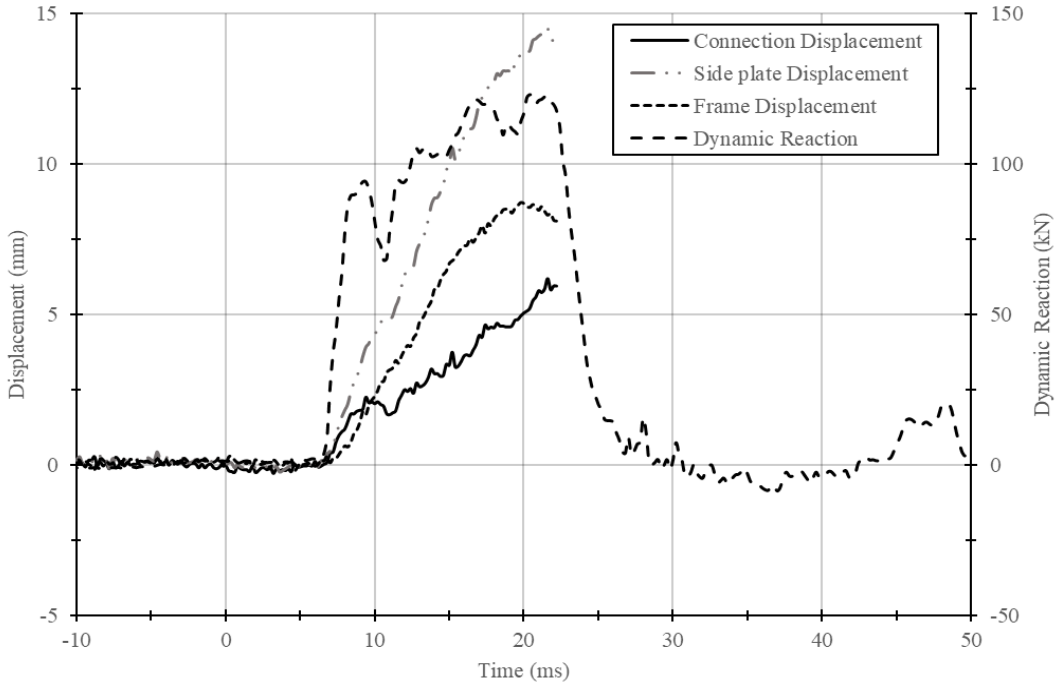

Figure B.22: Displacement and reaction time histories for E0D[5]

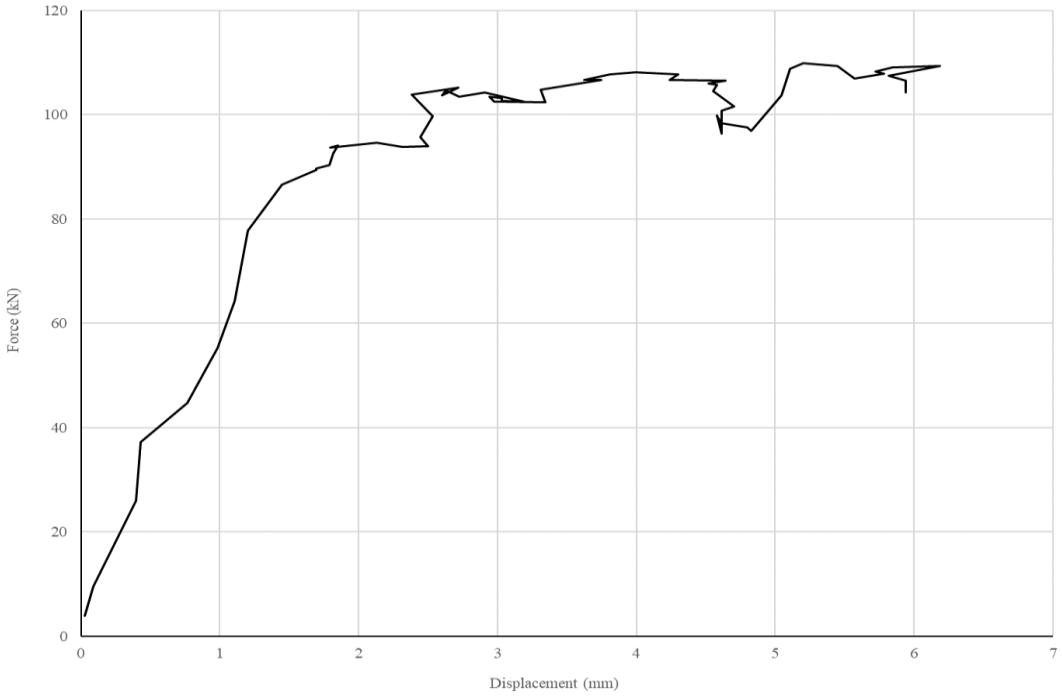

Figure B.23: Force displacement curve for E0D[5]

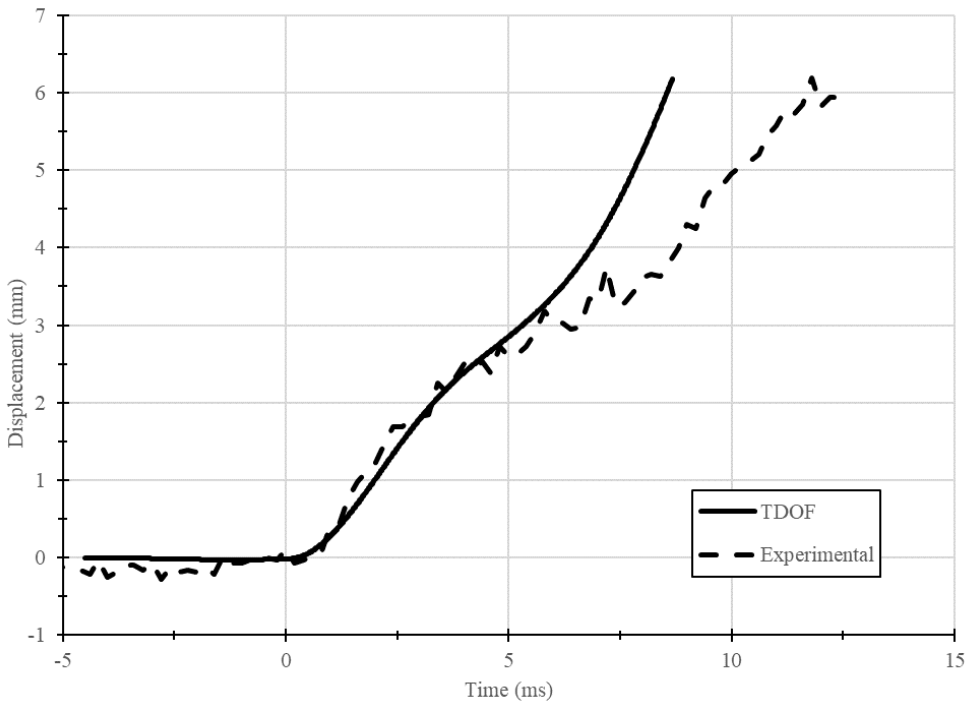

Figure B.24: TDOF prediction for E0D[5]

(a) Splitting failure

(b) Minimal crushing in bolt hole before splitting

(c) Slight bending in bolt

Figure B.25: Specimen E0D[5] after testing

Specimen: E0D[6]

Comments: Reinforced specimen. No ultimate failure

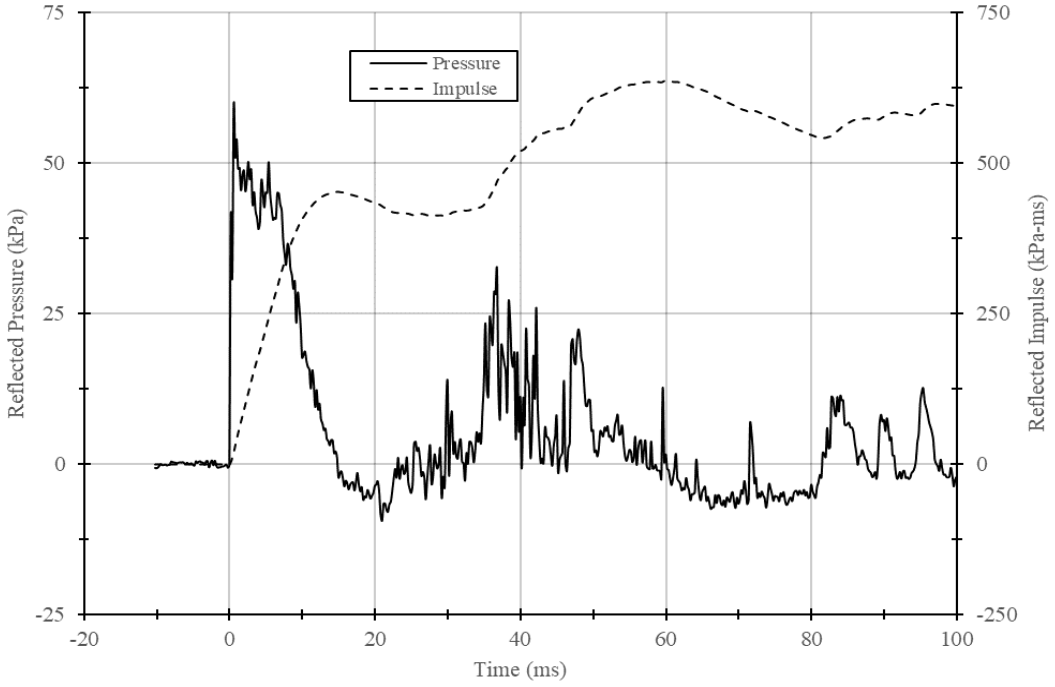

Figure B.26: Reflected pressure and impulse time histories for E0D[6]

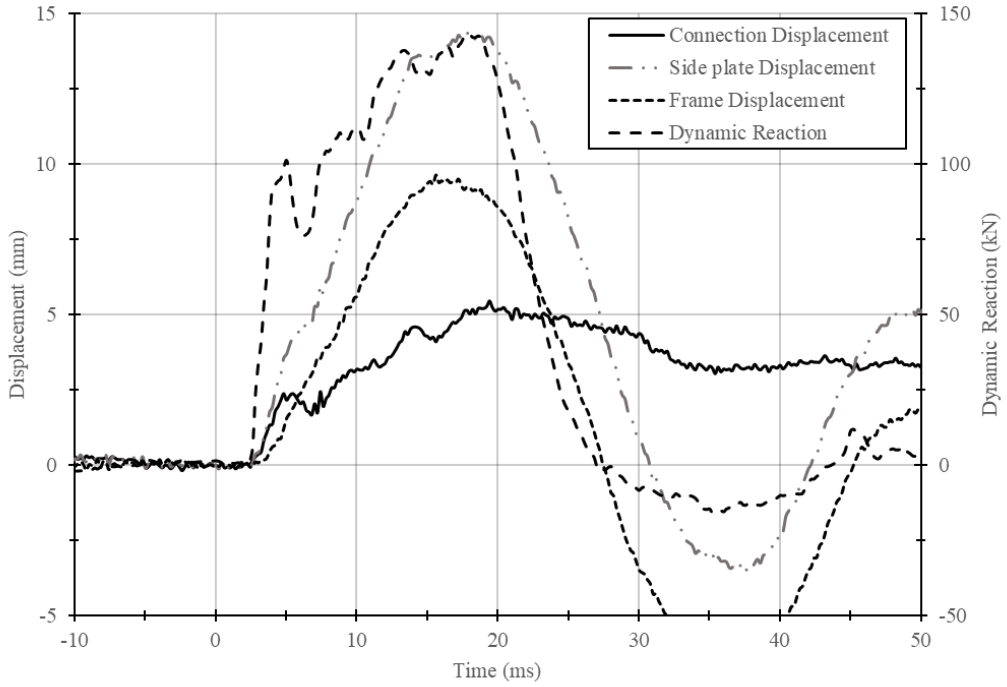

Figure B.27: Displacement and reaction time histories for E0D[6]

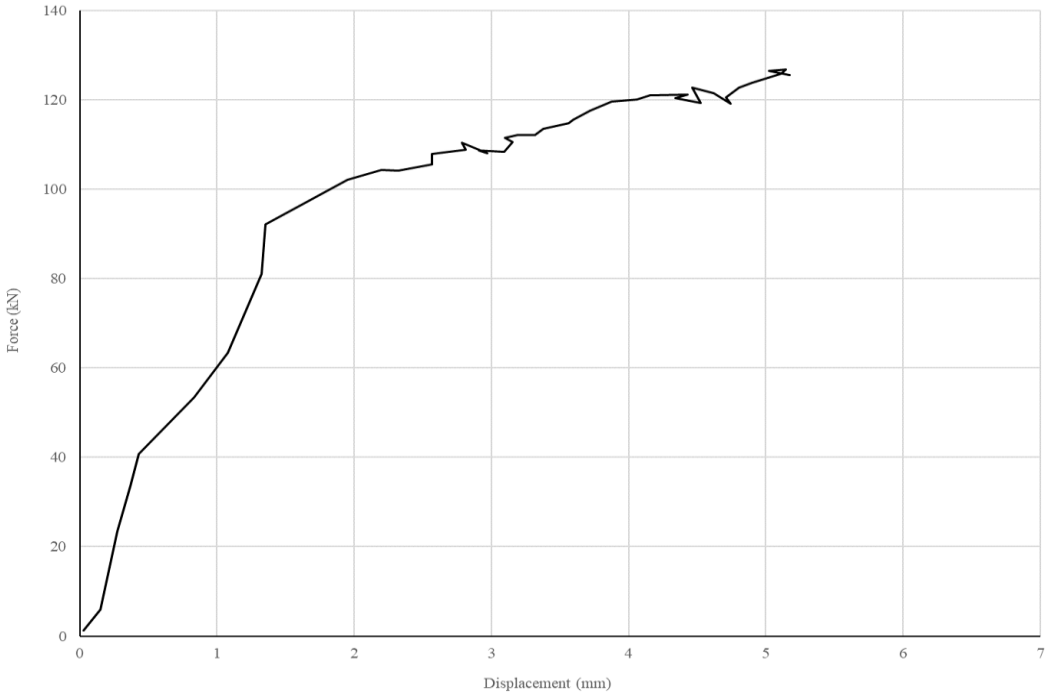

Figure B.28: Force displacement curve for E0D[6]

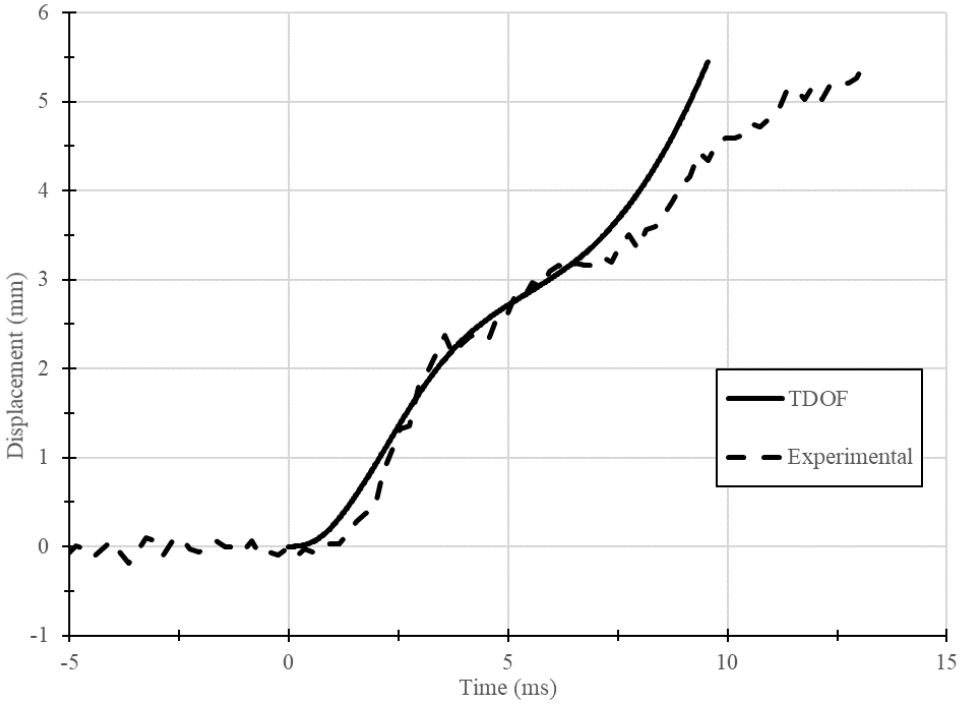

Figure B.29: TDOF prediction for E0D[6]

(a) Reinforcing configuration

(b) Specimen after testing

(c) Minimal crushing in bolt hole

(d) Slight bending in bolt

Figure B.30: Specimen E0D[6] after testing

Specimen: E0D[7]

Comments: Reinforced specimen. Failed in screw withdrawal and splitting

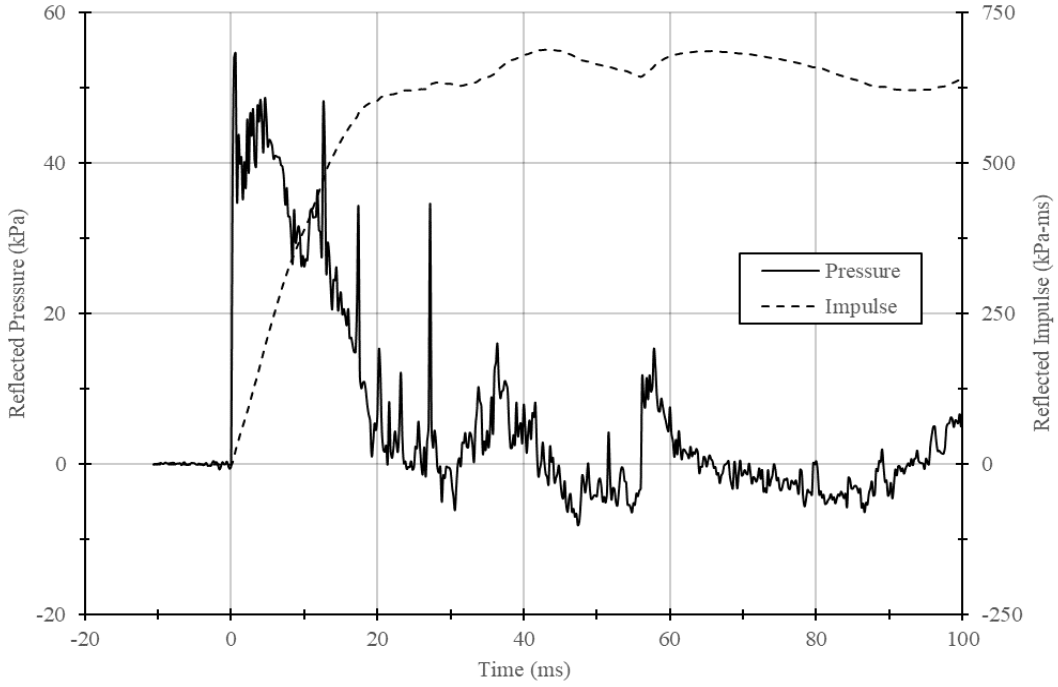

Figure B.31: Reflected pressure and impulse time histories for E0D[7]

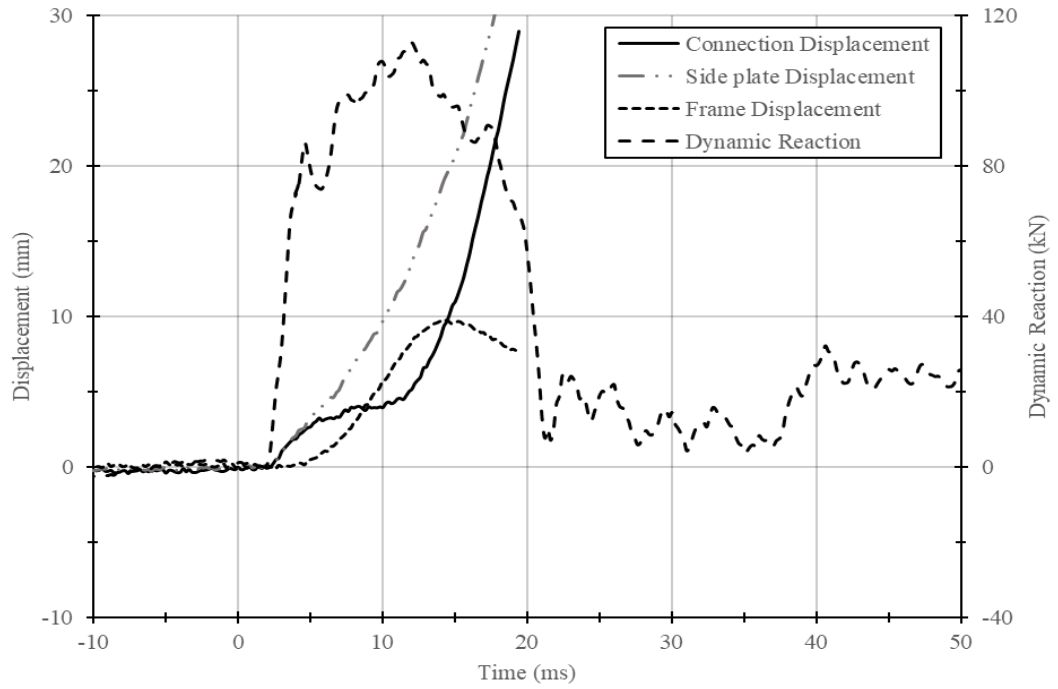

Figure B.32: Displacement and reaction time histories for E0D[7]

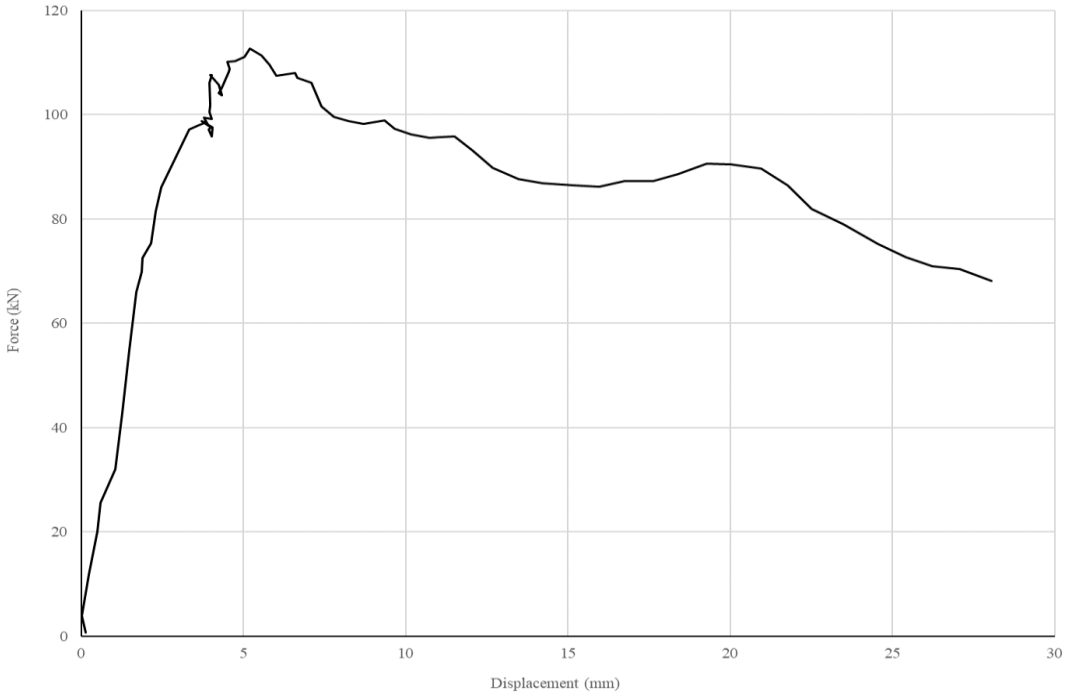

Figure B.33: Force displacement curve for E0D[7]

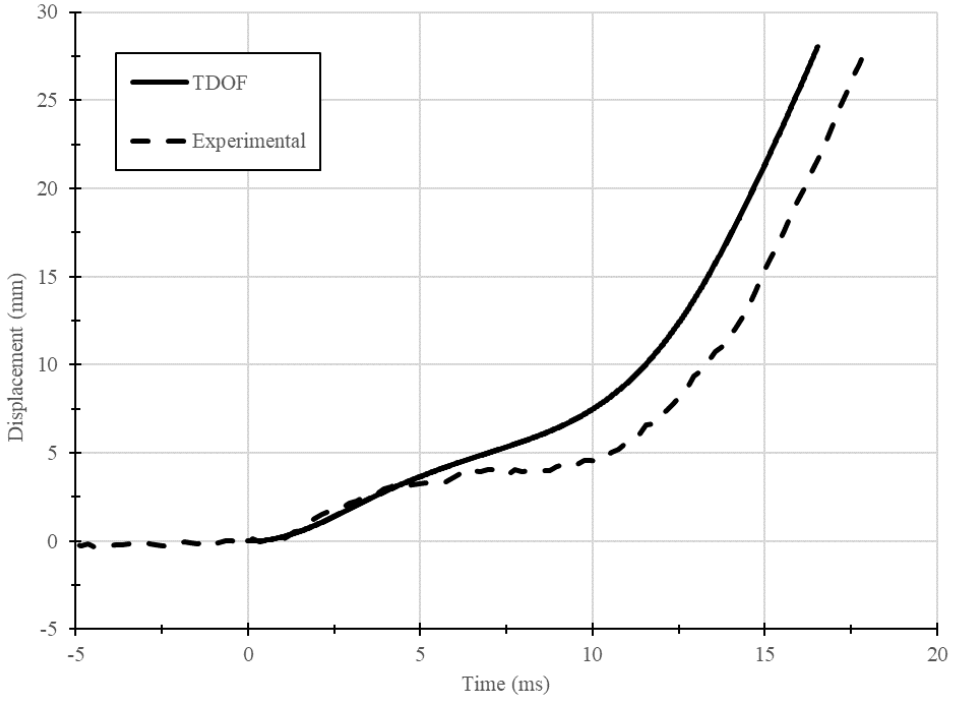

Figure B.34: TDOF prediction for E0D[7]

(a) Ultimate failure in screw withdrawal

(b) Extensive crushing in bolt hole before splitting

(c) Slight bending in bolt

Figure B.35: Specimen E0D[7] after testing

Specimen: E0D[8]

Comments: Reinforced specimen. No ultimate failure

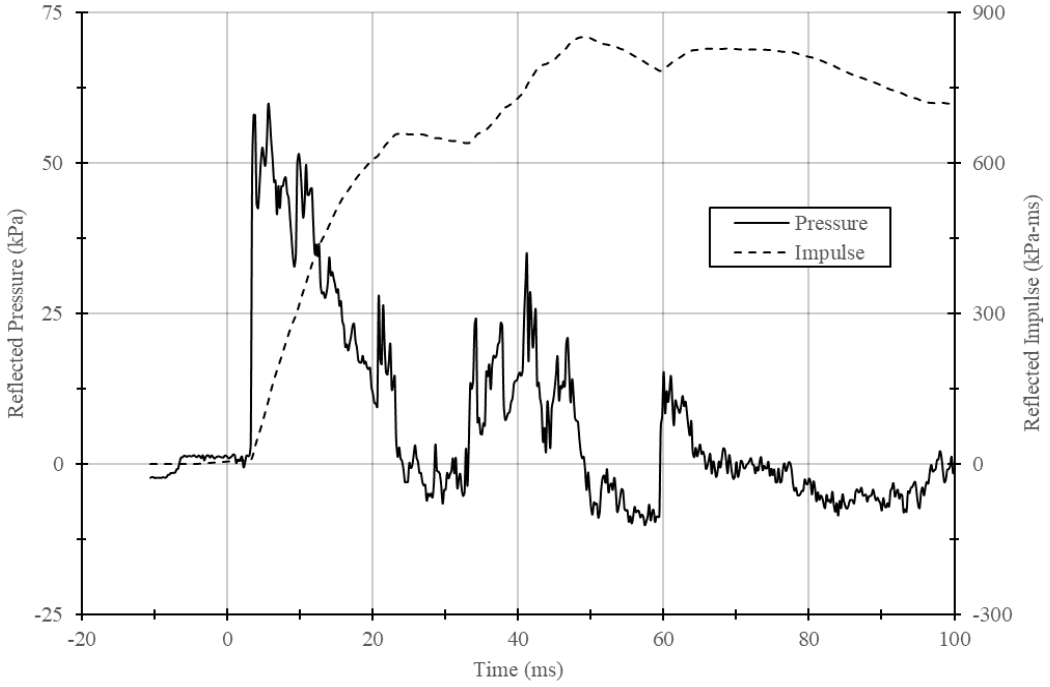

Figure B.36: Reflected pressure and impulse time histories for E0D[8]

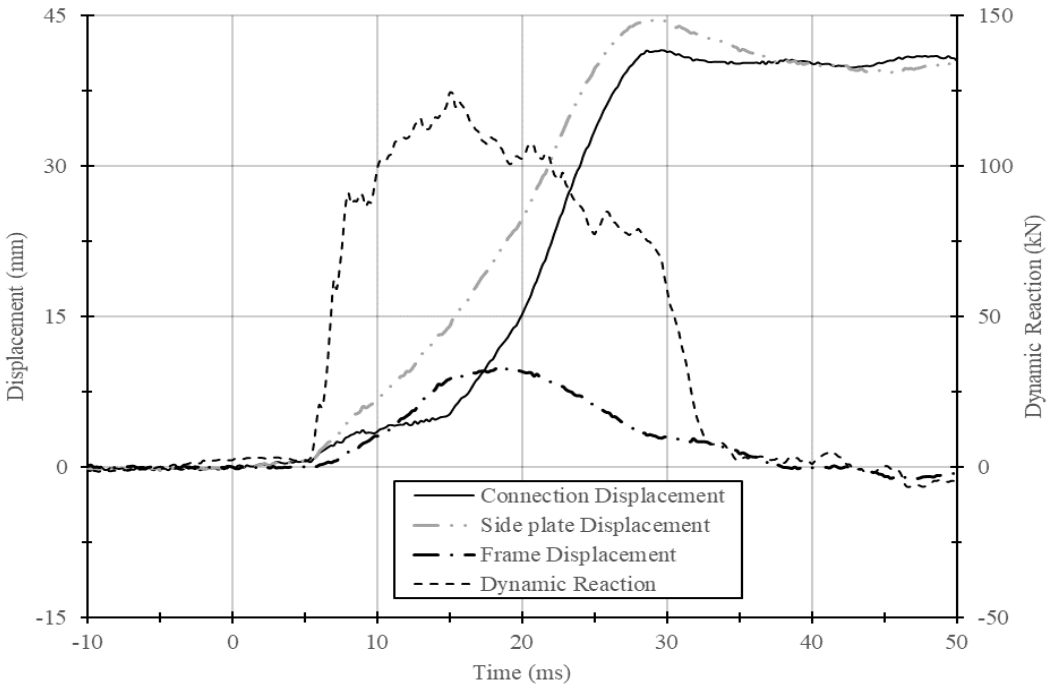

Figure B.37: Displacement and reaction time histories for E0D[8]

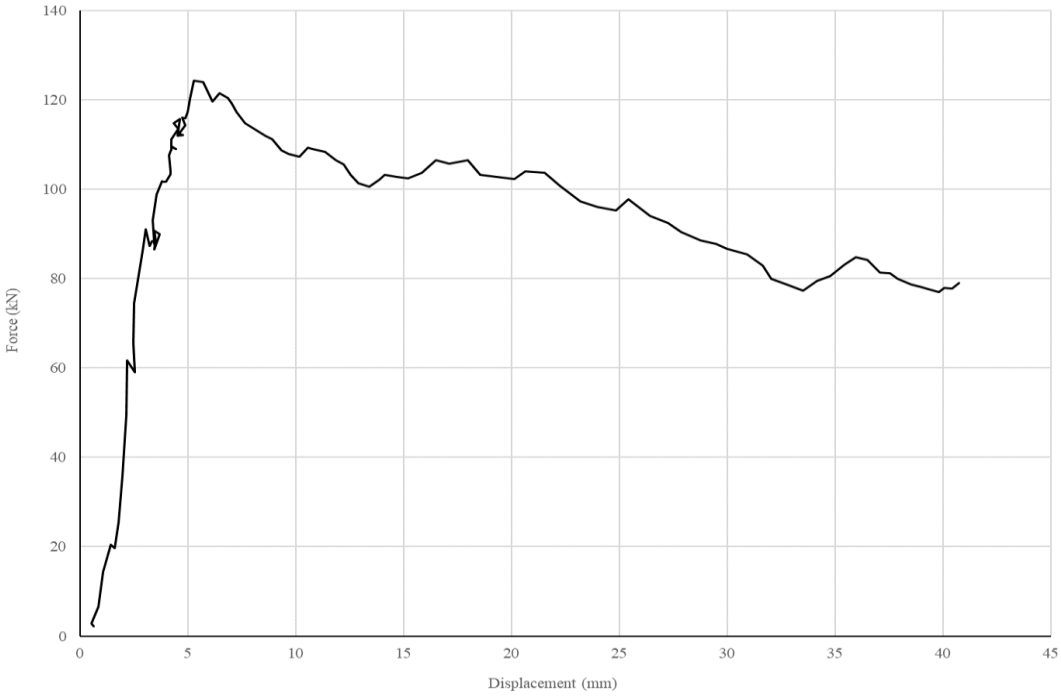

Figure B.38: Force displacement curve for E0D[8]

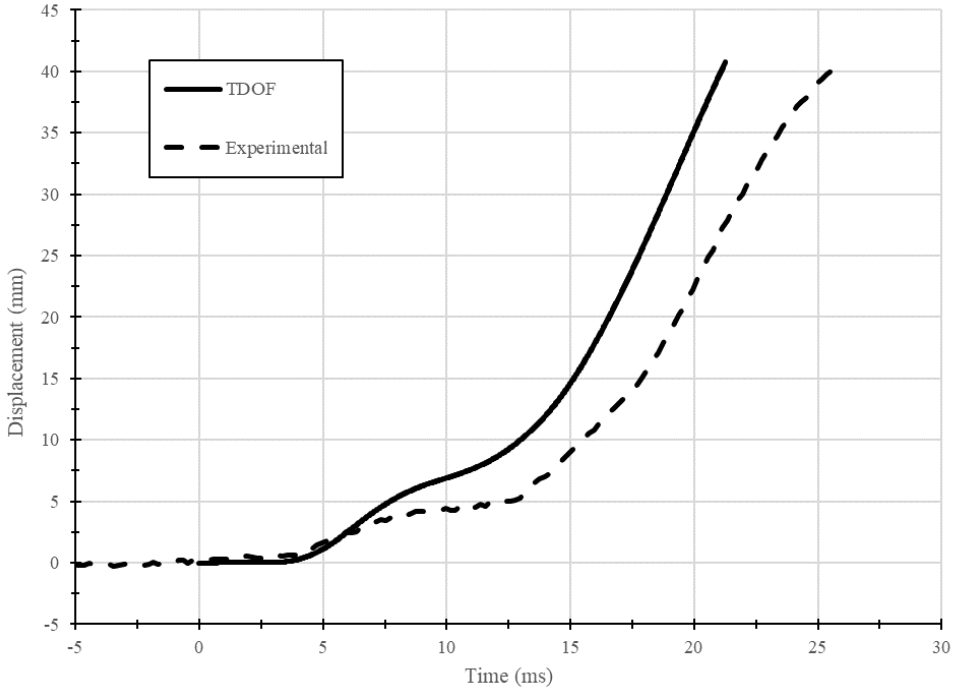

Figure B.39: TDOF prediction for E0D[8]

(a) No screw failure

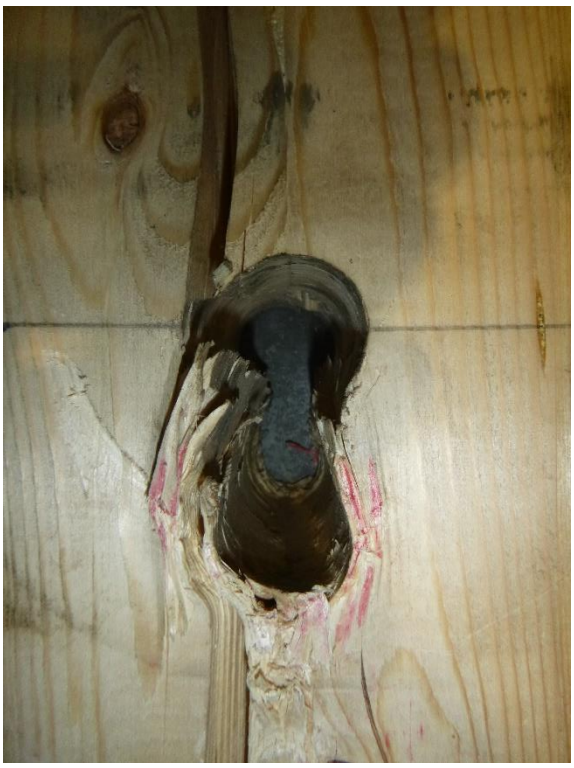

(b) Extensive crushing in bolt hole

(c) Slight bending in bolt

Figure B.40: Specimen E0D[8] after testing

Specimen: E0D[9]

Comments: Reinforced specimen. Failed in screw withdrawal and splitting

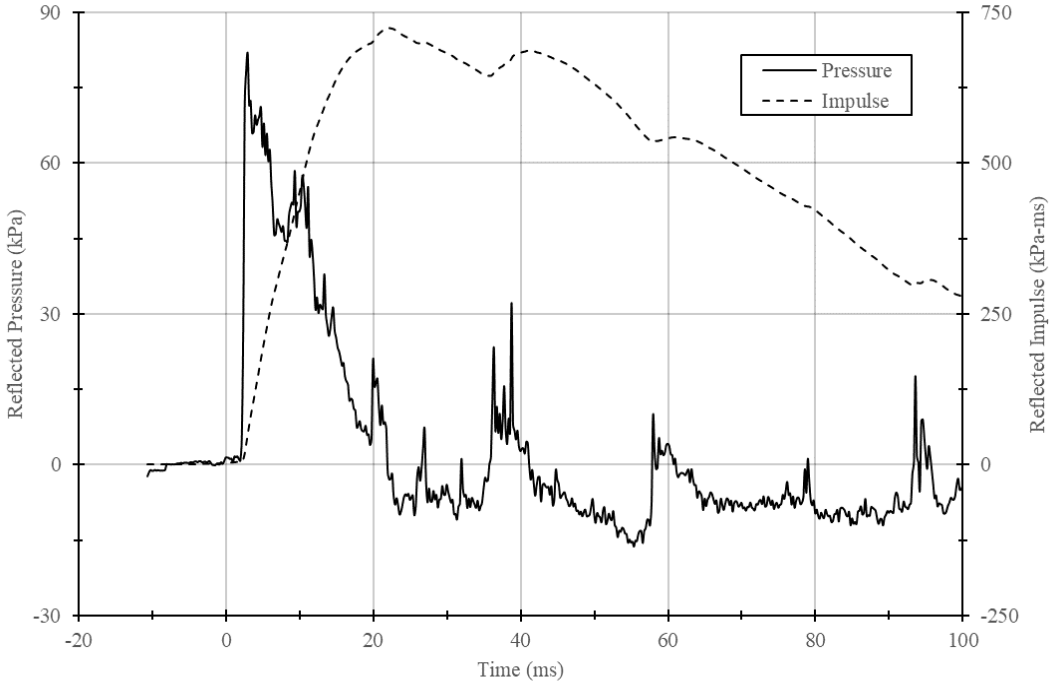

Figure B.41: Reflected pressure and impulse time histories for E0D[9]

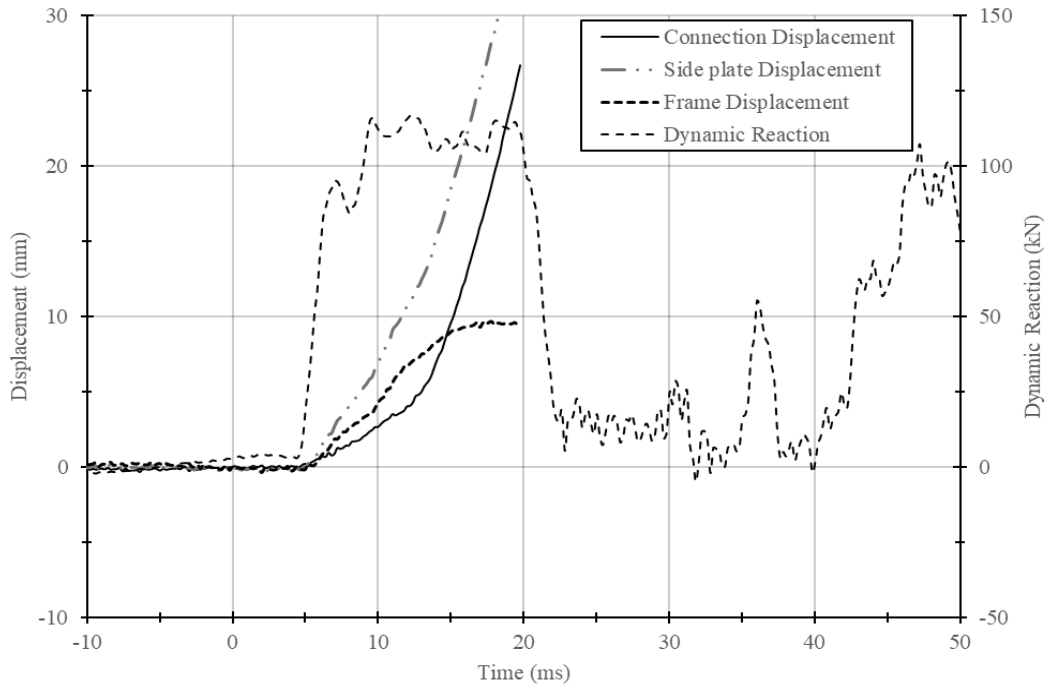

Figure B.42: Displacement and reaction time histories for E0D[9]

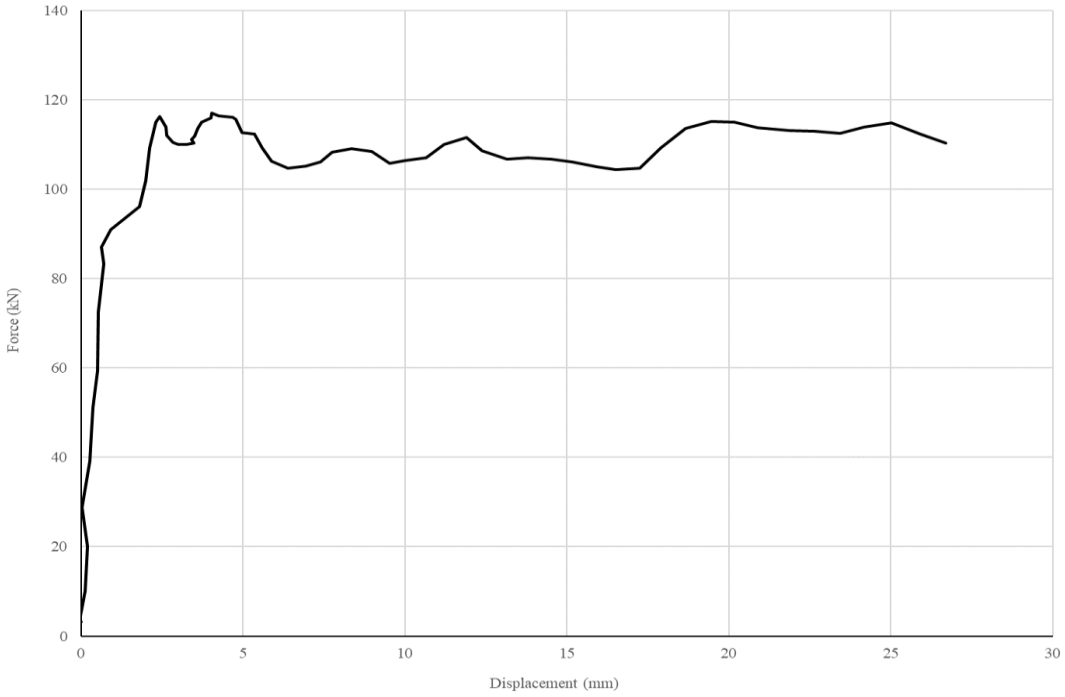

Figure B.43: Force displacement curve for E0D[9]

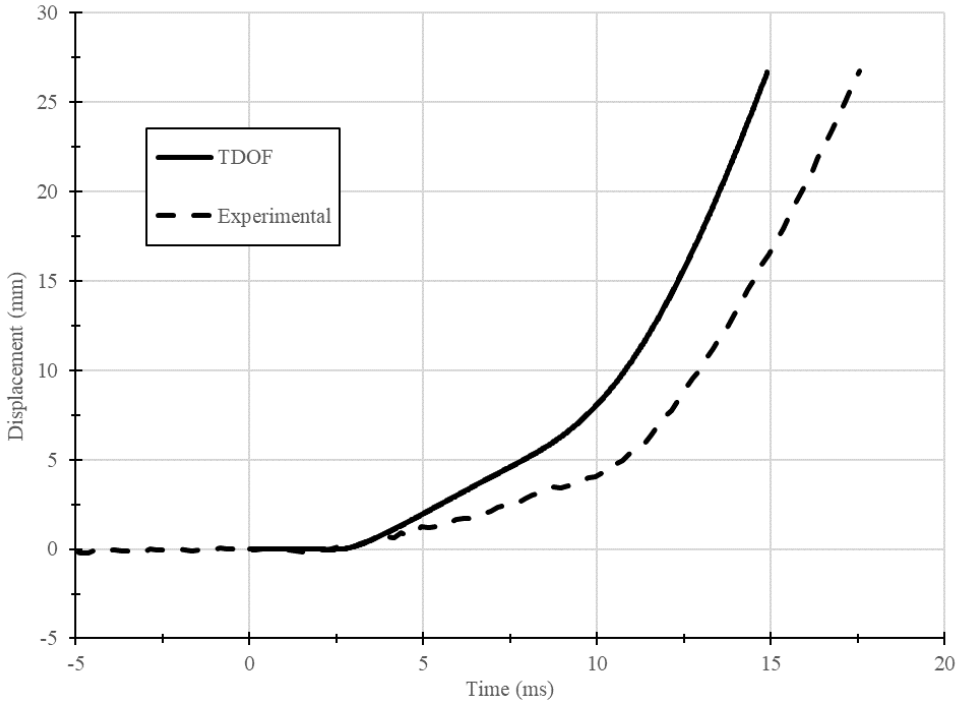

Figure B.44: TDOF prediction for E0D[9]

(a) Ultimate failure in screw withdrawal

(b) Extensive crushing in bolt hole before splitting

(c) Slight bending in bolt

Figure B.45: Specimen E0D[9] after testing

Specimen: E90D[1]

Comments: No ultimate failure.

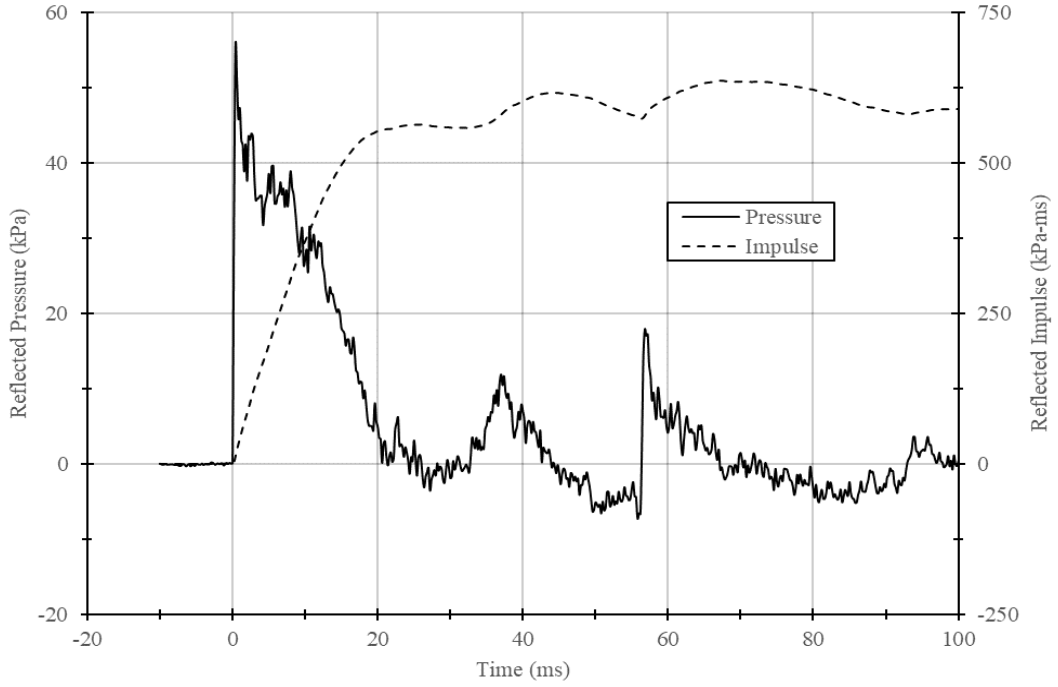

Figure B.46: Reflected pressure and impulse time histories for E90D[1]

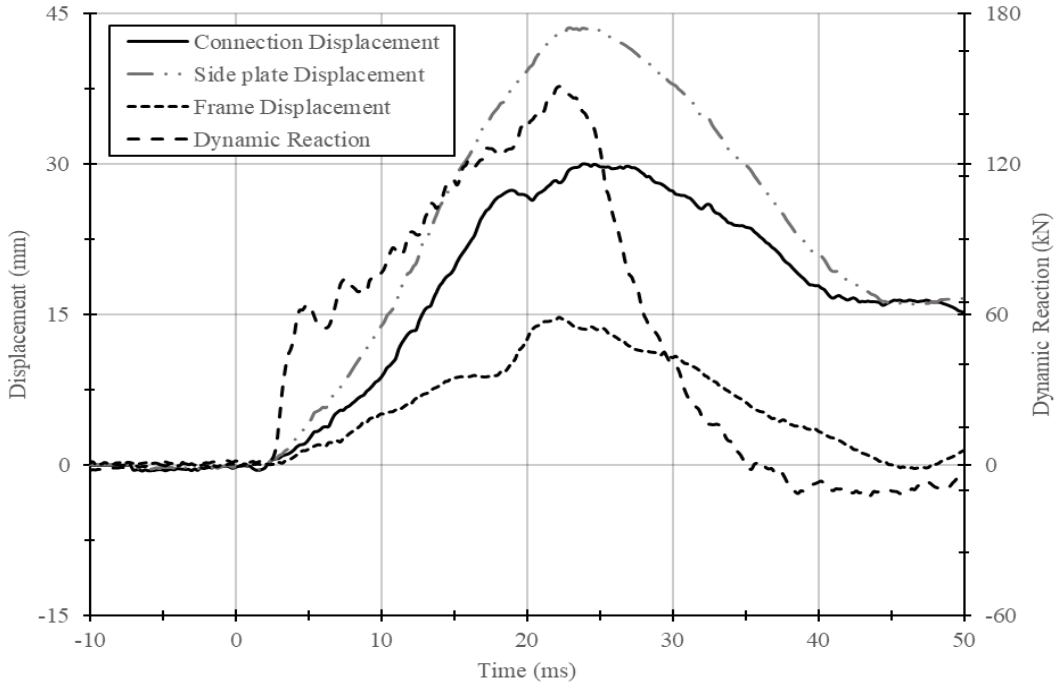

Figure B.47: Displacement and reaction time histories for E90D[1]

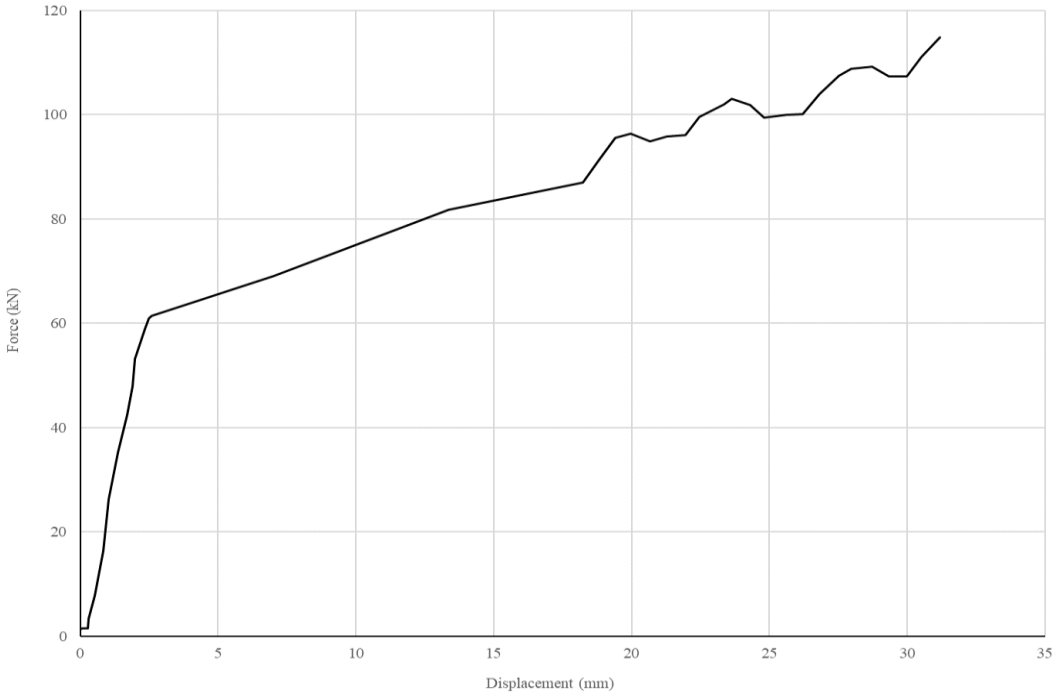

Figure B.48: Force displacement curve for E90D[1]

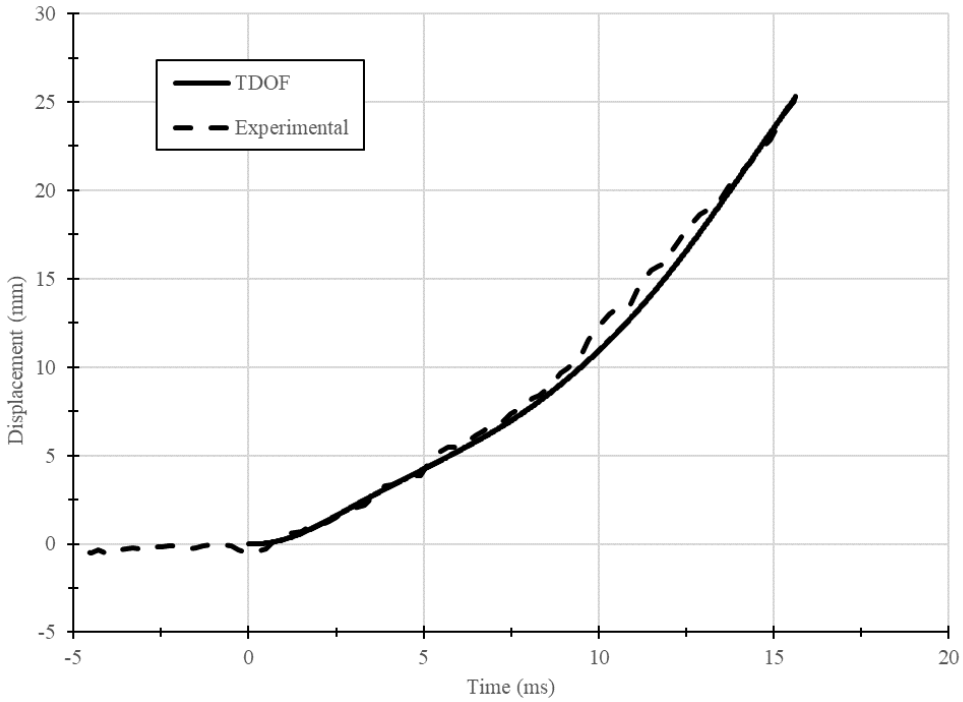

Figure B.49: TDOF prediction for E90D[1]

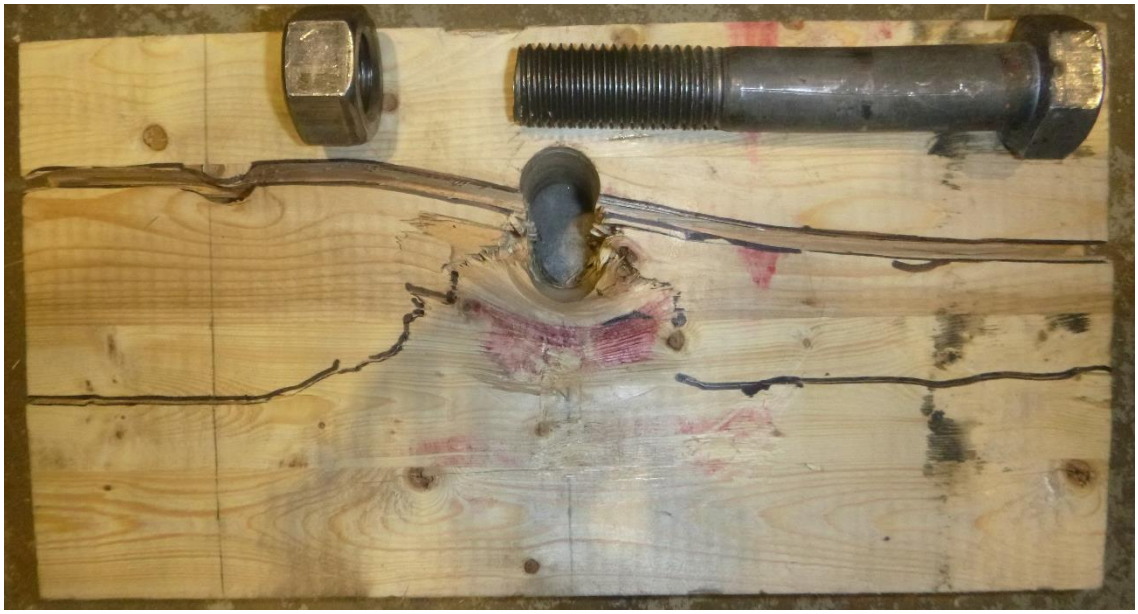

(a) Specimen after testing

(b) Crushing in bolt hole

(c) No bending in bolt

Figure B.50: Specimen E90D[1] after testing

Specimen: E90D[2]

Comments: No ultimate failure. At 18 ms the side plate contacted the frame LVDT. Readings after this were meaningless

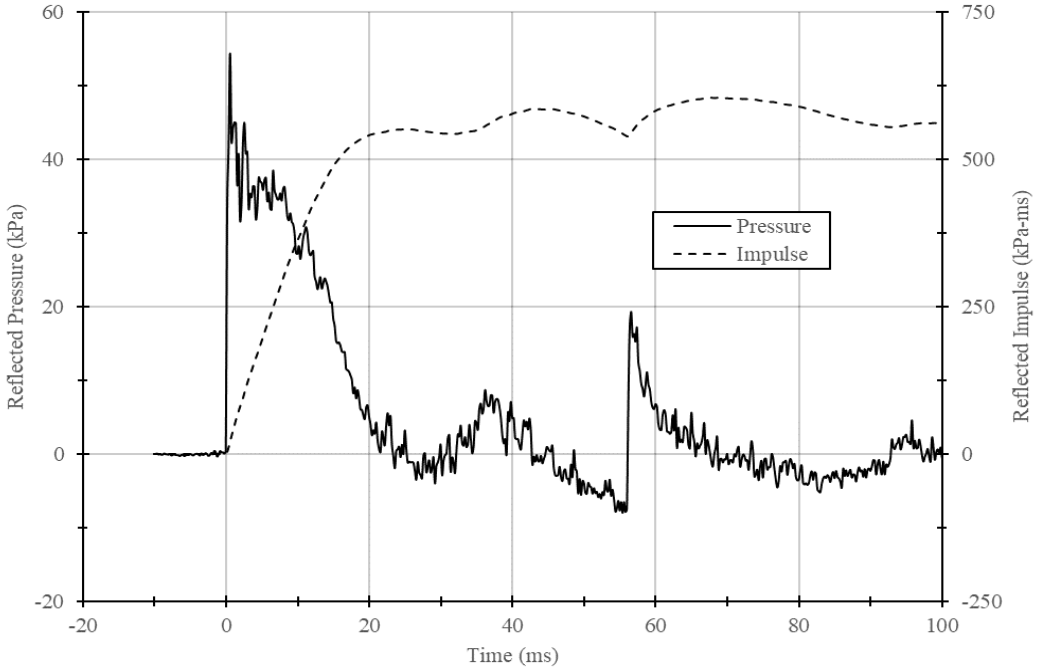

Figure B.51: Reflected pressure and impulse time histories for E90D[2]

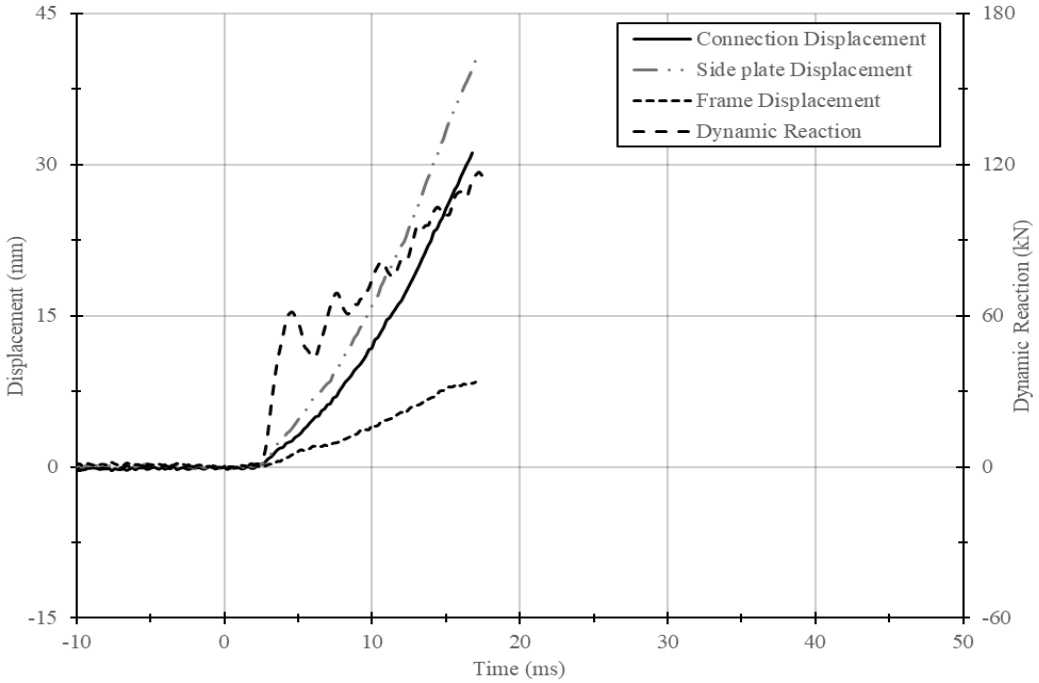

Figure B.52: Displacement and reaction time histories for E90D[2]

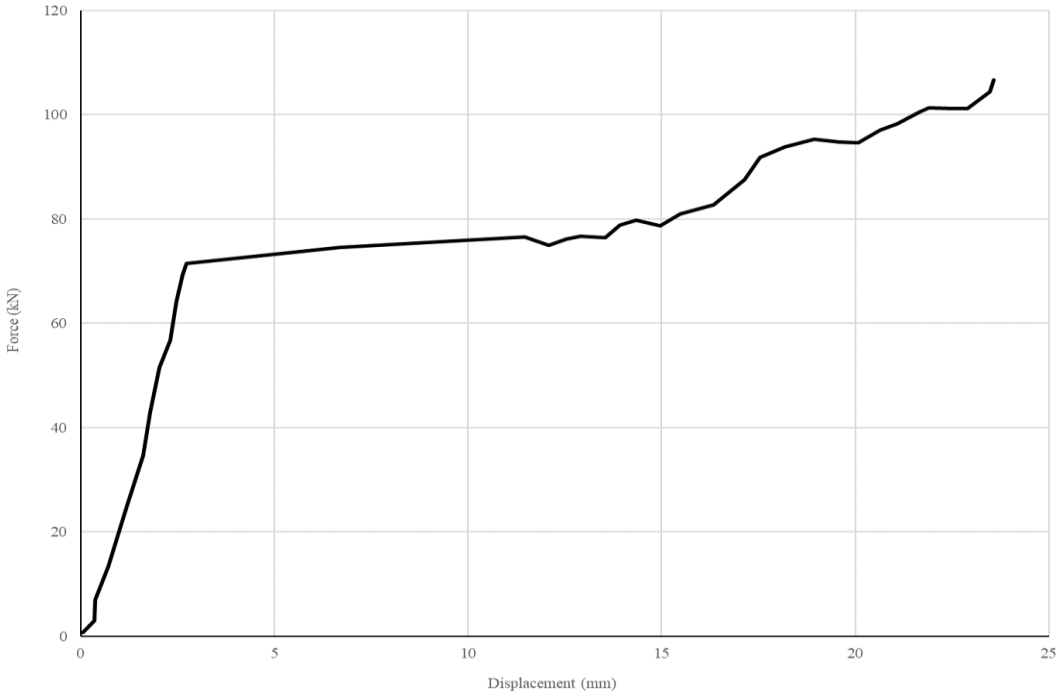

Figure B.53: Force displacement curve for E90D[2]

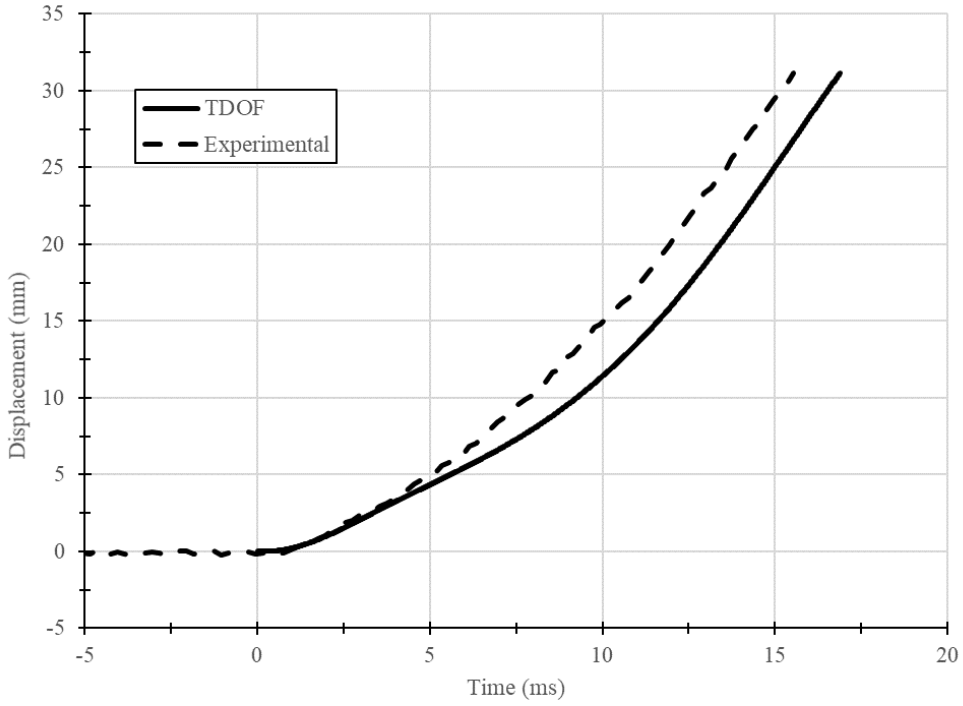

Figure B.54: TDOF prediction for E90D[2]

(a) Specimen after testing

(b) Crushing in bolt hole

(c) Slight bending in bolt

Figure B.55: Specimen E90D[2] after testing

Specimen: E90D[3]

Comments: No ultimate failure. At 16 ms the side plate contacted the frame LVDT. Readings after this were meaningless

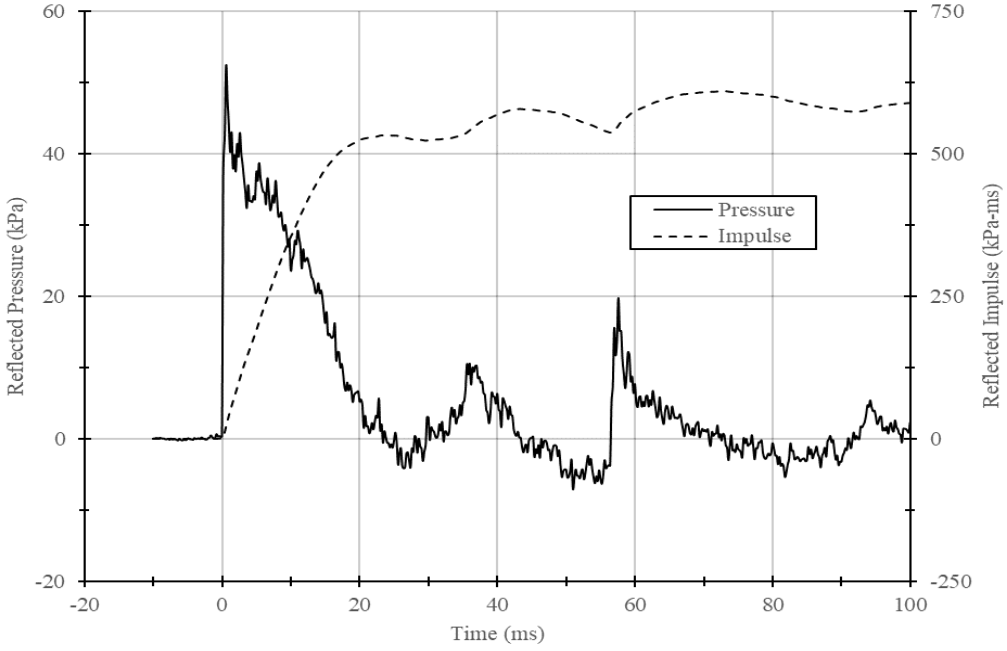

Figure B.56: Reflected pressure and impulse time histories for E90D[3]

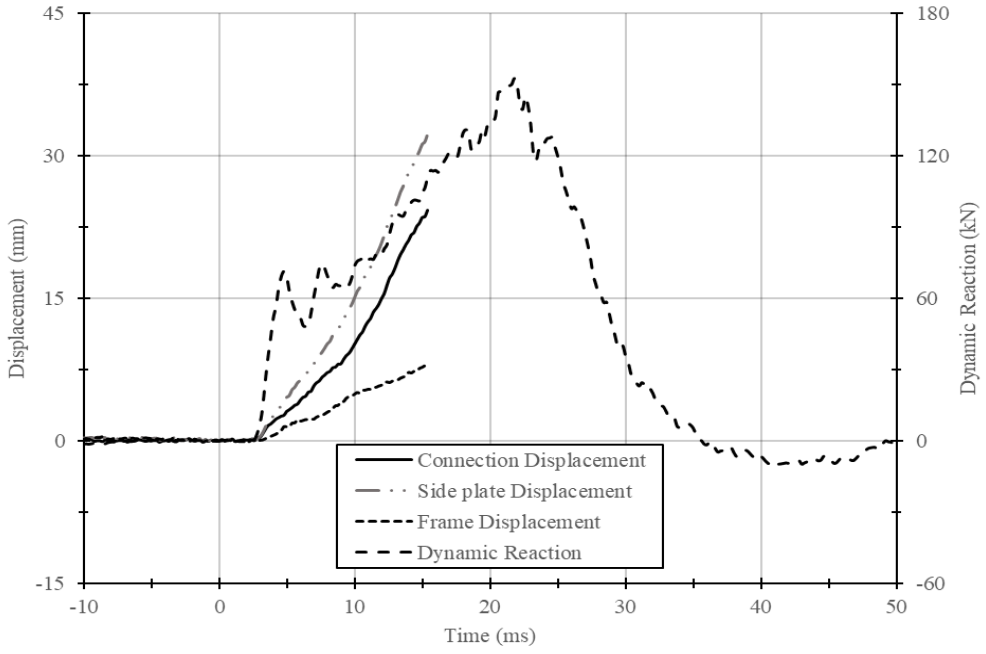

Figure B.57: Displacement and reaction time histories for E90D[3]

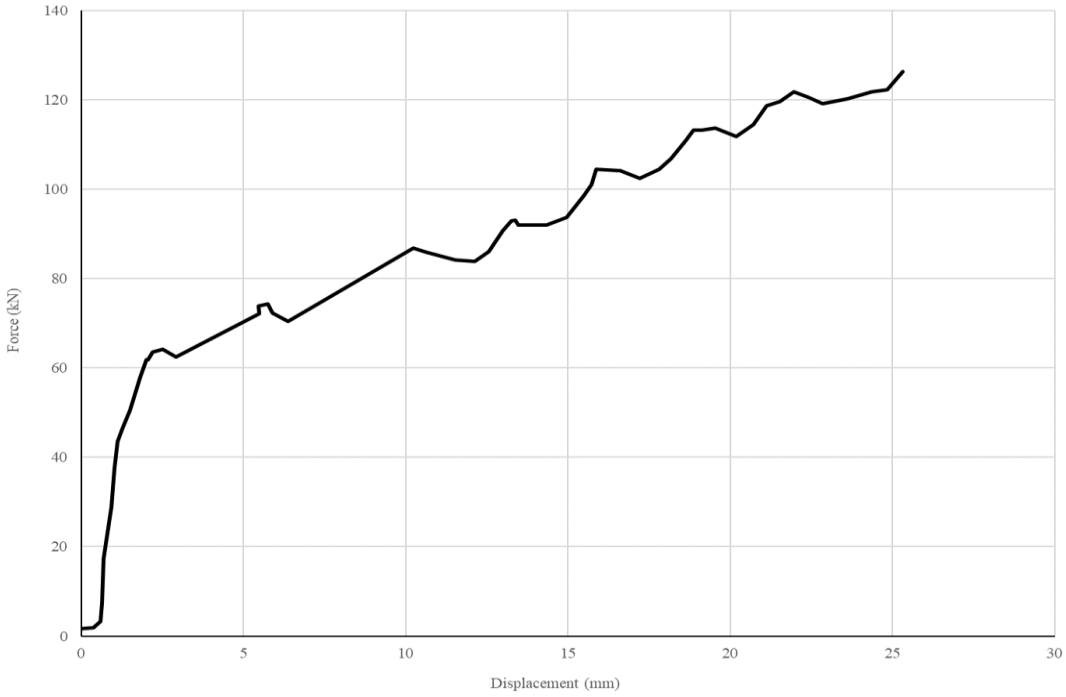

Figure B.58: Force displacement curve for E90D[3]

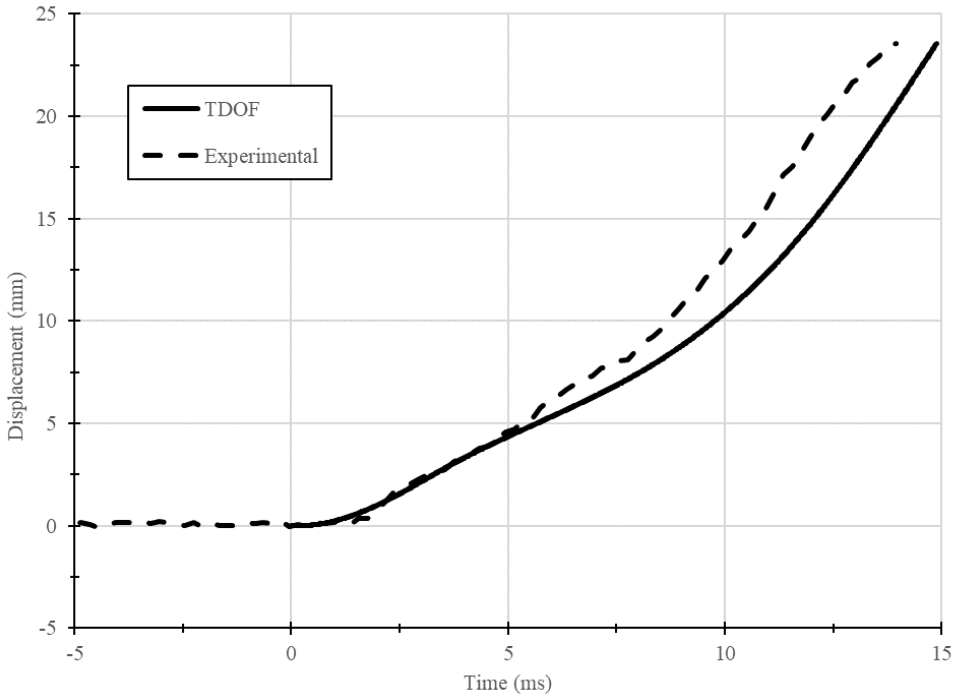

Figure B.59: TDOF prediction for E90D[3]

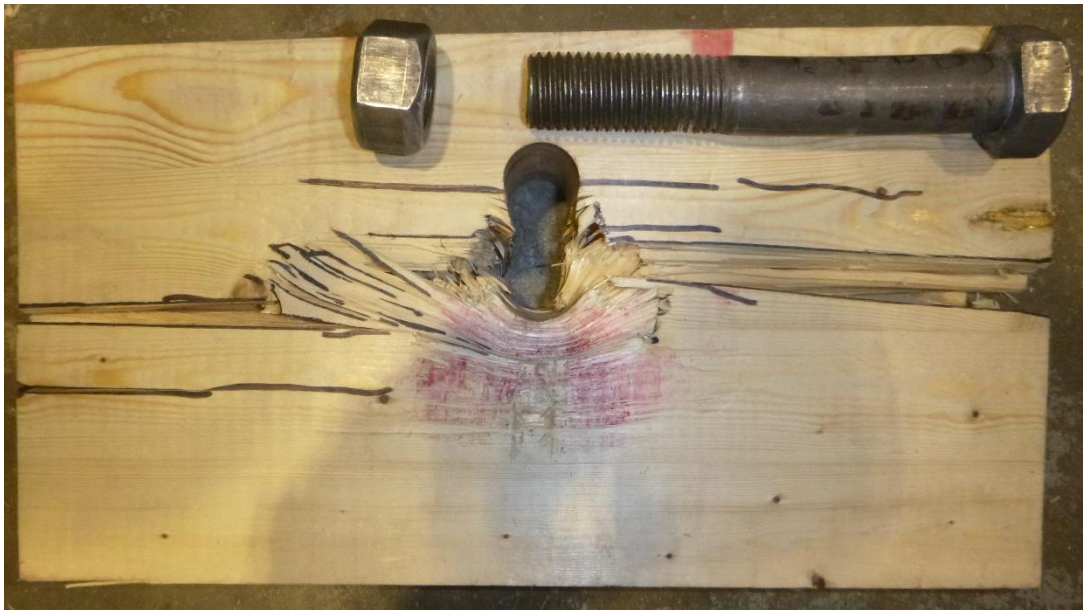

(a) Specimen after testing

(b) Crushing in bolt hole

(c) Slight bending in bolt

Figure B.60: Specimen E90D[3] after testing

Specimen: Y0D[1]

Comments: Specimen failed in splitting. After the specimen split, the bolt was pushed into the support frame, causing it to shear off

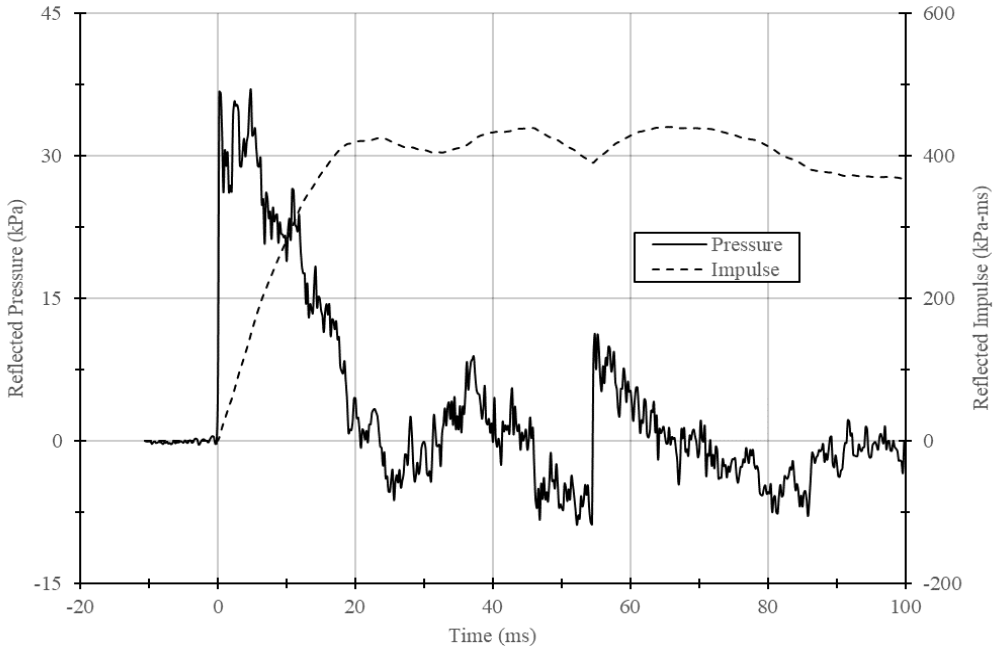

Figure B.61: Reflected pressure and impulse time histories for Y0D[1]

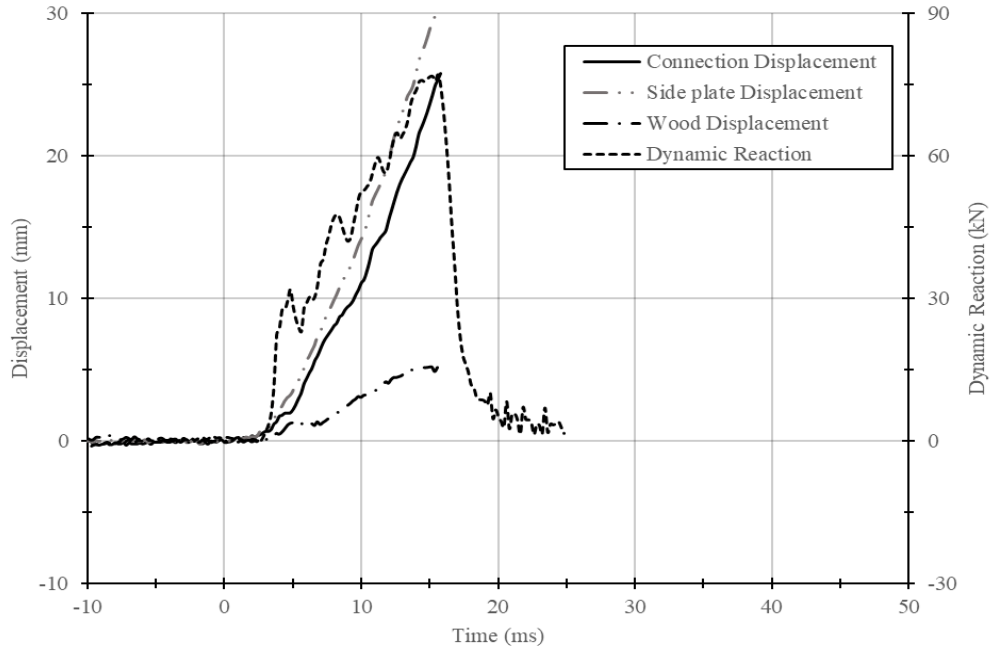

Figure B.62: Displacement and reaction time histories for Y0D[1]

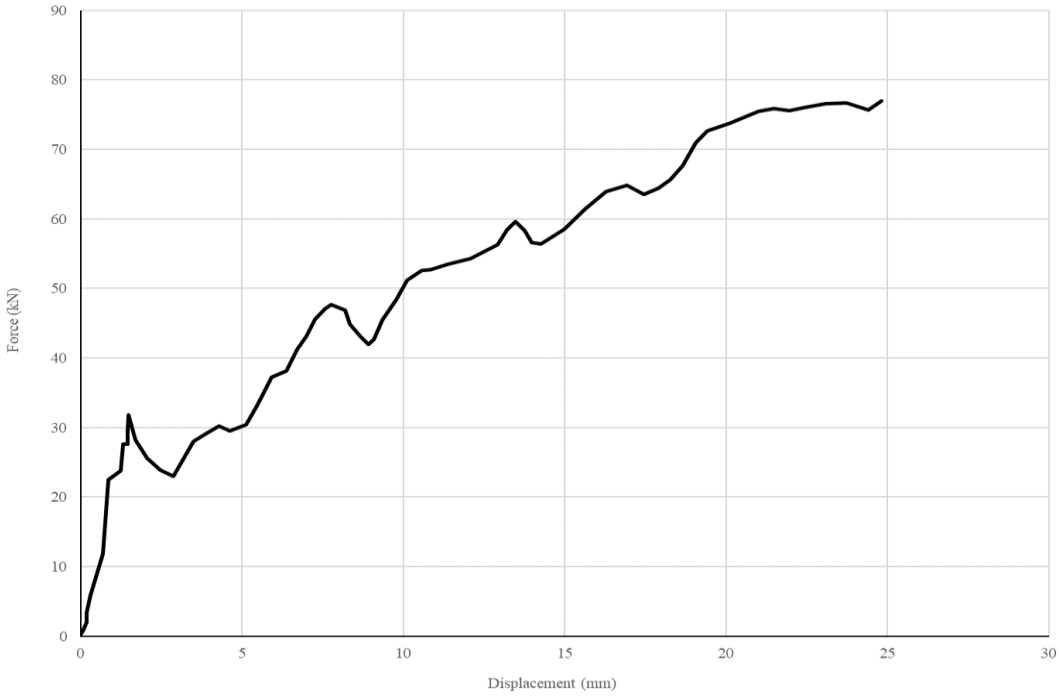

Figure B.63: Force displacement curve for Y0D[1]

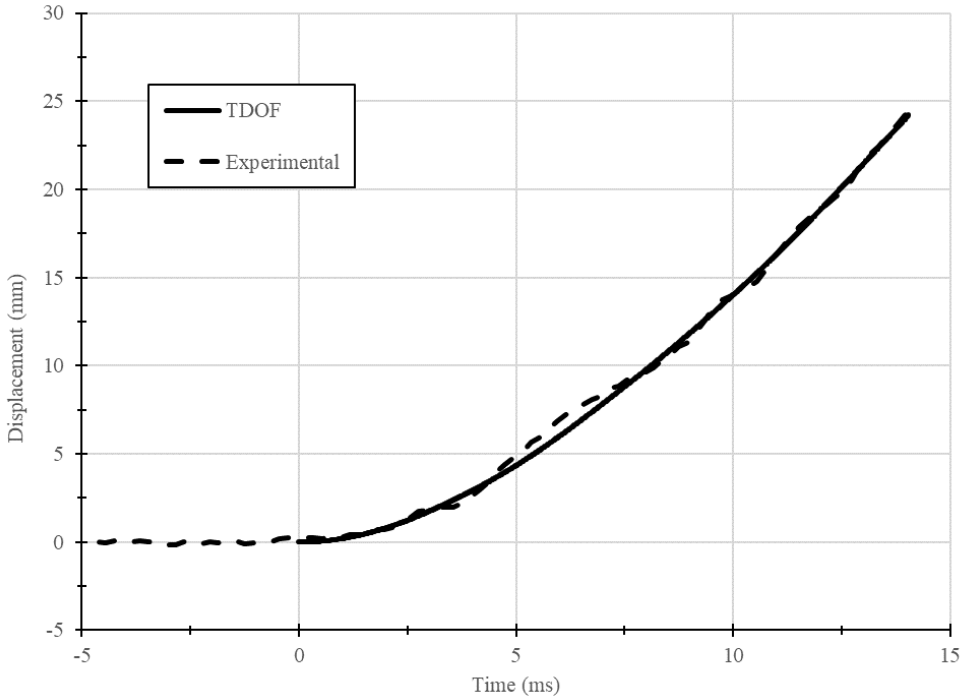

Figure B.64: TDOF prediction for Y0D[1]

(a) Inside of split specimen

(b) Splitting failure

(c) Crushing at bolt hole edge

(d) Bending in bolt

Figure B.65: Specimen Y0D[1] after testing

Specimen: Y0D[2]

Comments: No ultimate failure.

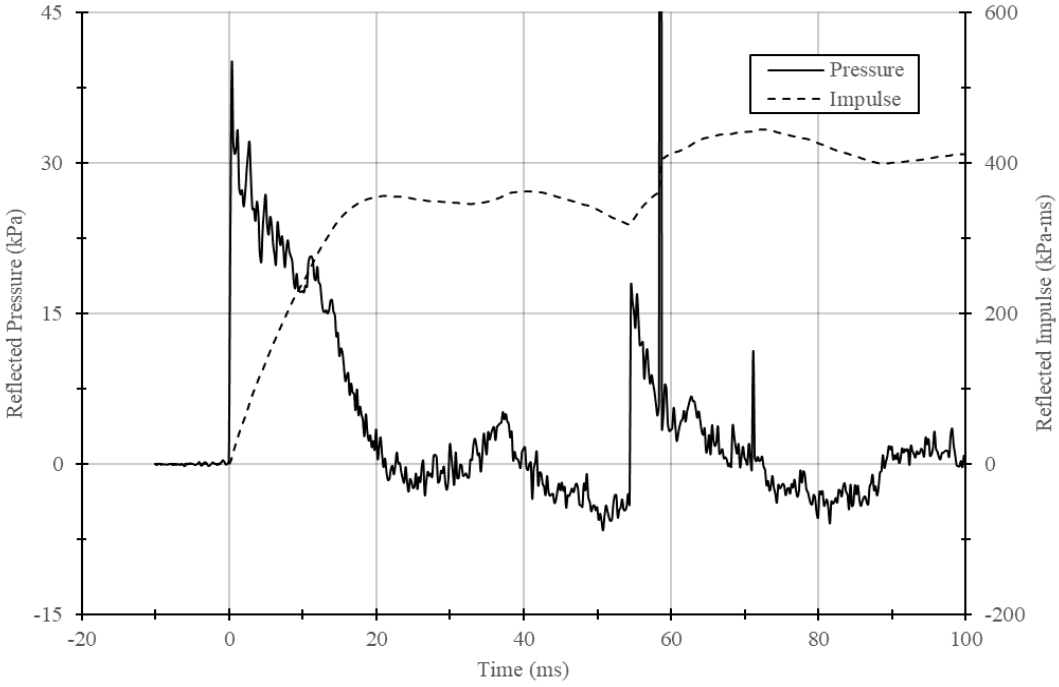

Figure B.66: Reflected pressure and impulse time histories for Y0D[2]

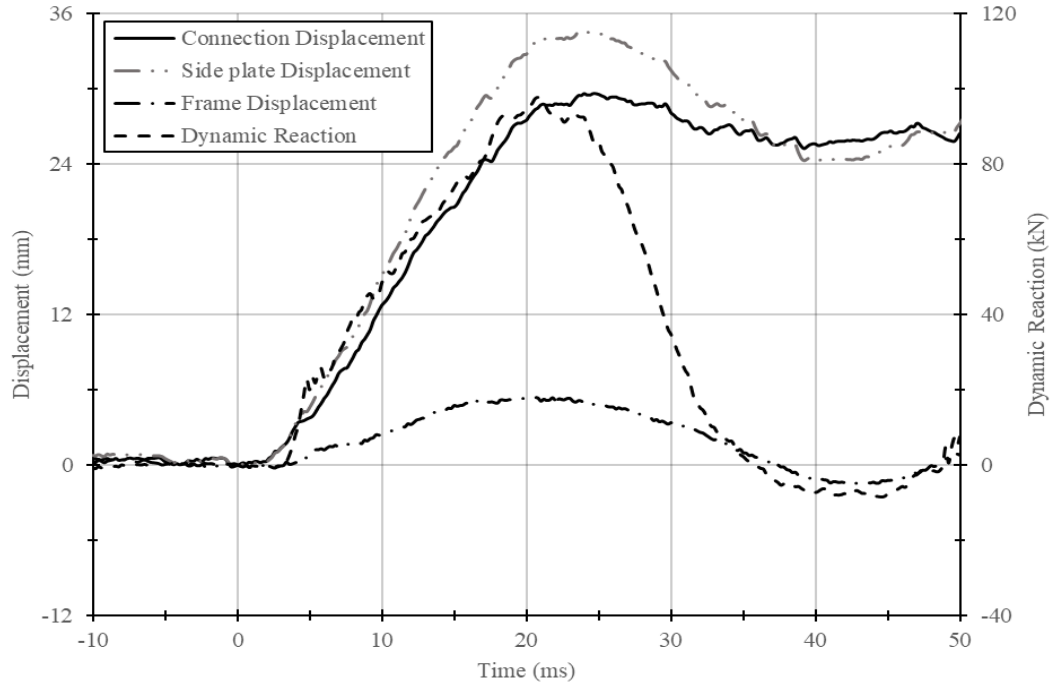

Figure B.67: Displacement and reaction time histories for Y0D[2]

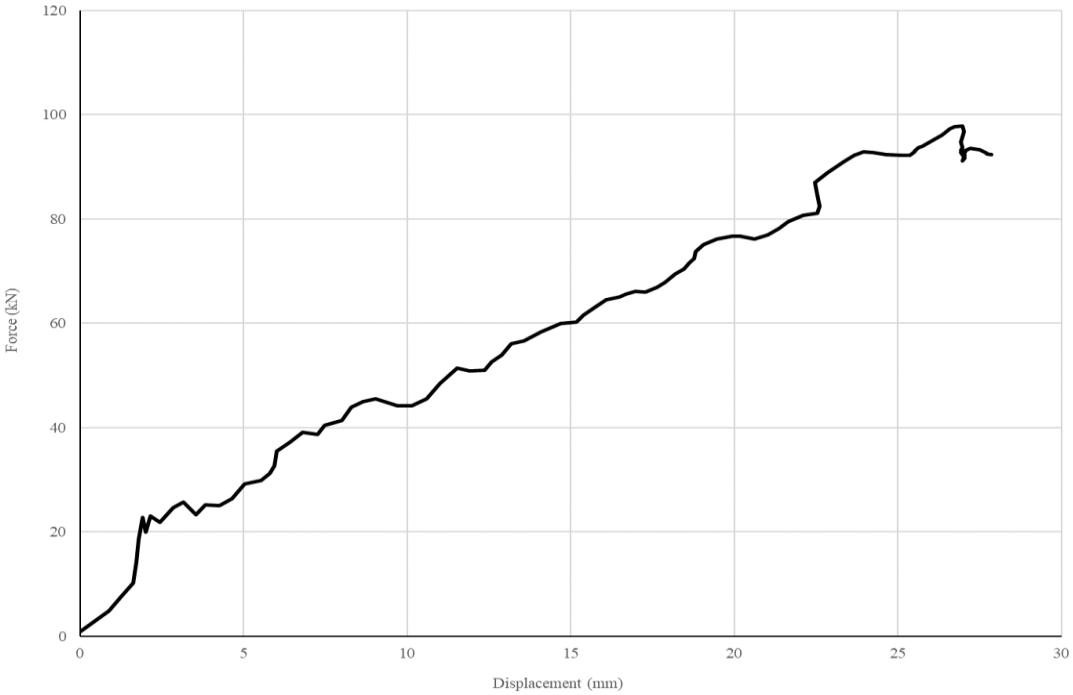

Figure B.68: Force displacement curve for Y0D[2]

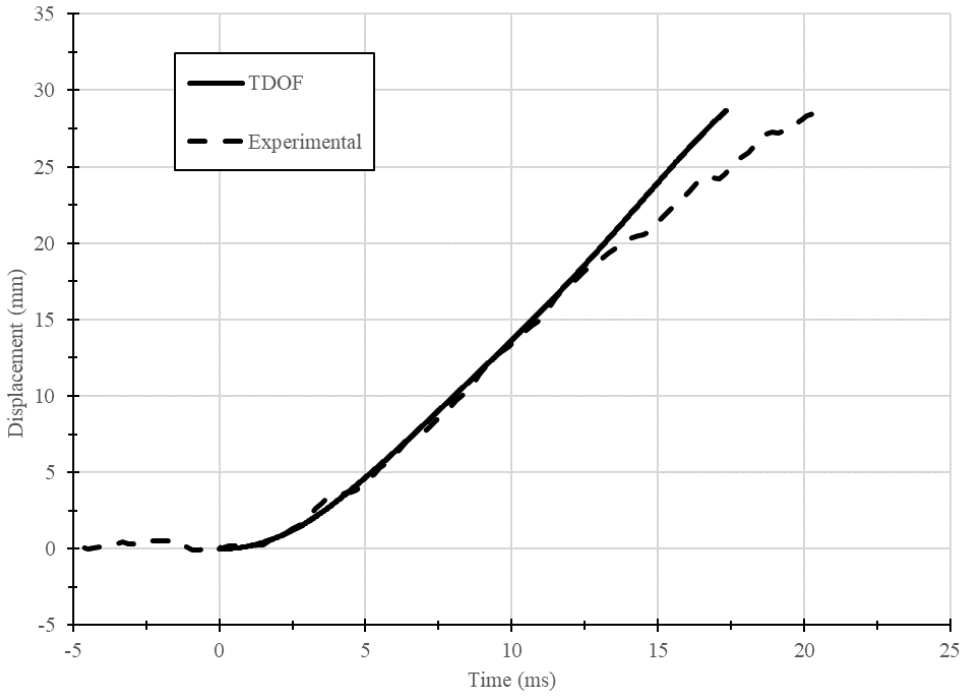

Figure B.69: TDOF prediction for Y0D[2]

(a) Specimen cut open to observe crushing in wood

(b) No ultimate failure

(c) Crushing at bolt hole edge

(d) Bending in bolt with no shear failure

Figure B.70: Specimen Y0D[2] after testing

Specimen: Y0D[3]

Comments: Specimen failed in splitting

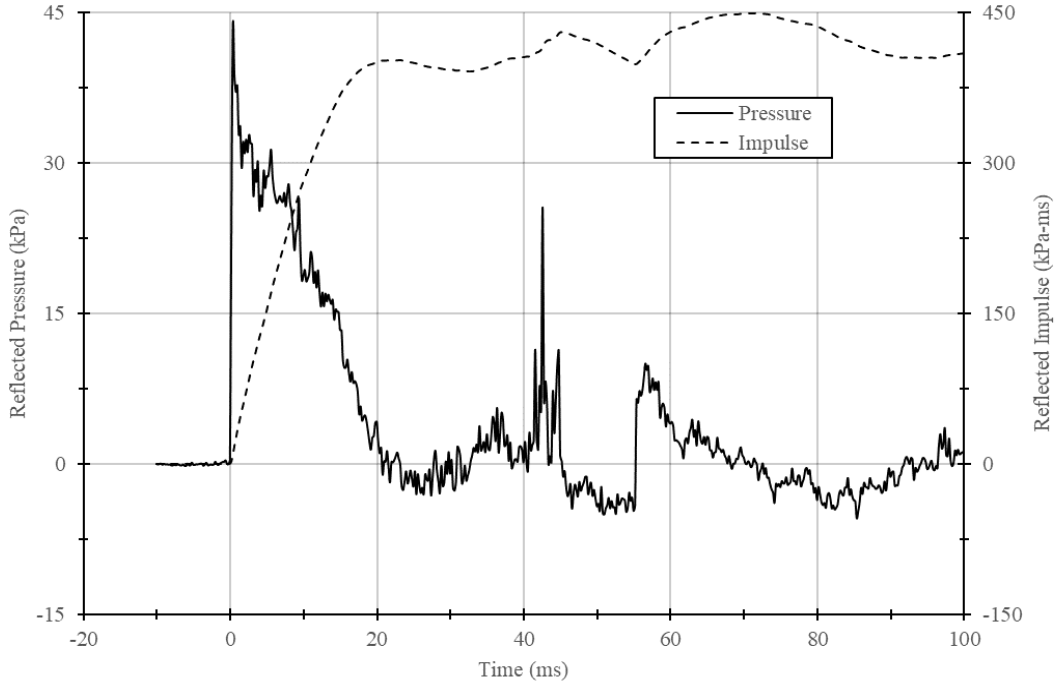

Figure B.71: Reflected pressure and impulse time histories for Y0D[3]

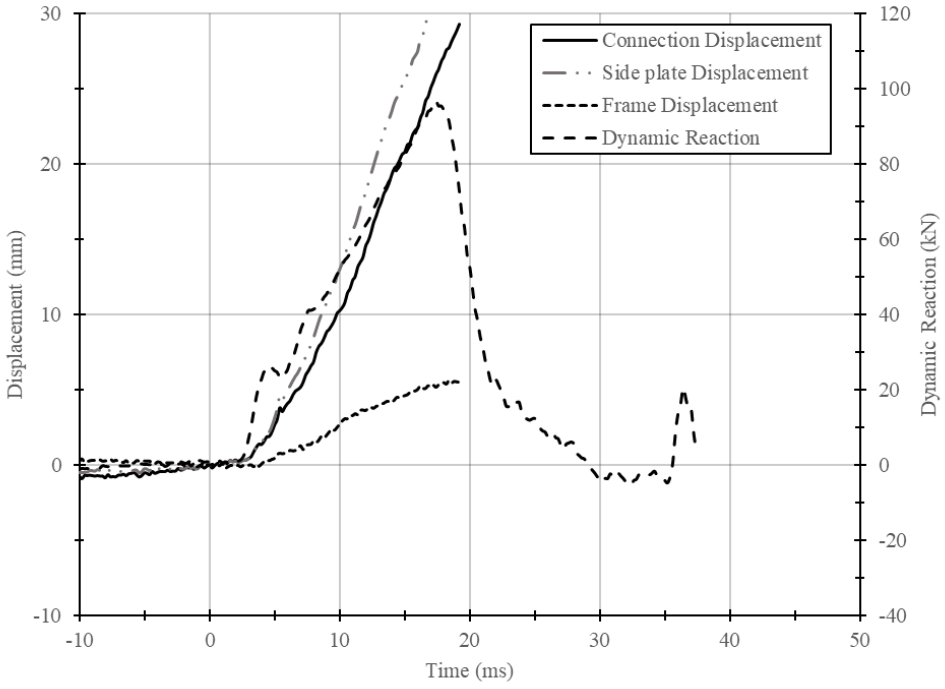

Figure B.72: Displacement and reaction time histories for Y0D[3]

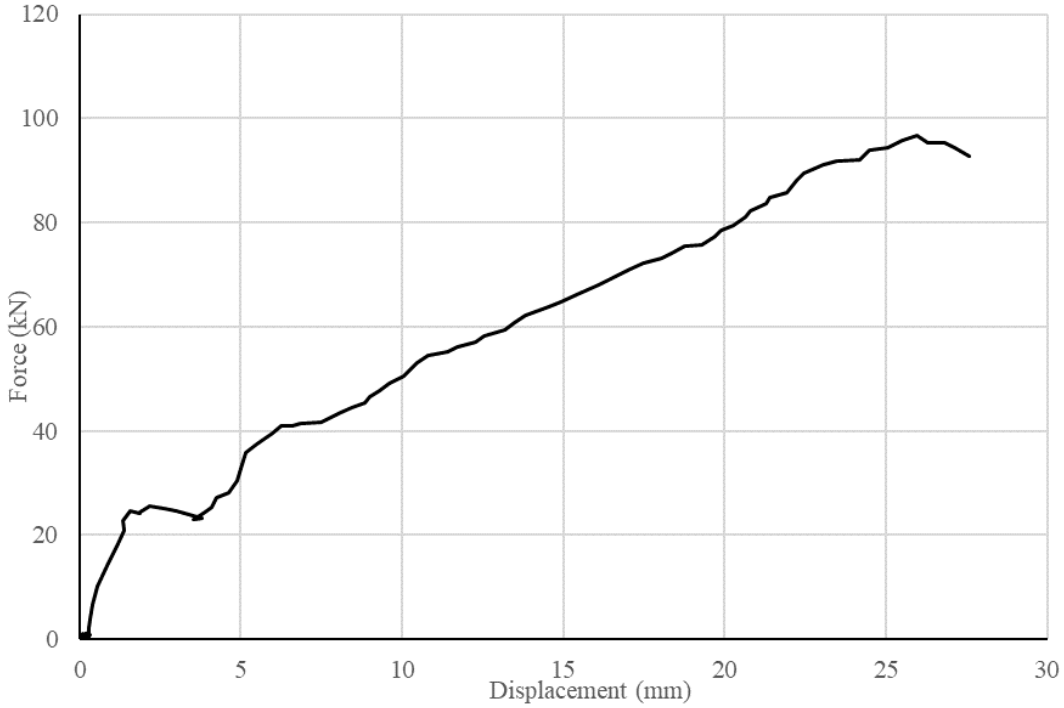

Figure B.73: Force displacement curve for Y0D[3]

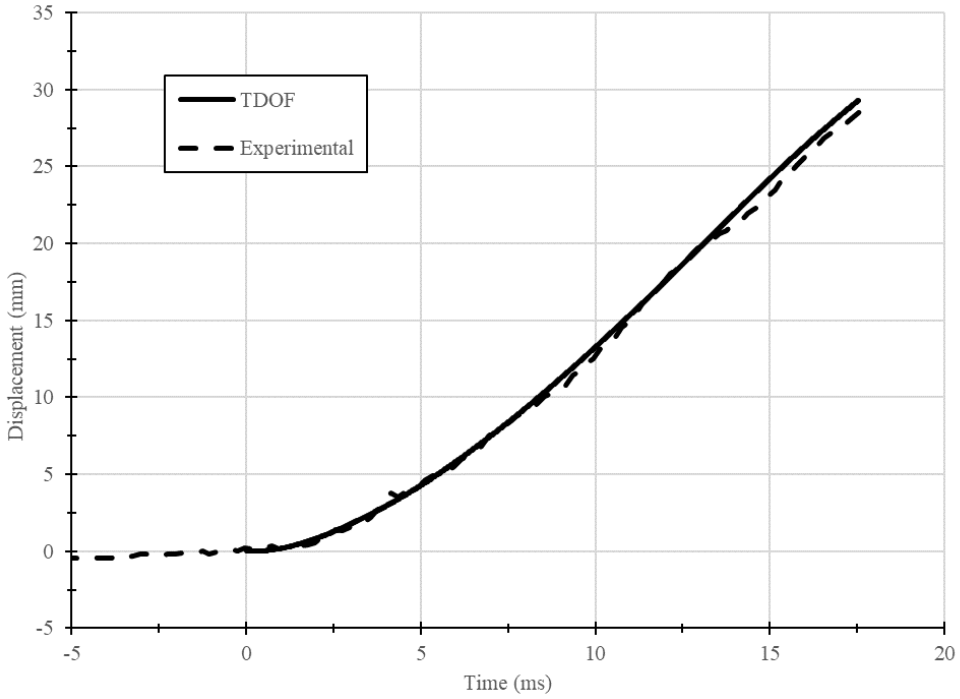

Figure B.74: TDOF prediction for Y0D[3]

(a) Inside of split specimen

(b) Splitting failure

(c) Crushing at bolt hole edge

(d) Bending in bolt with no shear failure

Figure B.75: Specimen Y0D[3] after testing

Specimen: Y0D[4]

Comments: Reinforced specimen. Ultimate failure in bolt shear. After the bolt failed in shear it was pulled out of the specimen and subsequently bent against the reaction frame. This explains the unusual deformed shape of the bolt.

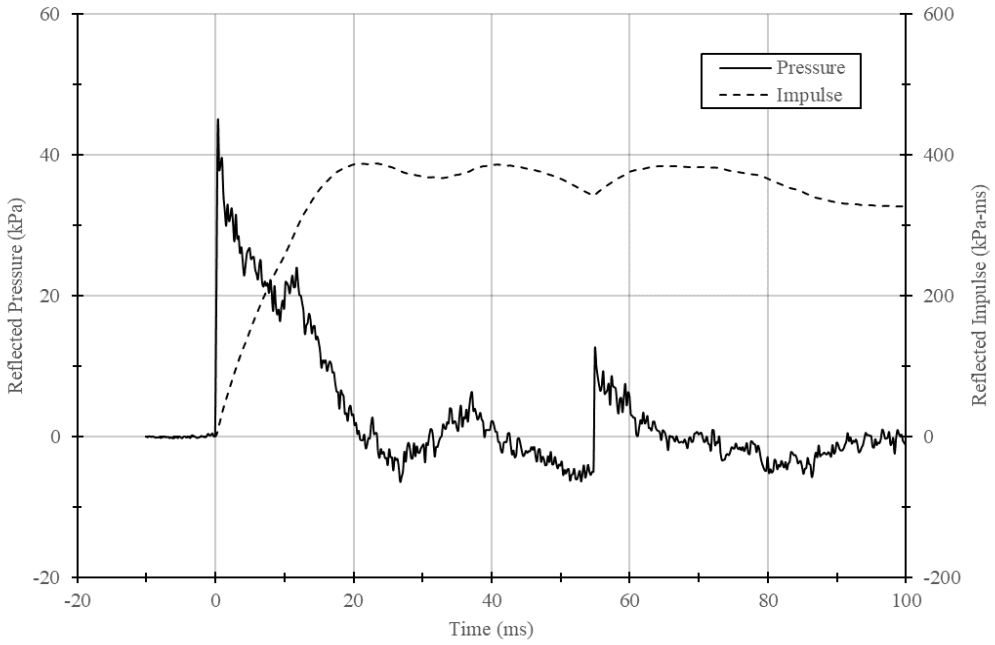

Figure B.76: Reflected pressure and impulse time histories for Y0D[4]

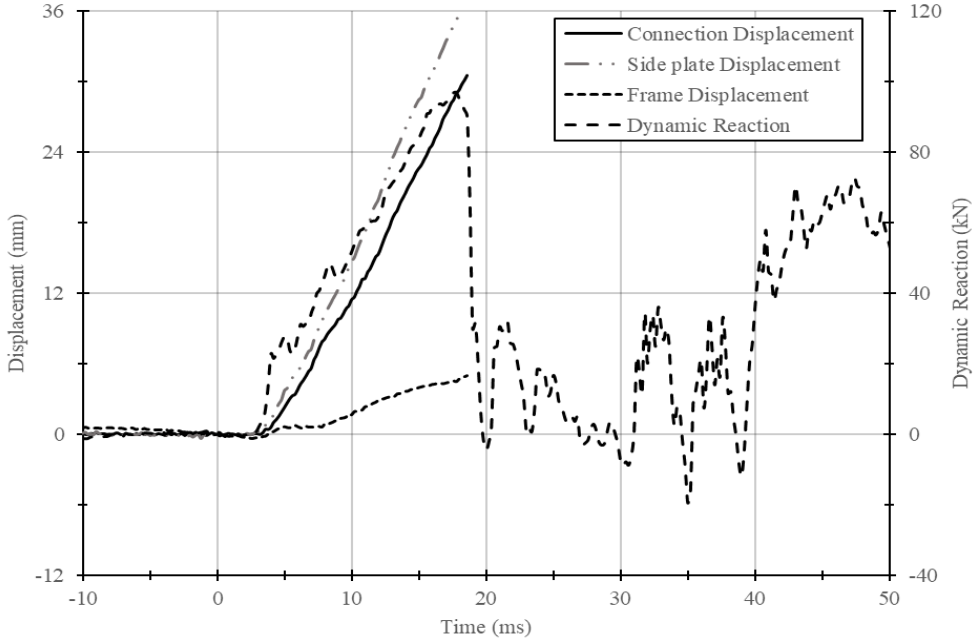

Figure B.77: Displacement and reaction time histories for Y0D[4]

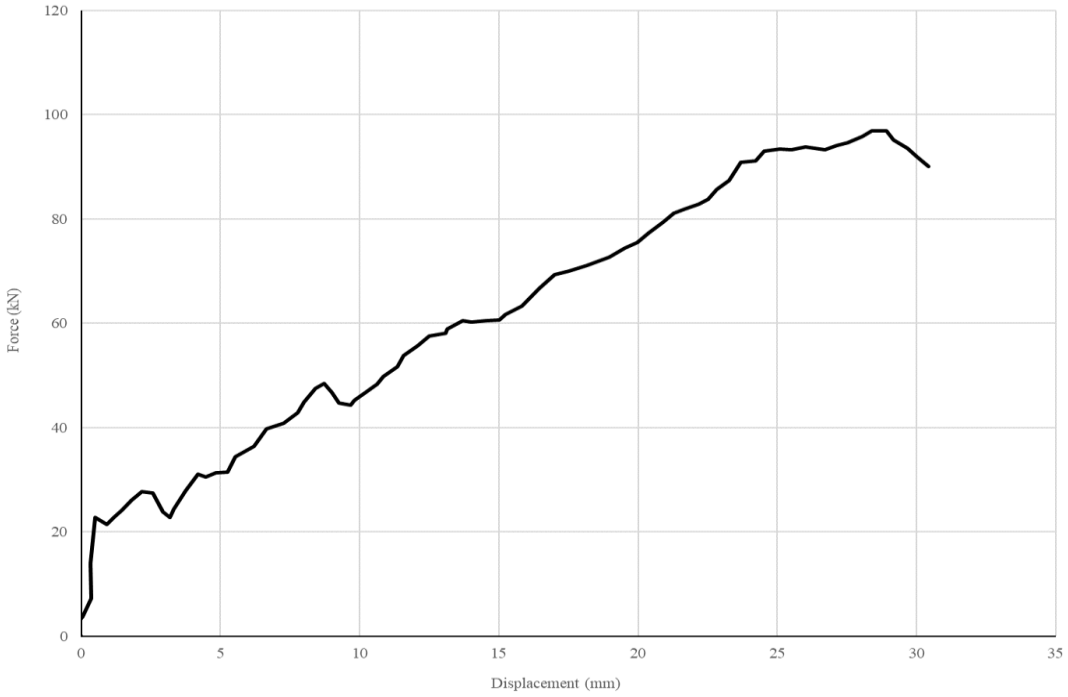

Figure B.78: Force displacement curve for Y0D[4]

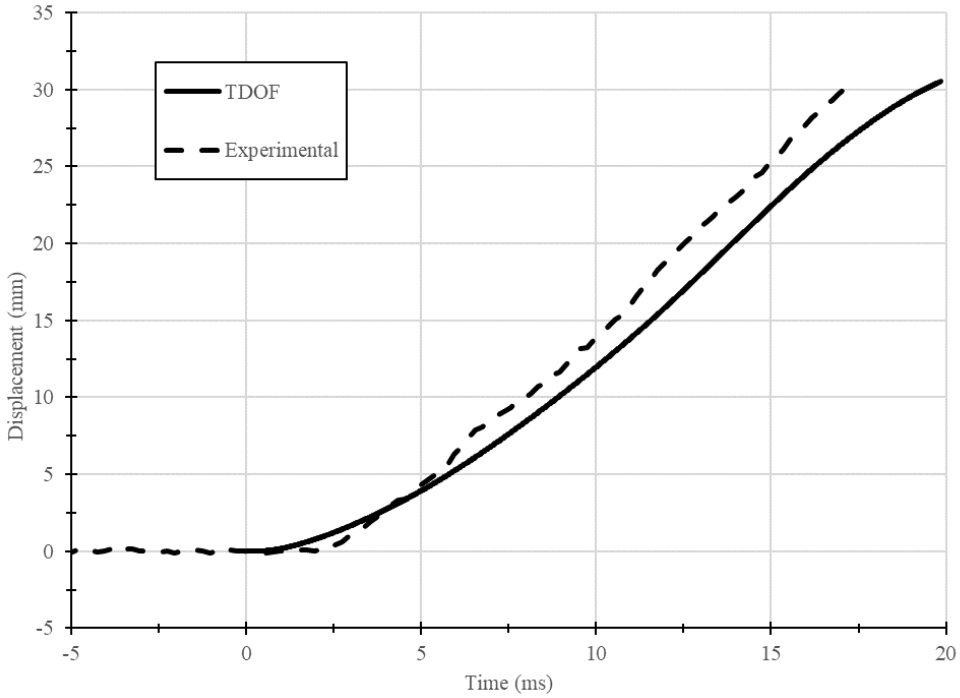

Figure B.79: TDOF prediction for Y0D[4]

(a) Self-tapping screw reinforcement configuration

(b) No splitting failure

(c) Crushing at bolt hole edge

(d) Deformed shape of bolt and shear failure on nut side

Figure B.80: Specimen Y0D[4] after testing

Specimen: Y0D[5]

Comments: Reinforced specimen. Ultimate failure in bolt shear. After the bolt failed in shear it was pulled out of the specimen and subsequently bent against the reaction frame. This explains the unusual deformed shape of the bolt.

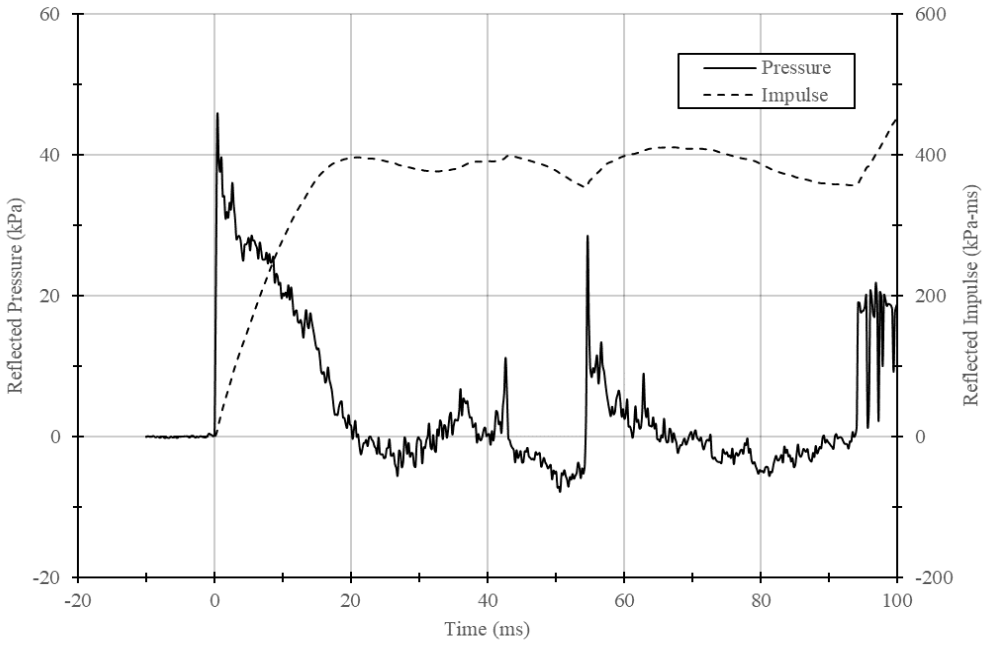

Figure B.81: Reflected pressure and impulse time histories for Y0D[5]

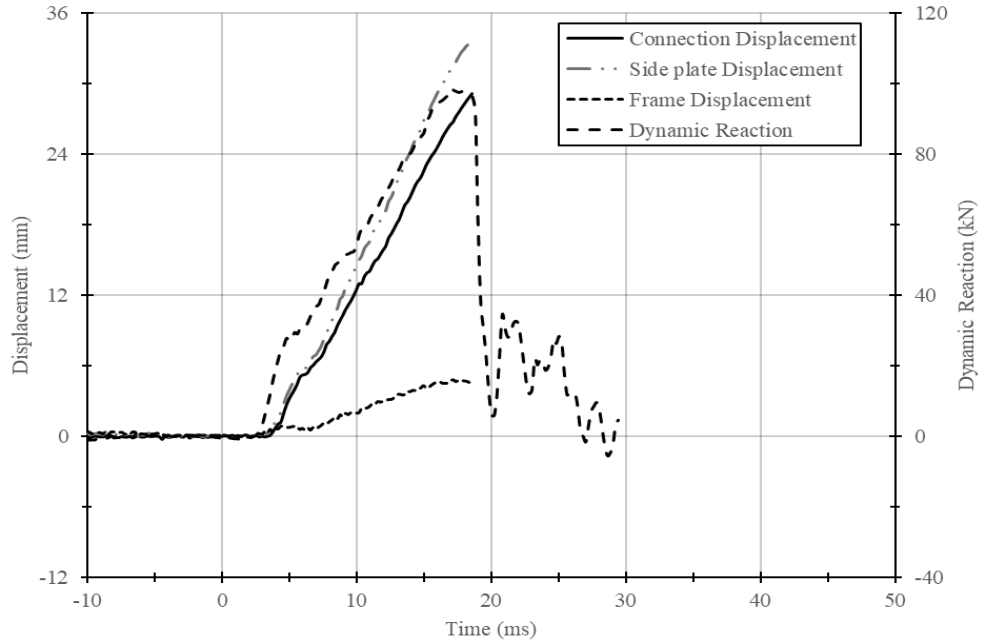

Figure B.82: Displacement and reaction time histories for Y0D[5]

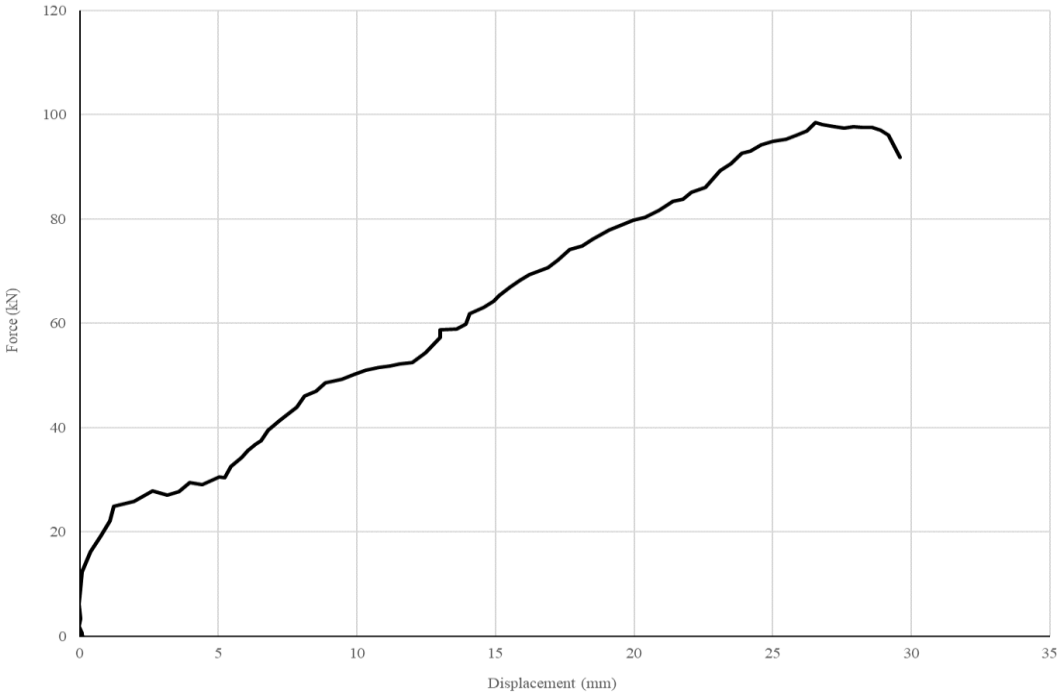

Figure B.83: Force displacement curve for Y0D[5]

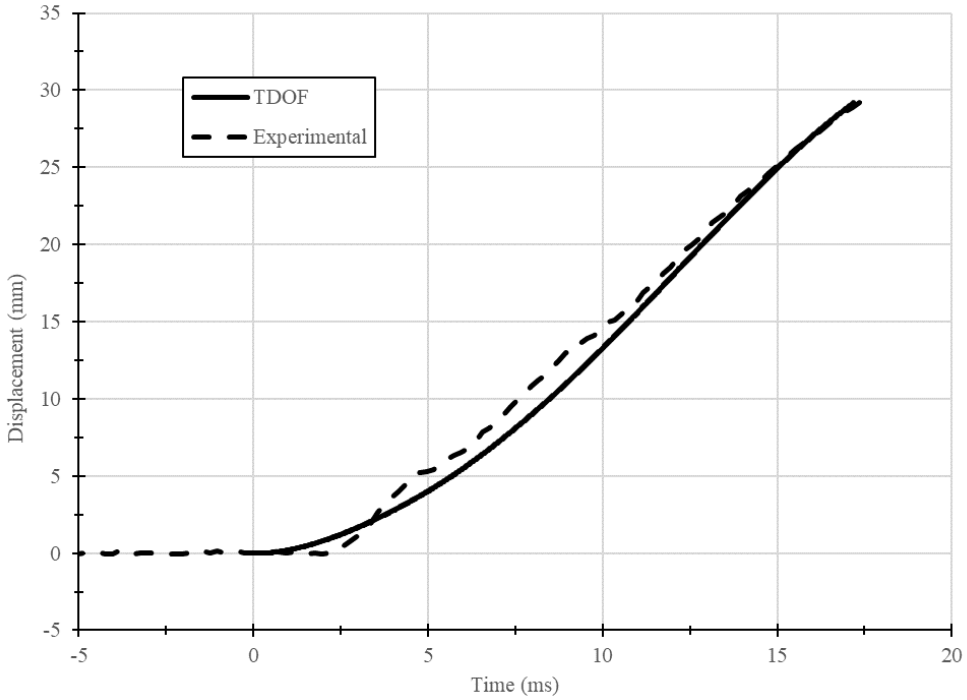

Figure B.84: TDOF prediction for Y0D[5]

(a) No splitting failure

(b) Crushing at bolt hole edge

(c) Deformed shape of bolt and shear failure on nut side

Figure B.85: Specimen Y0D[5] after testing

Specimen: Y0D[6]

Comments: Reinforced specimen. Ultimate failure in bolt shear. After the bolt failed in shear it was pulled out of the specimen and subsequently bent against the reaction frame. This explains the unusual deformed shape of the bolt.

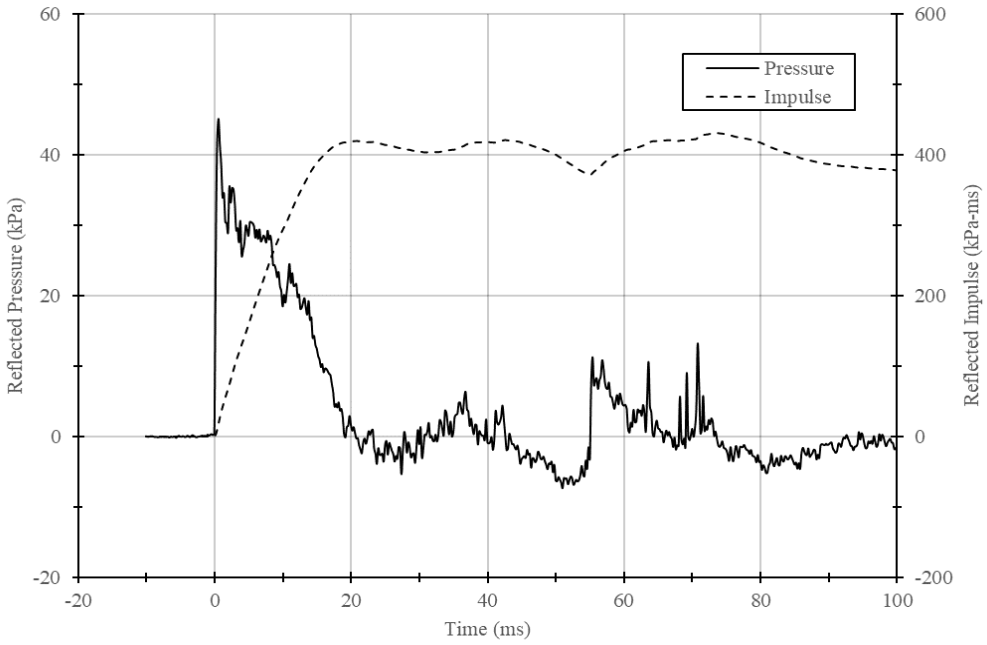

Figure B.86: Reflected pressure and impulse time histories for Y0D[6]

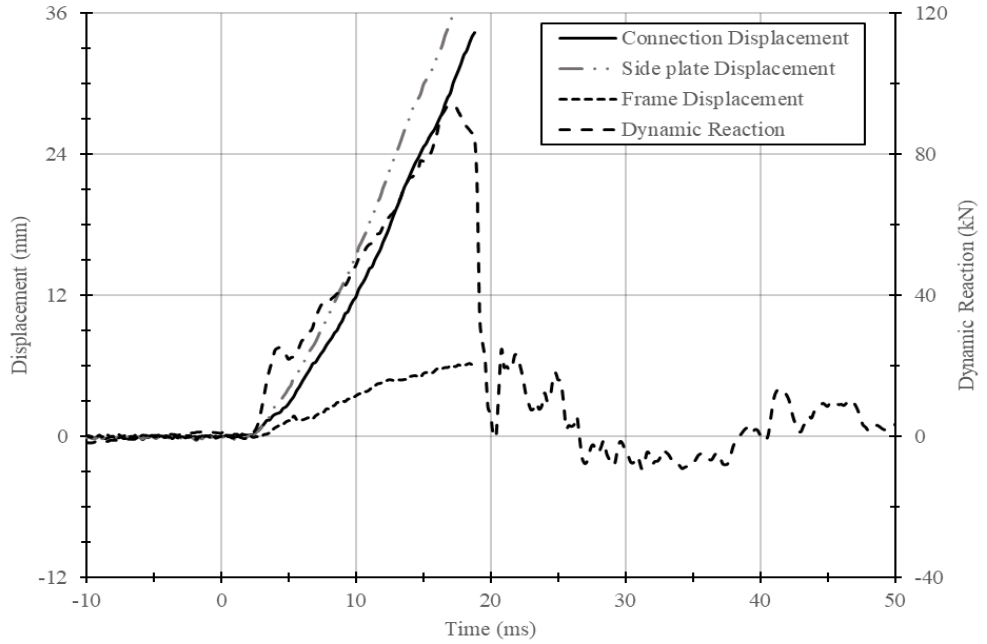

Figure B.87: Displacement and reaction time histories for Y0D[6]

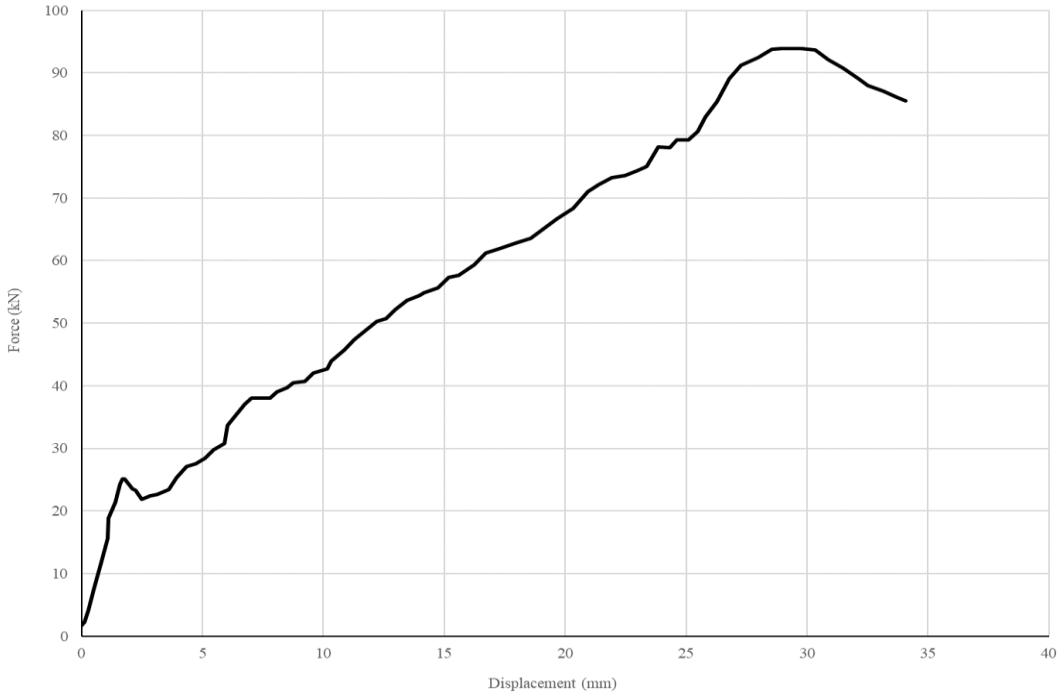

Figure B.88: Force displacement curve for Y0D[6]

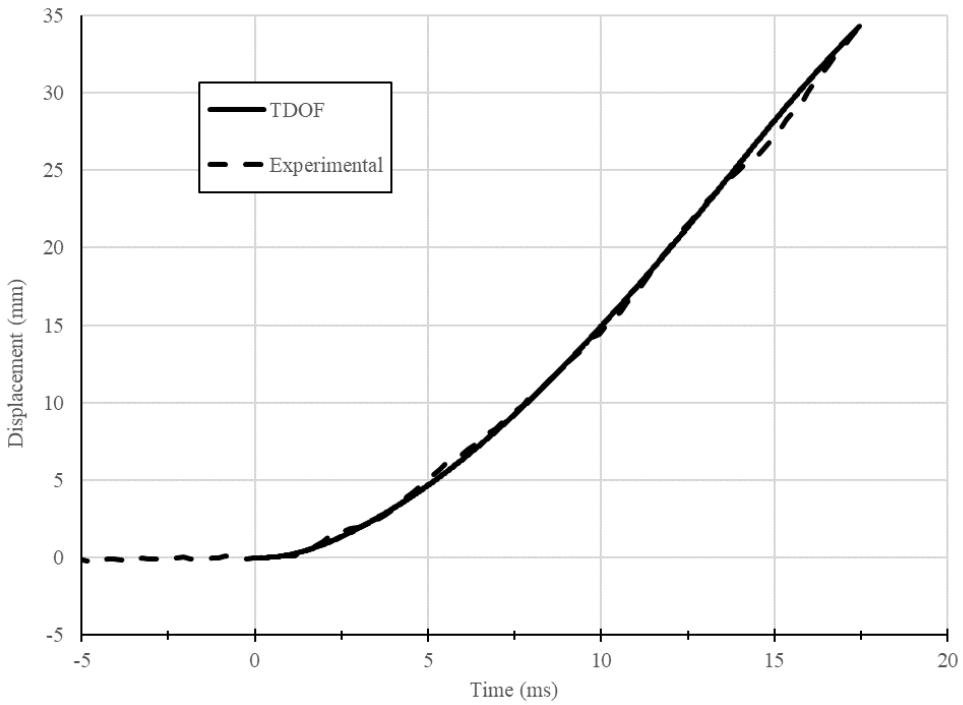

Figure B.89: TDOF prediction for Y0D[6]

(a) No splitting failure

(b) Crushing at bolt hole edge

(c) Deformed shape of bolt and shear failure on nut side

Figure B.90: Specimen Y0D[6] after testing

Specimen: Y90D[1]

Comments: Ultimate failure in bolt shear. Initial looseness of connection prevented yield load and stiffness from being determined. After the bolt failed in shear it was pulled out of the specimen and subsequently bent against the reaction frame. This explains the unusual deformed shape of the bolt.

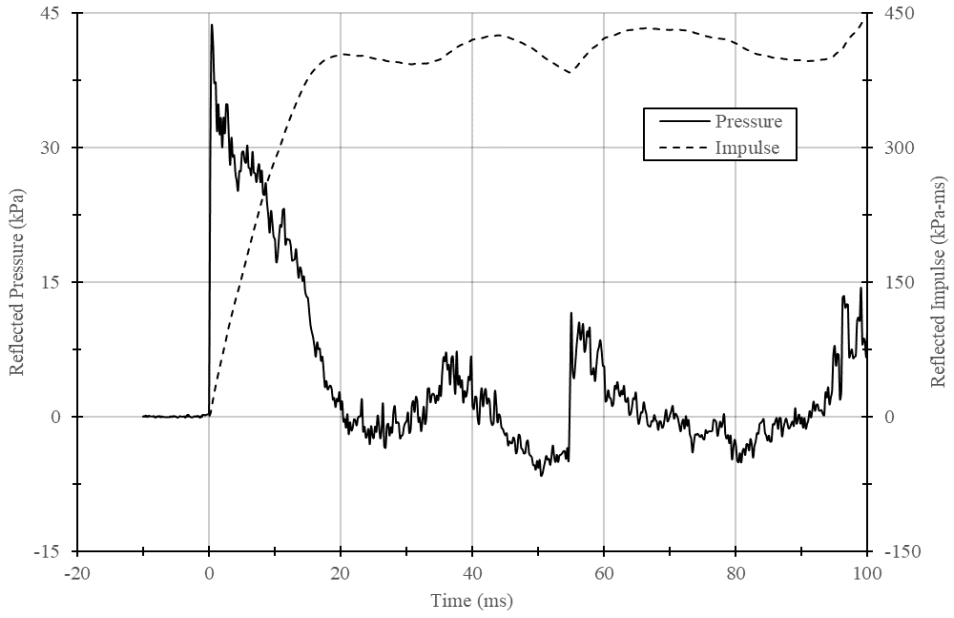

Figure B.91: Reflected pressure and impulse time histories for Y90D[1]

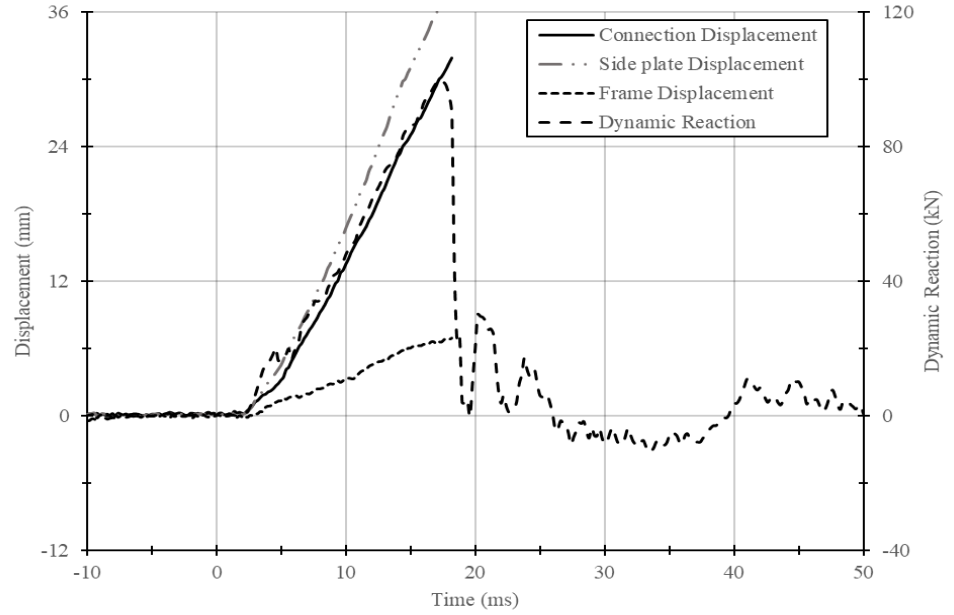

Figure B.92: Displacement and reaction time histories for Y90D[1]

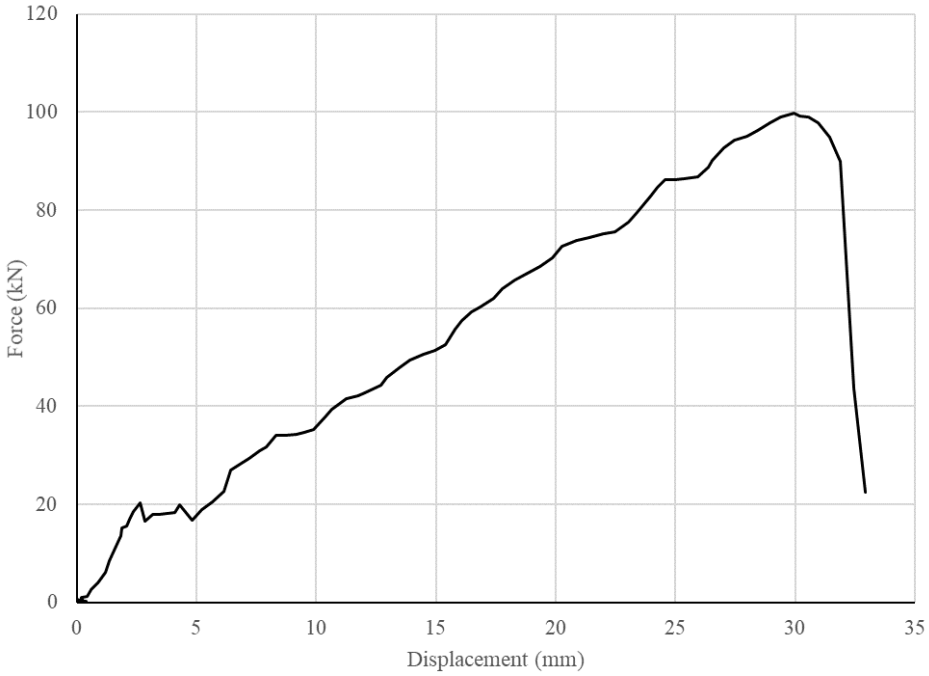

Figure B.93: Force displacement curve for Y90D[1]

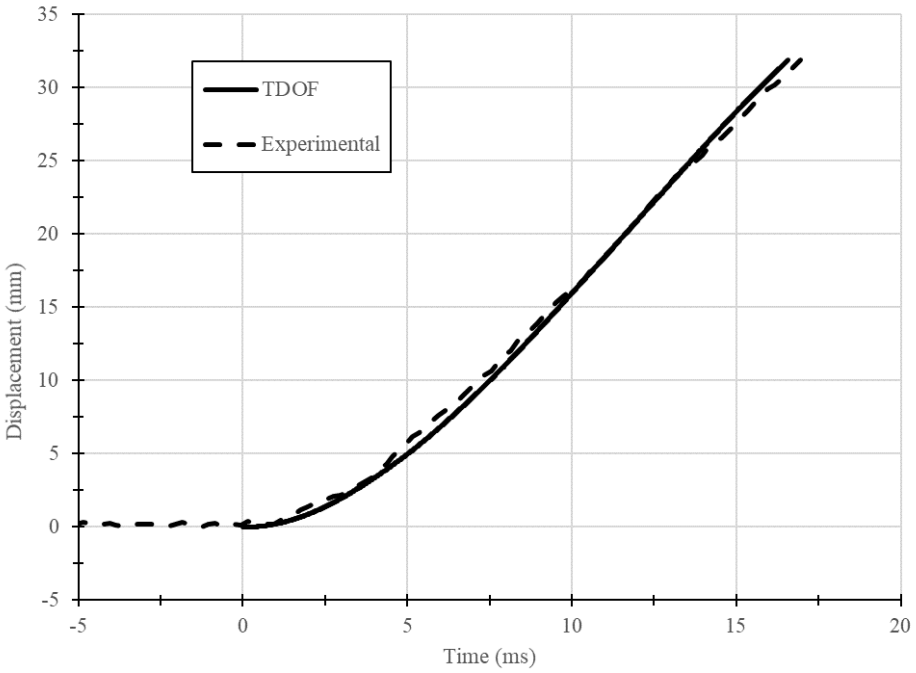

Figure B.94: TDOF prediction for Y90D[1]

(a) No splitting failure

(b) Crushing at bolt hole edge

(c) Deformed shape of bolt and shear failure on nut side

Figure B.95: Specimen Y90D[1] after testing

Specimen: Y90D[2]

Comments: Ultimate failure in bolt shear. Initial looseness of connection prevented yield load and stiffness from being determined. After the bolt failed in shear it was pulled out of the specimen and subsequently bent against the reaction frame. This explains the unusual deformed shape of the bolt.

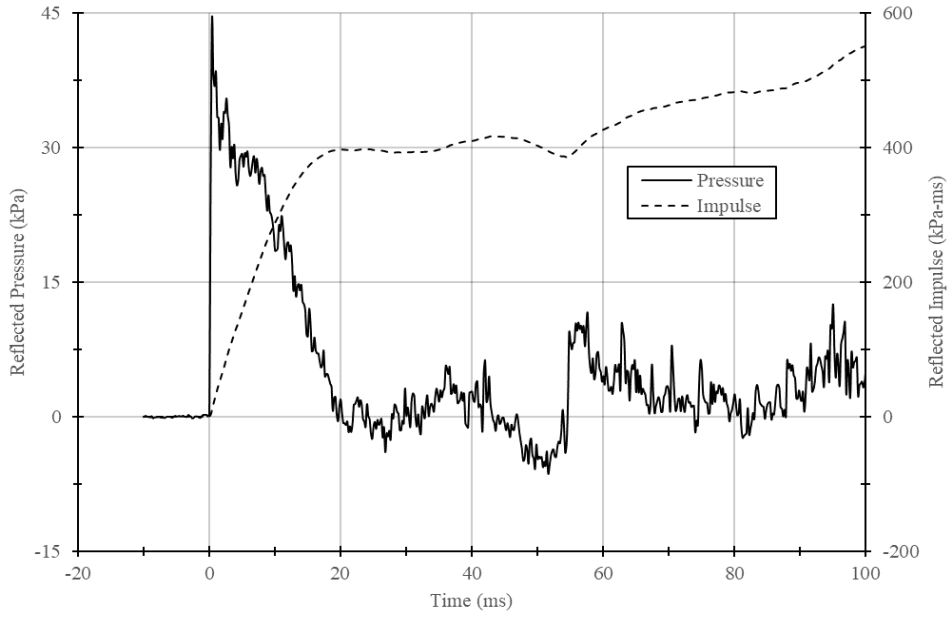

Figure B.96: Reflected pressure and impulse time histories for Y90D[2]

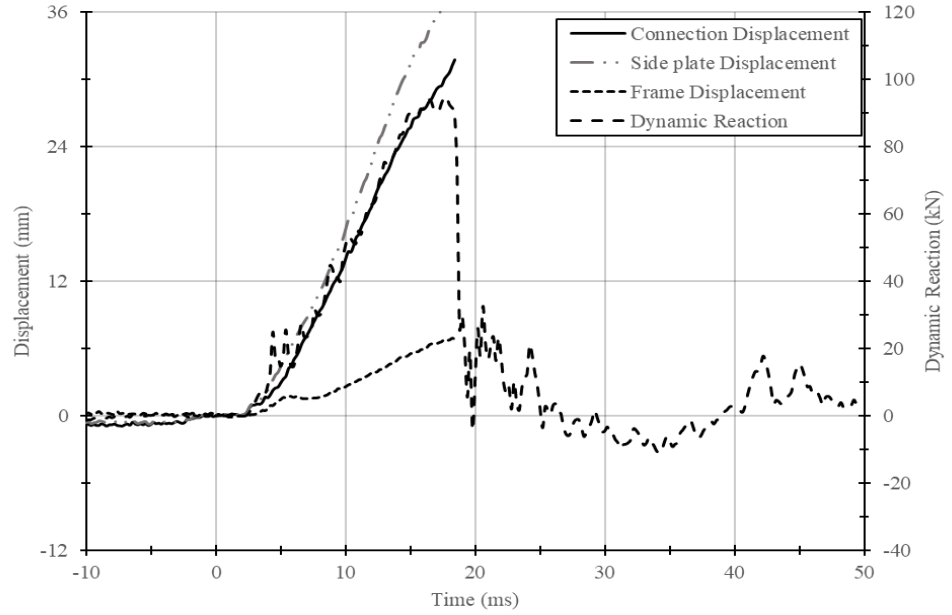

Figure B.97: Displacement and reaction time histories for Y90D[2]

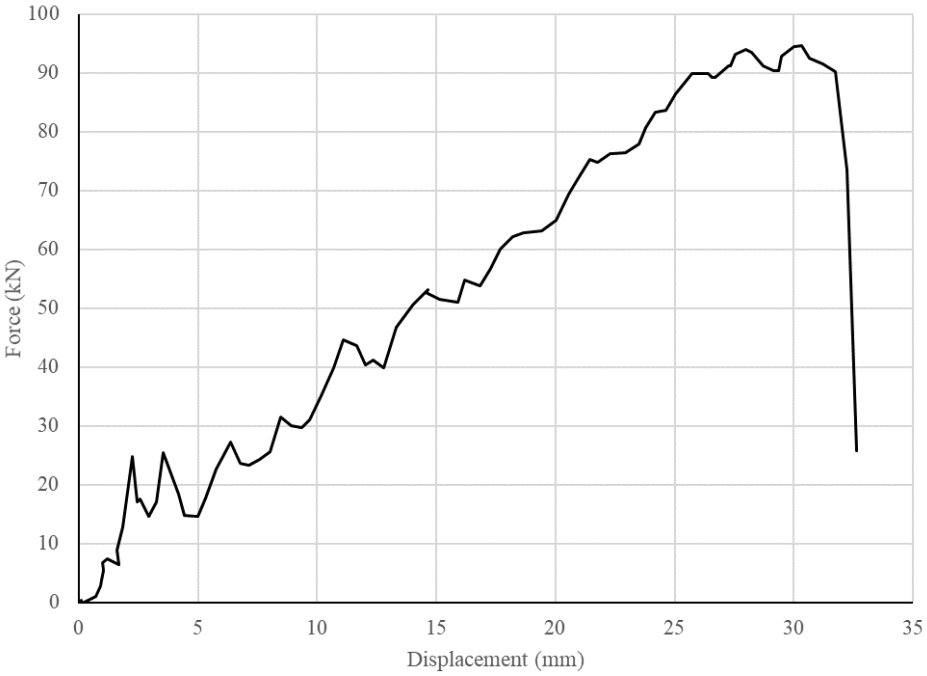

Figure B.98: Force displacement curve for Y90D[2]

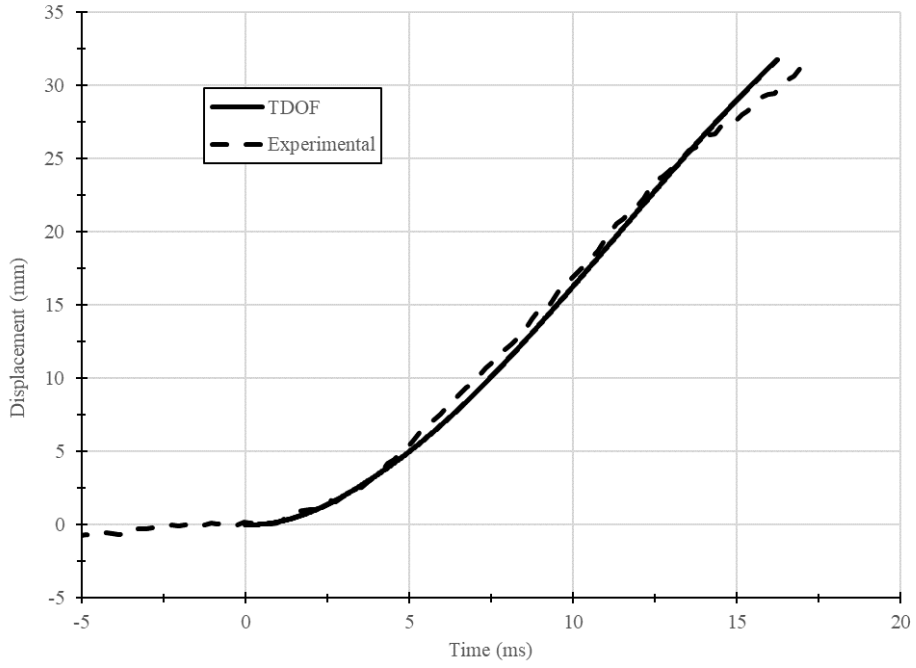

Figure B.99: TDOF prediction for Y90D[2]

(a) No splitting failure

(b) Crushing at bolt hole edge

(c) Deformed shape of bolt and shear failure on nut side

Figure B.100: Specimen Y90D[2] after testing

Specimen: Y90D[3]

Comments: Ultimate failure in bolt shear. After the bolt failed in shear it was pulled out of the specimen and subsequently bent against the reaction frame. This explains the unusual deformed shape of the bolt.

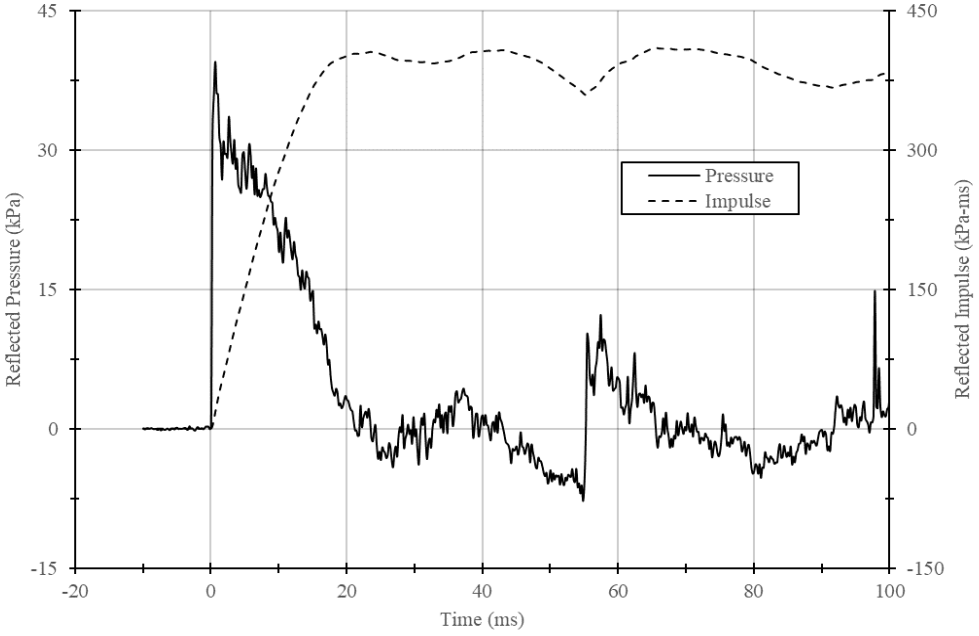

Figure B.101: Reflected pressure and impulse time histories for Y90D[3]

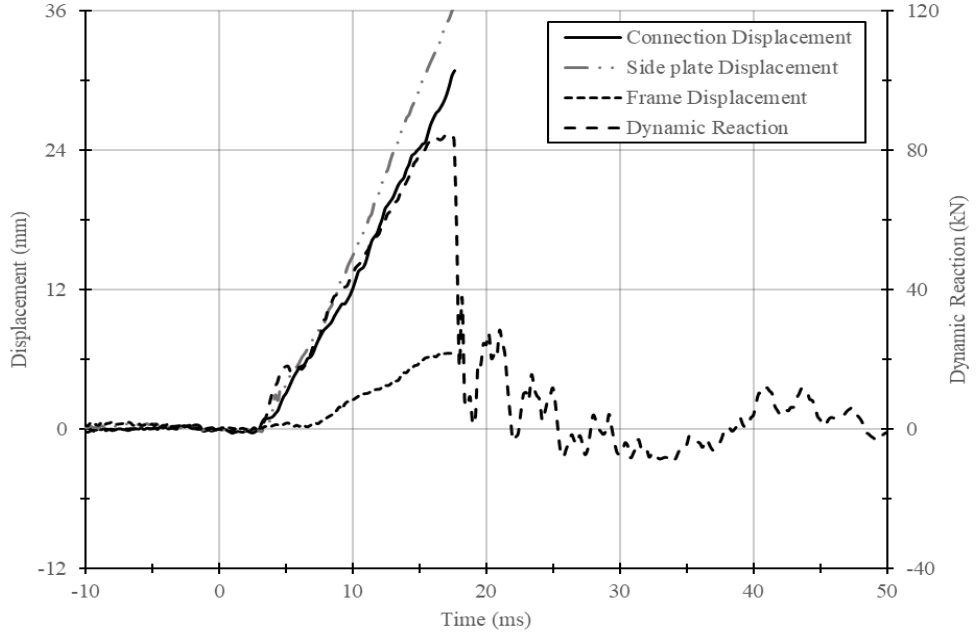

Figure B.102: Displacement and reaction time histories for Y90D[3]

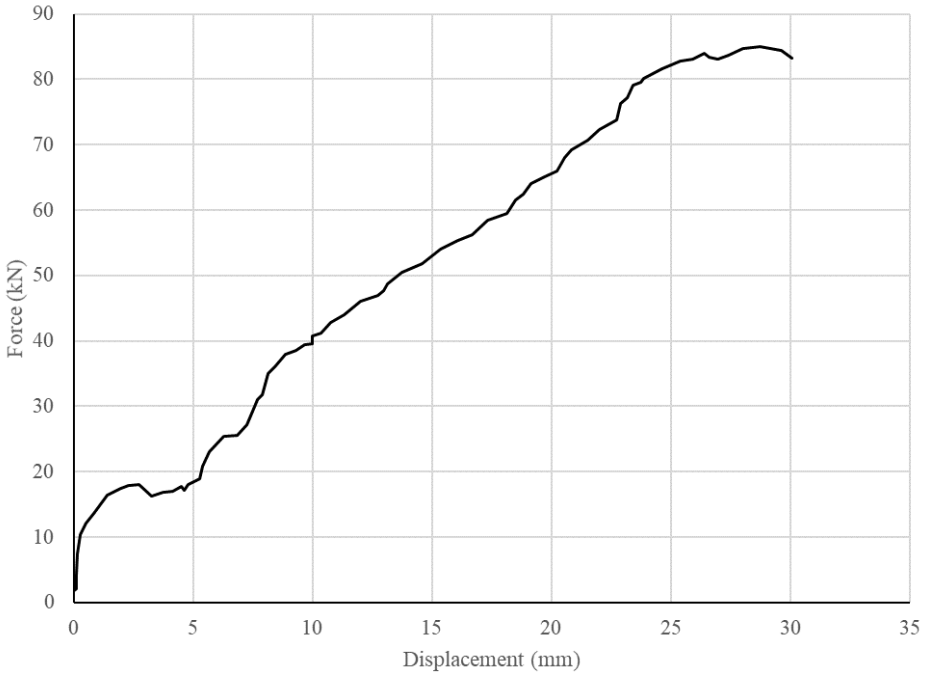

Figure B.103: Force displacement curve for Y90D[3]

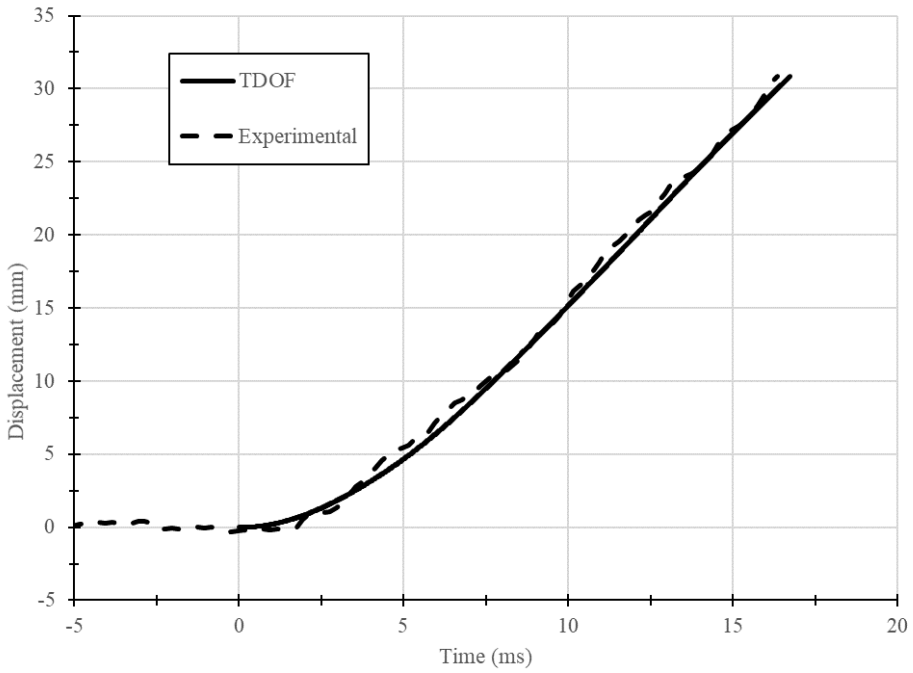

Figure B.104: TDOF prediction for Y90D[3]

(a) No splitting failure

(b) Crushing at bolt hole edge

(c) Crushing at bolt hole edge

(d) Deformed shape of bolt and shear failure on nut side

Figure B.105: Specimen Y90D[3] after testing